UNIVERSITAT POLITÈCNICA DE CATALUNYA BARCELONATECH

Application of dynamic vibration absorbers on double-deck circular railway tunnels to mitigate railway-induced ground-borne vibration

by

Behshad Noori

Departament d'Enginyeria Mecànica

UNIVERSITAT POLITÈCNICA DE CATALUNYA

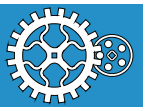

Application of dynamic vibration absorbers on double-deck circular railway tunnels to mitigate railway-induced ground-borne vibration

by

Behshad Noori

directed by

Robert Arcos Villamarín

Arnau Clot Razquin

tutored by

Teresa Pàmies Gómez

A dissertation submitted in fulfillment of the requirements for the Doctoral degree

in the

Universitat Politècnica de Catalunya (UPC)

June 4, 2019

Abstract

Application of dynamic vibration absorbers on double-deck circular railway tunnels to mitigate railway-induced ground-borne vibration

by Behshad Noori

This dissertation is concerned with investigating the efficiency of dynamic vibration absorbers (DVAs) as measures to mitigate ground-borne vibrations induced by railway traffic in double-deck tunnels. The main topics of the dissertation are the coupling of a set of longitudinal distributions of DVAs to the interior floor of a double-deck tunnel dynamic model, the computation of the response of this coupled system due to train traffic and obtaining the optimum design parameters of the DVAs to minimize this response. To address the first concern, a methodology for coupling a set of longitudinal distributions of DVAs to any railway subsystem in the context of a theoretical dynamic model of railway infrastructure is developed. The optimum design parameters of the DVAs are obtained using an optimization process based on a genetic algorithm. The effectiveness of the DVAs is assessed by two response parameters, which are used as objective functions to be minimized in the optimization process: the energy flow radiated upwards by the tunnel and the maximum transient vibration value (MTVV) in the building near the tunnel. The model used to compute the former is a two-and-a-half dimensional (2.5D) semi-analytical model of a train-track-tunnel-soil system that considers a full-space soil model, and the one used to compute the latter is a hybrid experimental-numerical model of a train-track-tunnel-soil-building system. In the hybrid model, a numerical model of the track-tunnel system based on 2.5D coupled finite element-boundary element formulation along with a dynamic rigid multi-body model of the vehicle is used to compute the response in the tunnel wall, and then, the response in the building is computed using experimentally obtained transfer functions between the tunnel wall and the building. The triaxial response in the building is used to compute the MTVV. An alternative option to evaluate the MTVV in a building is to use a fully theoretical model of the train-track-tunnel-soil-building system. In the context of this modeling strategy,

a computationally efficient method to calculate the 2.5D Green's functions of a layered soil is also presented. The results show that the DVAs would be an effective mitigation measure for railway-induced vibrations in double-deck tunnels as reductions up to 6.6 dB in total radiated energy flow and up to 3.3 dB in the vibration inside a nearby building are achieved in the simulations presented in this work.

Acknowledgements

Firstly, I would like to express my sincere gratitude to the directors of this dissertation Dr. Robert Arcos and Dr. Arnau Clot for the continuous support on my Ph.D. studies and related research, for their endless patience, motivation, and enormous knowledge. Their guidance helped me in all the time for the research involved and for writing this dissertation. I am also very grateful to Prof. Jordi Romeu for his interest in this project and for all his support and advises which help me through not only my career but also my personal life.

I would also like to thank Prof. Luis Baeza and Prof. David Thompson from the Institute of Sound and Vibration Research (ISVR), University of Southampton, UK. Being visiting researcher in ISVR helped me enriching my research and taking the last steps to finalize my dissertation.

I am also grateful to the funding received through the Industrial Doctorates Plan from AV Ingenieros and Agència de Gestió d'Ajuts Universitaris i de Recerca (AGAUR) from Generalitat de Catalunya. Special thanks to Mr. Joan Cardona and employees of AV Ingenieros for their support and for their efforts to make the funding possible. I would like to express my gratitude to Universitat Politècnica de Catalunya (UPC) for its financial support.

I would like to thank all the members of the LEAM for all the discussions, the help, the supports. Thanks to Santi, Andreu and, Tere for all their practical and wise advice. Thanks to Jay, my office mate, and Memo for sleepless Friday nights we were working together; and thanks to my girlfriend and all my friends, who helped me overcome living abroad challenges and made it enjoyable for me.

Finally, I want to express my deepest gratitude to my parents and siblings without whom I would never have enjoyed so many opportunities and I would not have had the courage to begin this adventure in the first place. Thank you for believing in me and encouraging me to follow my dreams.

Contents

Abstract i

Acknowledgements iii

List of Figures vi

List of Tables x

1 Introduction 1
- 1.1 Justification of the research . . . 2
- 1.2 Outline of the dissertation . . . 4

2 Literature review 6
- 2.1 Railway ground-borne vibration problem . . . 7
- 2.2 Soil dynamics: Half-space modeling strategies . . . 8
- 2.3 Railway-induced vibration prediction models . . . 10
- 2.4 Railway-induced ground-borne vibration countermeasures . . . 12
- 2.5 Dynamic vibration absorbers . . . 14

3 Control of vibration energy flow radiated upwards from double-deck tunnels by means of DVAs 16
- 3.1 Introduction . . . 17
- 3.2 Modeling of the vehicle-track-tunnel-soil system . . . 17
  - 3.2.1 Track-tunnel-soil model . . . 18
  - 3.2.2 Vehicle-track coupling . . . 19
- 3.3 Application of DVAs on an underground railway system . . . 22
- 3.4 DVAs optimization approach . . . 27
- 3.5 Application and results . . . 29
  - 3.5.1 Parameters used to model subsystems . . . 29
  - 3.5.2 Computation of the Green's functions . . . 31
  - 3.5.3 Train pass-by response . . . 33
  - 3.5.4 Optimum parameters of DVAs . . . 35

4 Application of DVAs as vibration countermeasures: Case study of L9 Barcelona metro 45

4.1 Introduction . . . 46
4.2 Hybrid vibration prediction model . . . 46
4.2.1 Modeling of tunnel-soil system . . . 47
4.2.2 Modeling of track-interior floor system . . . 47
4.2.3 Modeling of train-track interaction . . . 50
4.2.4 Building response prediction . . . 51
4.3 DVAs optimization approach . . . 52
4.4 Application and results . . . 53
4.4.1 Computation of the Green's functions of the tunnel/soil system 53
4.4.2 Train pass-by response prediction . . . 56
4.4.3 Experimental measurements required for the hybrid model . 60
4.4.4 Application of DVAs . . . 65

5 Fast computation of 2.5D elastodynamic Green's functions in half-spaces 68
5.1 Introduction . . . 69
5.2 3D Stiffness matrices in Cartesian coordinates . . . 69
5.2.1 Stiffness matrix of a layer . . . 73
5.2.2 Stiffness matrix of a lower half-space . . . 75
5.3 2.5D Green's functions for homogeneous and layered half-spaces . . 76
5.4 Results and discussion . . . 78
5.4.1 Case 1: Surface response of a homogeneous half-space subjected to a buried load . . . 79
5.4.2 Case 2: Buried response of a homogeneous half-space subjected to a buried load . . . 81
5.4.3 Case 3: Buried response of a layered half-space subjected to a buried load. . . . 85
5.4.4 Case 4: An extension of the fictitious force method . . . 88

6 Conclusions and further work 95
6.1 Conclusions . . . 96
6.2 Further work . . . 99

Bibliography 101

List of Figures

1.1 A cross-section of the double-deck tunnel with platforms in L9 [1]. . 3

2.1 Schematize of ground-borne vibration propagation. 8
2.2 A cross-section of a double-deck tunnel with superstructures proposed by Clot et al. [2]. 11

3.1 A scheme of a double-deck tunnel and its subsystems embedded in a full-space. 18
3.2 A track system with one longitudinal distribution of DVAs. 22
3.3 DVAs modeled as a SDOF. 23
3.4 The track-tunnel-soil model in full-space with one distribution of DVAs. 27
3.5 A finite cylindrical strip through which the radiated energy flow is calculated. 28
3.6 Train configuration. 31
3.7 Geometrical scheme of the receivers located at the soil and at the interior floor. 32
3.8 Time history of the vertical velocity of the left rail due to the train passing at speeds of (a) $v_t = 20$ m s^{-1} and (b) $v_t = 25$ m s^{-1}. 34
3.9 Time history of the radial velocity of the soil at $\theta = \pi/2$ and $r_s = 12$ m due to the train passing at speeds of (a) $v_t = 20$ m s^{-1} and (b) $v_t = 25$ m s^{-1}. 35
3.10 Frequency spectrum of the radial velocity for the hard soil (top) and soft soil (bottom) at $\theta = \pi/2$ rad and $r_s = 12$ m due to the train passing at speeds of (a,c) $v_t = 20$ m s^{-1} and (b,d) $v_t = 25$ m s^{-1}. 36
3.11 Mean power flow radiated upwards over the cylindrical strip in the time domain for the cases (a) H20, (b) H25, (c) S20 and (d) S25. The grey and black lines represent the results with and without DVAs, respectively. The total radiated energy is presented for each case. 38
3.12 ESD for cases (a) H20, (b) H25, (c) S20 and (d) S25. The grey and black lines represent the results with and without DVAs, respectively. The total radiated energy is also presented for each case. . . 40

3.13 One-third octave bands for cases (a) H20, (b) H25, (c) S20 and (d) S25. The grey and black lines represent the results with and without DVAs, respectively. 41
3.14 Energy radiated over cylindrical strip in J as a function of θ for cases (a) H20, (b) H25, (c) S20 and (d) S25. The grey and black lines represent the results with and without DVAs, respectively. . . 42
3.15 The radial velocity Green's functions of the hard soil in dB (dB reference 1 m $N^{-1}s^{-1}$) at the receivers located at $r_s = 12$ m and (a) $\theta = 0$, (b) $\theta = \pi/2$ rad and (c) $\theta = \pi$ rad for $v_t = 25$ m s^{-1}. Inclined dashed black lines denote points of constant $\tilde{\omega}$ for the specific speed of 25 m s^{-1}. 43
3.16 Contact forces caused by wheel-rail interaction associated to $v_t = 20$ m s^{-1} (grey) and $v_t = 25$ m s^{-1} (black). 43
3.17 One-third octave band spectrum of the vertical velocity of the left rail in dB (dB reference 10^{-8} m s^{-1}) for the train speeds of (a) $v_t = 20$ m s^{-1} and (b) $v_t = 25$ m s^{-1}. The grey and black lines represent the results with and without DVAs, respectively. 44

4.1 Mesh of the 2.5D FE-BE model of the double-deck tunnel for the specific section studied. The boundary element nodes are shown by diamonds. The FE nodes used to couple the rails (three nodes for each rail, r_1 and r_2), the ones used to evaluate the response of the system at the tunnel wall (t_1 and t_2), and the ones considered as possible positions of DVAs (d_1 to d_{12}) are shown by circles. 54
4.2 Schematic of 2D MDOF rigid body model of each car. 57
4.3 Time history of the vertical velocity of the rail r_1 (a) and the rail r_2 (b), at $x = 0$, in the absence of DVAs. 58
4.4 Time history (a) and frequency spectrum (b) of the vertical velocity of the interior floor d_3. 58
4.5 Time history (a) and frequency spectrum (b) of the velocity of the tunnel wall at t_1 associated to y direction. Superimposed (in gray) time history and frequency spectrum of the vertical velocity at t_1. . 59
4.6 Wheel-rail interaction contact force at the first wheel. 59
4.7 Schematic representation of the setup of accelerometers used for the vibration measurements inside the tunnel (a). Accelerometers used to record time history of the tunnel wall (b), the interior floor (c) and the building (d) due to train pass-by. 61
4.8 One-third octave band spectra of the vertical vibration acceleration of the interior floor for the passage of the train in dB (dB reference 10^{-6} m s^{-2}): (a) Numerical prediction response (dashed black line) at d_3, five measured responses (gray lines) and the average of measured responses (dashed black line) at a_1; (b) Numerical prediction response (dashed black line) at d_{12}, five measured response (gray lines) and the average of measured responses (dashed black line) at a_3. 62

4.9 One-third octave band spectra of the vibration acceleration of the tunnel wall in y direction in dB (dB reference 10^{-6} m s^{-2}). Dashed black line, gray lines and solid black line represent numerical prediction response, five measured responses and the average of measured responses, respectively. 63
4.10 Experimentally obtained transfer functions between the tunnel wall and the targeted building (gray lines) and average of all transfer functions (black line). 64
4.11 One-third octave band spectra of the vibration acceleration at the targeted building floor in dB (dB reference 10^{-6} m s^{-2}). Dashed black line, gray lines, and solid black line represent numerical prediction response, five measured responses and the average of measured responses, respectively. 65
4.12 One-third octave band spectra of the vibration acceleration of the targeted building in dB (dB reference 10^{-6} m s^{-2}) before (solid black line) and after (dashed black line) the application of the DVAs in the tunnel. 67

5.1 Free body diagram of a layer without body forces. 73
5.2 Free body diagram of a lower half-space without body forces. 75
5.3 A homogeneous half-space with a virtual interface (dashed lines) placed at the position of the buried load; the receiver-point placed on the surface. 80
5.4 Amplitude (a) and phase values (b) of the 2.5D Green's functions at 30 Hz for case 1. Solid and dotted lines are used to represent the results obtained using Tadeu's method and the new one, respectively. 82
5.5 Relative errors of the 2.5D Green's functions with respect to the reference solution for new method (solid lines) and for Tadeu's method (dashed lines) for case 1. 83
5.6 A homogeneous half-space with buried receiver-point and buried load; the virtual interface (dashed lines) placed at the position of the buried load. 83
5.7 Amplitude (a) and phase values (b) of the 2.5D Green's functions at 30 Hz for case 2. Solid and dotted lines are used to represent the results obtained using Tadeu's method and the new one, respectively. 84
5.8 Relative errors of the 2.5D Green's functions with respect to the reference solution for new method (solid lines) and for Tadeu's method (dashed lines) for case 2. 85
5.9 A three-layered half-space with the virtual interfaces, dashed lines, considered for buried load and receiver-point. 86
5.10 Amplitude (a) and phase values (b) of the 2.5D Green's functions at 30 Hz for case 3. Solid and dotted lines are used to represent the results obtained using the stiffness matrix method in cylindrical coordinate [3] and the new one, respectively. 87

5.11 Sampling grid obtained directly using the proposed method (black solid points). The required points are denoted by grey circles. . . . 88
5.12 Sampling grid obtained directly from the method based on the stiffness matrices in cylindrical coordinates (black solid points). The required points are denoted by grey circles. 89
5.13 Schematic representation of (a) first (b) second and (c) third step of the fictitious force method. 90
5.14 A circular tunnel embedded in a layered half-space. 91
5.15 Amplitude (a) and phase values (b) at $(y_{rp}, z_{rp}) = (10, 6)$ at 60 Hz. Solid and dotted lines are used to represent the results obtained using the present method and using EDT [4], respectively. 93
5.16 Amplitude (a) and phase values (b) at $(y_{rp}, z_{rp}) = (10, 0)$ at 60 Hz. Solid and dotted lines are used to represent the results obtained using the present method and using EDT [4], respectively. 94

List of Tables

3.1 Mechanical parameters used to model the soil. 29
3.2 Mechanical parameters used to model the tunnel. 30
3.3 Mechanical parameters used to model the interior floor. 30
3.4 Mechanical parameters used to model the rail. 30
3.5 Mechanical parameters used to model the fastener. 30
3.6 Mechanical parameters used to model the train. 31
3.7 The optimum values of DVAs parameters and resulting IL. 37

4.1 Mechanical parameters used to model the tunnel/interior floor system and soil. 54
4.2 Parameters used to model the rails. 55
4.3 Mechanical parameters used to model the train. 57
4.4 The optimum values of DVAs parameters and resulting IL. 66

5.1 Mechanical parameters used to model the soil in sections 5.4.1 and 5.4.2 80
5.2 Mechanical parameters used to model the soil in section 5.4.3. . . . 86
5.3 Mechanical parameters used to model the soil in section 5.4.4. . . . 92
5.4 Mechanical parameters used to model the tunnel in sections 5.4.4. 92

To my family

Chapter 1

Introduction

This chapter begins with a brief introduction to the underground railway-induced vibration problem and justifies the necessity of introducing novel countermeasures for new tunnel designs to tackle this problem. The main objectives and the structure of the dissertation are also presented briefly in this chapter.

1.1 Justification of the research

Underground railway systems play a major role in transporting passengers within urban and suburban areas. However, the vibrations caused by trains circulation in underground tunnels are one of the major sources of ground-borne vibrations. These vibrations propagate through the soil and structural foundations into nearby buildings, resulting in vibration and re-radiated noise in the buildings. These can cause discomfort for residents of the buildings, affect the operation of sensitive equipment and damage buildings with structural weakness, i.e. old historical buildings.

Several countermeasures have been proposed and applied in practice to address underground-railway induced vibration problems. These vibration mitigation measures can be categorized according to the location at where they are applied: i) the source; ii) the propagation path and iii) the receiver. Mitigation measures at the source mainly target the mechanisms of ground-borne vibration generation to reduce the forces appearing in the vehicle-track interaction and their transmission to the surroundings. The ones applied at the propagation path are all based on the idea of interrupting the propagation path of waves through the soil. The ones applied at the receiver or building are based on the installation of resilient elements like rubber blocks or steel springs between the building and its foundation.

In recent years, innovative tunnel structure designs have been constructed in several cities worldwide. Double-deck circular tunnel is one of these new designs, in which the tunnel is divided into two sections by an interior floor supported on the tunnel walls. Trains can circulate along both sections of the tunnel. Line 9 (L9) of Barcelona metro is one of the projects in which this new design has been considered and finally implemented. Fig. 1.1 shows a cross-section of a double-deck tunnel section with platforms in L9 [1].

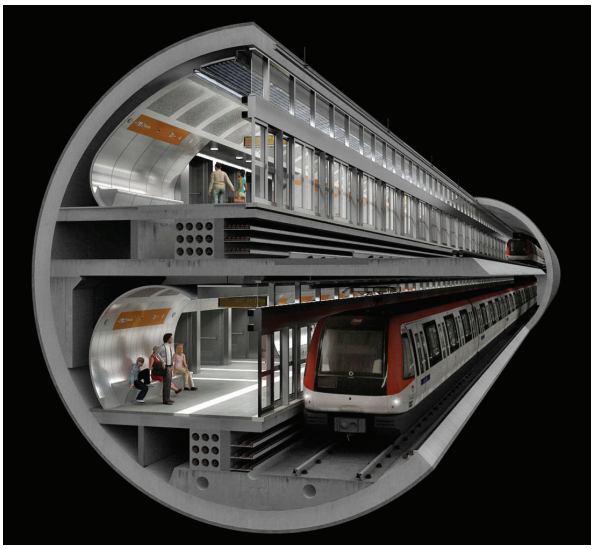

FIG. 1.1: A cross-section of the double-deck tunnel with platforms in L9 [1].

Various experimental measurements showed that the levels of vibration induced in nearby buildings due to train circulations in the upper section of the tunnel are 10 dB larger than the ones induced by trains pass-by in the lower section.

Introducing effective countermeasures for vibrations induced due to train pass-by over the upper section of a double-deck tunnel is one of the main challenges for this type of infrastructures. There are four reasons behind this issue:

1. In order to explain the 10 dB difference between the vibration induced by train passage at upper and lower sections, theoretical studies about the dynamic response of double-deck tunnels were done. Comparing the vibrations radiation from this type of tunnel due to the line load applied on the interior floor with the one from the simple circular tunnels showed clear differences with respect to the pattern and the magnitude of the radiated vibration by both structures [5, 6]. A smooth vibrations radiation pattern has been observed for the simple circular tunnel, however, the ones radiated form a double-deck tunnel include sharp peaks;

2. Floating slab track system, one of the most common and effective countermeasures applied at the source, cannot be used for the upper section due to geometrical limitations;

3. Only a few studies have been reported on measures to mitigate ground-borne vibration for double-deck tunnels [7, 8];

4. The efficiency of common vibration countermeasures applied in the vibration path has not been assessed for this type of tunnel.

A well-established system that has been widely used to control the vibration of mechanical, civil and aerospace structures is the dynamic vibration absorbers (DVAs), also known as tuned mass dampers (TMDs). DVAs have been used to address some issues in the railway-induced vibration field such as the vibration of car-bodies of a low-floor train at a certain frequency [9], rail radiated noise [10] and growth of rail corrugation [11]. However, the application of DVAs as a countermeasure for ground-borne railway-induced vibrations has not been considered yet, being the present thesis the first study on the matter.

Thus, this dissertation is focused on the application of DVAs on the interior floor of double-deck tunnel infrastructures to mitigate ground-borne vibrations induced by the train pass-by over the upper section of the tunnel. The potential of DVAs as a vibration countermeasure for this specific case is investigated for the full- and half-space models of the soil. The full-space model is more appropriate to generally evaluate the effect of DVAs by controlling the vibration energy radiated upwards by the tunnel structure. On the other hand, the half-space model would be convenient to study the vibration mitigation for specific buildings. General methodologies for simulating and optimizing the performance of DVAs are developed. These methodologies can also be employed to evaluate the performance of DVAs in any underground railway infrastructure.

1.2 Outline of the dissertation

The dissertation is divided into six chapters. In this chapter, the motivation to do this research is explained and the contents of each chapter are outlined as well.

Chapter 2 is concerned with presenting a review on previous research works regarding prediction models for ground-borne vibrations induced by underground railways. Moreover, different methods to address railway-induced vibration problems are discussed in this chapter. In addition, an introduction to the concept of the DVAs as vibration countermeasures and their applications in different fields, specifically, in railway-induced noise and vibration field, are presented.

Chapter 3 focuses on general methodology to evaluate the efficiency of DVAs as vibration countermeasures by controlling the vibration energy radiated upwards by the tunnel structure due to the train traffic. This chapter begins with a description of a semi-analytical model of a train-track-tunnel-soil system where the locally surrounding soil is modelled as a full-space. Afterward, a methodology to couple DVAs to any subsystem of railway infrastructure and the application of this methodology for the case of a double-deck tunnel is explained. Moreover, the optimization approach used to determine the optimal parameters of DVAs is explained and the objective function used in the optimization process is defined. Finally, the efficiency of optimal DVAs as a countermeasure to minimize the energy flow radiated upwards by the tunnel is investigated.

The efficiency of DVAs in vibration control of a particular building over the double-deck tunnel in L9 of Barcelona metro is assessed in chapter 4. A hybrid model of the train-track-tunnel-soil-building system is initially described. Following the methodology for coupling DVAs to the interior floor of a double-deck tunnel and optimization process described in the previous chapter, the efficiency of the application of the optimized DVAs on the interior floor of the L9 double-deck tunnel in minimizing the maximum vibration transient (MTVV) value in a particular building is evaluated.

The potential of DVA as a vibration countermeasure for underground railway-induced ground-borne vibration problems can be also investigated considering that the model of the soil is a half-space. With this attitude, the efficiency of the DVAs on reducing the soil surface vibration or the vibration field in a building (if a building dynamic model is used on this regard) can be simulated. In this approach, an accurate and computationally efficient modeling of the wave propagation in the layered half-space is one of the key elements. A new method to calculate Green's functions for two-and-a-half dimensional (2.5D) elastodynamic problems in homogeneous and horizontally layered half-spaces subjected to point loads is presented in chapter 5.

The conclusions from this investigation are summed up in chapter 6. Some guidelines for future works are also pointed out in the same chapter.

Chapter 2

Literature review

This literature review consists of five sections. It begins with a general introduction to the ground-borne vibrations induced by underground railway traffic and its generation mechanisms. Then, a review of previous research works regarding half-space modeling strategies and the prediction models for ground-borne vibration induced by underground railways is presented. Afterward, several vibration mitigation measures proposed to address railway-induced ground-borne vibration problem are reviewed, and their advantages and drawbacks are detailed. Finally, the concept behind the DVA as a vibration mitigation measure and its applications in different fields, specifically in the framework of the underground railways, are discussed.

2.1 Railway ground-borne vibration problem

Over the past decades, underground railway networks are expanding considerably as not only they provide faster and cheaper communication means in comparison with the other type of transportation, but also they can solve the traffic congestion and air pollution issues. However, the ground-borne vibrations induced by underground railways are of great concern in modern societies. The vibrations generated due to the train pass-by in tunnels propagates through the soil into the nearby buildings as shown in Fig. 2.1. These vibrations can be directly perceived by inhabitants of the nearby buildings as vibratory motions of the building walls, ceilings, and floors which are significant in a frequency range of 1 to 80 Hz [12–14], and can make disturbances as re-radiated noise mainly in a frequency range of 16 to 250 Hz [15]. Both vibratory surfaces and re-radiated noises can negatively affect the quality of day-to-day life of the dwellers of these buildings [16], and can cause sensitive equipment malfunction [17].

There are two excitation mechanisms that mostly contribute to the vibration induced by railway traffic: i) the quasi-static excitation ii) the dynamic excitation. The former is induced by the static component of the moving loads applied by the train to the track and is of great importance for high-speed trains. The latter can be attributed to various mechanisms [18], mainly the wheel/rail unevenness and the longitudinal variability of the track's mechanical parameters. Noteworthy, the response of a building to the excitation would also depend on the characteristics of

the building and its foundation, distance from the excitation source, and geology of the area.

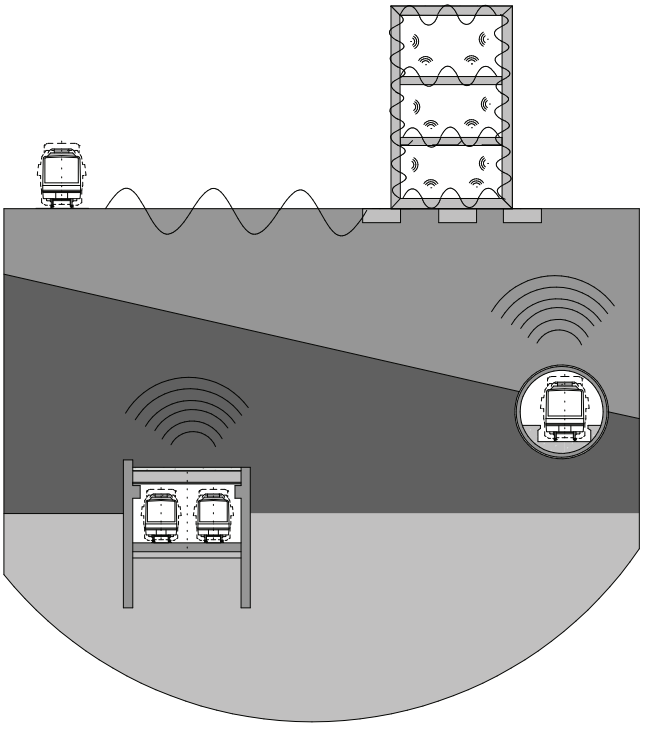

FIG. 2.1: Schematize of ground-borne vibration propagation.

2.2 Soil dynamics: Half-space modeling strategies

The propagation of elastic waves is one of the most important topics in such fields as seismology, soil dynamics, noise and vibration, and soil-structure interaction. Specifically, the fundamental solutions for homogeneous and layered elastic solid media are of great interest in ground modeling. The fundamental solutions, also known as Green's functions, of these types of problems provide the relation between stresses or displacements at the receiver-points due to the sources acting within medium. A useful domain for longitudinally invariant problems is the 2.5D domain, in where the 3D Green's functions are expressed in terms of the wavenumber associated to the invariant direction and the two remaining spatial coordinates.

Regarding to homogeneous elastic solid media modeling, a semi-analytical solution of a homogeneous half-space subjected to a spatially harmonic line load with sinusoidal varying amplitude was presented by Tadeu et al. [19]. This solution was presented subsequent to the Green's functions for 2.5D elastodynamic problem in full-space developed by Tadeu and Kausel [20]. These analytical expressions have been employed by numerous authors in various problems such as railway-induced vibration [21, 22], acoustics [23, 24] and soil-structure interaction [25]. The usefulness of the method in many engineering applications demonstrates its significant value.

Numerous researches have also focused on determining the solution for the isotropic layered media which provides better representation of the dynamic response of the soil in comparison to the homogeneous one. Some of the major studies on the subject were reviewed in details by Nayfeh [26]. Green's functions for an isotropic layered half-space have been determined by Waas et al. [27], Kausel [28] and Oliveira and Kausel [29] by employing Thin Layer Method (TLM). Van Der Hijten employed Cagniard-de Hoop method to solve differential equation of the wave motion in the layered medium in order to obtain the Green's functions [30]. The dual vector representation of the wave motion equation and the Precise Integration Method (PIM) are the other methods which have been used to calculate Green's functions for a layered half-space in wavenumber-frequency domain [31, 32]. The propagator matrix method or transfer matrix method, proposed firstly by Thomson [33] to model horizontally isotropic layered media, has been also used by several authors [34–36] to find the dynamic response of the system. Due to computational instabilities of the method, different reformulations have been presented, like reflection and transmission coefficients method [37]. A survey of the computationally efficient improvements of the method was presented by Lowe [38]. Assembling the global matrix of the system with employing the elemental stiffness matrices of the layers, known as stiffness matrix method, was presented by Kausel and Roësset [39]. More computationally efficient versions of his method have been presented later [40–42]. For longitudinally invariant problems, numerous authors obtained the 2.5D Green's functions from the stiffness matrix method of Kausel and Roësset [3, 4]. François et al. [43] used the 2.5D Green's functions in a 2.5D boundary element formulation as an alternative to the 2.5D fundamental solution of a homogeneous full-space. Hussein et al. [22] employed these 2.5D Green's functions as a part of a methodology to calculate underground railway-induced vibration from a

tunnel embedded in a layered half-space.

2.3 Railway-induced vibration prediction models

Accurate prediction models should be used to assess the efficiency of mitigation measures for railway-induced ground-borne problems. Numerical, hybrid models and semi-analytical models can provide the desired level of accuracy.

In the framework of numerical models, there are different existing modeling alternatives: a three-dimensional (3D) coupled Finite Element-Boundary Element Methods (FEM-BEM) approach [44], a 3D periodic FEM-BEM approach [45] and 2.5D approaches based on FEM-BEM [46–48], based on the Method of Fundamental Solutions (MFS) coupled with FEM [49] and based on a scaled boundary FEM coupled with FEM [50]. The 2.5D approach has been employed in most of the existing models. It considers that the track, the tunnel and the ground can be approximately treated as a longitudinally invariant structures.

Hybrid models that combine numerical methodologies with empirical models/experimental measurements can provide an increment on the accuracy with respect to conventional numerical models for specific sites [51, 52]. A higher level of confidence in predicted results is expected in hybrid models as some sources of uncertainties related to the input parameters would be addressed by the use of experimental measurements. Kouroussis et al. [53] proposed a hybrid experimental-numerical approach to enhance ground-borne vibration predictions accuracy in the presence of rail discontinuities, such as switches, crossings and rail joints. Lopez-Mendoza et al. [54] presented a model to predict ground-borne vibration levels within structures near railway lines for the cases where the free-field response due to train pass-by is known. For the existing railway lines, this model along with the in situ measurements can be used to make a hybrid prediction model. Kou et al. [55] developed two hybrid models based on separating source and propagation mechanism, where each can be quantified using in situ measurements or prediction models results.

Another alternative that stands out because of their computational benefits are the semi-analytical models. In this category, probably the most well-established

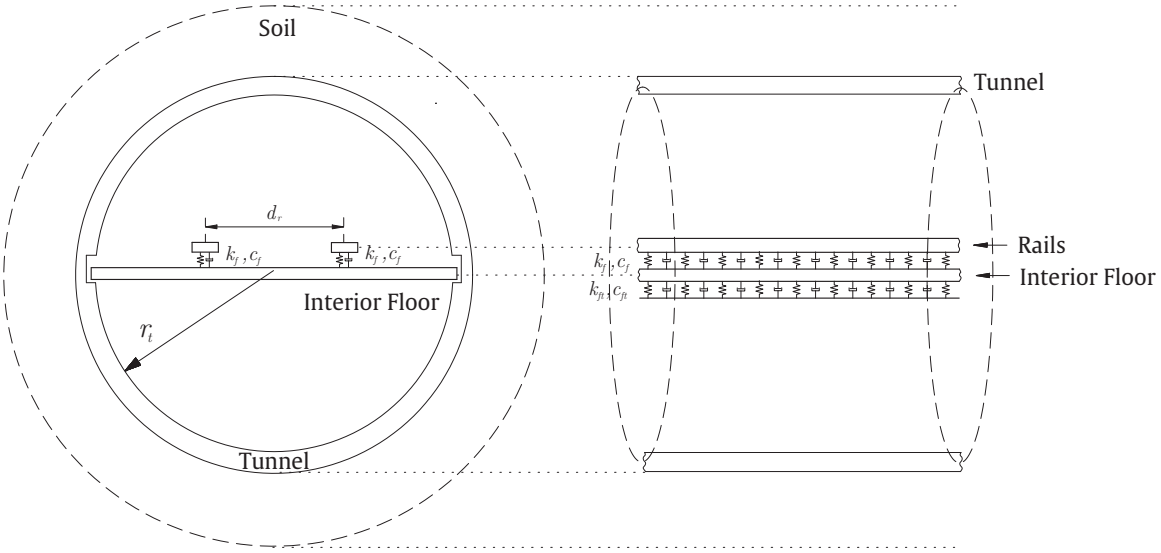

FIG. 2.2: A cross-section of a double-deck tunnel with superstructures proposed by Clot et al. [2].

models for at-grade trains and for underground railway traffic are the one presented by Sheng et al. [56] and the Pipe-in-Pipe (PiP) model [57, 58], respectively.

In the context of the double-deck tunnel, a 2.5D semi-analytical model of a double-deck tunnel embedded in a full-space presented by Clot et al. [2] is one of the few proposed models. A schematic representation of the track-tunnel-soil system used in this model is shown in Fig. 2.2. The track consist of two rails connected to the interior floor of the double-deck tunnel structure by means of direct fixation fasteners (DFF), and the tunnel is assumed to be embedded in a homogeneous full-space. The system is considered to be invariant in the longitudinal direction, i.e., the train's circulation direction. In this model, the rails are modelled as Euler-Bernoulli beams of infinite length. The DFF are represented by a continuous mass-less distribution of springs and dashpots. The interior floor is modeled as a homogeneous isotropic thin strip plate with a rectangular cross-section. The tunnel and soil subsystems are described using the PiP model, developed by Forrest and Hunt [57], which assumes that they can be represented as an infinite thin cylindrical shell and as a infinite homogeneous elastic media, respectively.

2.4 Railway-induced ground-borne vibration countermeasures

Several solutions have been proposed to address the problem of ground-borne vibration induced by railways. Targeting the mechanisms of ground-borne vibration generation in order to reduce transmitted forces by the vehicle to the track would be the most efficient approach. For instance, rail grinding [59] can be employed to eliminate the vibration caused by roughness or unevenness at the wheel-rail interface. Due to high cost of these maintenance actions, countermeasures are necessary to address railway-induced ground-borne vibration problem at a more reasonable cost. The mitigation measures can be categorized according to the location at where they are applied: i) the source; ii) the receiver and iii) the propagation path.

Mitigation measures at the source mainly target the track and its resiliency to reduce vibration transmission into the ground. An effective measure to reduce the vibration at the point of the emission is using floating-slab track (FST). Different methods have been proposed for modeling of FST with continuous and discontinuous slabs [60–62]. The efficiency of FST as a mitigation measure has been investigated using different methods [63, 64]. The FSTs are efficient in reducing the vibration at the frequencies above its resonance frequency [65]. The insertion of resilient materials beneath the ballast and sub-ballast is another commonly used countermeasure for ballasted tracks. The efficiency of ballast mats and under-ballast mats depend on the range of the frequencies which are intended to be isolated [66]. Other source isolation measures include under-sleeper pads [67] and soft railpads [68]. However, one should note that introducing resilient elements on the track to modify its stiffness, aiming vibration attenuation at high frequencies, may amplify the vibration level at low frequencies [69].

Damping treatments, localized stiffening or mass addition are some mitigation measures at receivers, i.e. buildings, that can be used to reduce the post-construction vibration. The base isolation, which is based on the installation of resilient elements like rubber blocks or steel springs between the building and its foundation, is another effective method to reduce the transmission of vibration into buildings. However, this countermeasure would be cost effective if it is incorporated during

the design phase [69]. A review of different methods employed to predict base isolation performance was discussed by Talbot and Hunt [70]. The difference between pre- and post-construction vibration levels need to be considered in assessment of base isolation performance [71]. The box-in-box technique is another method to mitigate the vibration at the receiver. In this method, a particular part of the building is mounted on isolation bearings to isolate it from the rest of the building [72]. The efficiency of a FST, base isolation and box-in-box arrangement in mitigating subway traffic induced ground-borne noise and vibration in buildings have been compared by Fiala et al., and it has been found that the former is the most effective mechanism [73].

The countermeasures applied at the propagation path are all based on the same idea of interrupting the propagation of waves through the soil. Wave-impeding blocks (WIP) [74], subgrade stiffening [75] and wave barriers [76] are the most common mitigation measures in the category. The latter category includes vibration isolation screens [77], open/in-filled trenches [78] and rows of piles [79]. These countermeasures are more effective for reducing ground-borne vibrations due to trains running at-grade rather than in the underground tunnels.

In the framework of the double-deck tunnels, only a few studies have been reported on measures to mitigate ground-borne vibration. Modification of the rail pads stiffness/damping values and implementation of an elastomeric mat between the interior floor and the tunnel structure are two mitigation measures studied by Clot et al. [7]. In their work, a 2.5D semi-analytical model of a double-deck tunnel, previously developed by the authors in [2], was used to investigate the effectiveness of a elastomeric mat to be added between the interior floor and the tunnel wall in reducing the upwards radiated energy flow from a double-deck tunnel subjected to a moving harmonic load [80]. It is found out that while in the absence of the vehicle, the modification of the rail pads stiffness/damping values cannot be completely understood, implementation of the elastomeric mat would be an effective countermeasure. Recently, Clot et al. [8] computed the response of the previously developed models to a train pass in order to study the efficiency of the implementation of an elastomeric mat in more real scenario. It was found that implementing a soft elastomeric mat results in a considerable reduction of the soil vibration velocity.

2.5 Dynamic vibration absorbers

A well-established system that has been widely used to control the vibration of mechanical, civil and aerospace structures is the DVA. In the last century, the application of DVAs as passive, active and semi-active countermeasures to attenuate undesirable vibration has been extensively studied [81, 82]. Some of the prominent application of DVAs around the globe are the ones in Taipei World Financial Center (also known as Taipei 101) [83], Millennium bridge [84] and Doha sport city tower[85]. DVA works as a secondary oscillatory system applied on a primary system at where the vibration needs to be controlled. DVAs are usually modelled as a single-degree-of-freedom (SDOF). The concept of a DVA was outlined by Watts in 1883 [86]. However, the practical design of DVA, as a spring-supported mass, was proposed by Frahm in 1911 [87]. Later, a damping element were introduced to DVAs to widen the controlled frequency range [88]. DVAs can be used to attenuate the vibration at a specific frequency or over a particular range of frequencies. In the former case, the natural frequency of the DVA should be tuned to the specific frequency, and the damping should be chosen as low as possible [89]. In the latter case, in which the host structure is considered as a SDOF system with the parameters of the selected mode, an optimization criterion is required. Optimum selection of the parameters of a DVA (mass, natural frequency and damping coefficient) has been investigated in many studies [88, 90–94] as the effectiveness of a DVA in vibration attenuation depends on its parameters.

Recently, DVAs have been used to address some issues in railway-induced vibration field. A study on the effectiveness of DVAs in suppressing the low-frequency vibrations of FST with discontinuous slabs was conducted by Zhu et al. [95] using a FEM model. They used two DVAs to minimize first- and second-mode vibrations of a slab which was treated as a SDOF system with the parameters of the selected mode, and the optimal parameters of DVAs were found using fixed-point theory [96]. Reducing the vibration of car-bodies of a low-floor train at certain frequency by means of a DVA was investigated by Wang et al. [9], in which DVA was found to be an effective countermeasure for excessive vertical vibration of car-bodies. TMDs have been also found to be effective in reducing the rail radiated noise. Thompson et al. [10] designed TMDs of steel masses and elastomeric material with high damping loss factor, placed at both sides of the rail. The system of absorbers results in reduction of radiated noise by about 5–6 dB. These TMDs

were reported to be effective in decreasing rail corrugation growth if they can fully suppress the pinnedpinned resonance [11]. Ho et al. developed multiple TMDs each consisting of a mass sandwiched between resilient materials [97]. This multiple mass–spring system has been put into practice and the system is found to be effective not only in attenuating rail vibration and tunnel noise level [97] but also in decreasing rail corrugation growth [98].

DVA parameters are crucial factors in their performance as a vibration mitigation measure. Several types of optimization procedures with analytical or numerical approaches can be considered to determine the optimal value of DVAs parameters. A complete review of some of the well-established theories for optimal tuning of DVAs can be found in [81]. Typically, the host structure is referred to the structure on which the DVAs are applied. Most of the analytical optimization procedures employed to find optimal value of DVAs parameters consider a SDOF system as the model of the host structure [93]. In these methodologies, the parameters of this SDOF model are obtained from the dominant mode of the host structure response. However, there are other optimization procedures in which there is no need to determine beforehand which mode is needed to be controlled. Among those, genetic algorithms (GA) have been widely used for tuning DVAs parameters in order to accomplish an optimal reduction of the vibration in specific locations of the system or in a global point of view. Some of the studies that apply GA for this purpose are [93, 99–102].

Chapter 3

Control of vibration energy flow radiated upwards from double-deck tunnels by means of DVAs

3.1 Introduction

The aim of this chapter is to investigate the efficiency of DVAs as a vibration abatement solution for railway-induced vibrations in the framework of a double-deck circular railway tunnel infrastructure. A previously developed semi-analytical model of the track-tunnel-ground system is employed to calculate the energy flow resulting from a train pass-by. A methodology for the coupling of a set of longitudinal distributions of DVAs over a railway system is presented as a general approach, as well as its specific application for the case of the double-deck tunnel model. In the basis of this model, a Genetic Algorithm (GA) is used to obtain the optimal parameters of the DVAs to minimize the vibration energy flow radiated upwards by the tunnel. The parameters of the DVAs set to be optimized are the natural frequency, the viscous damping and their positions. The results show that the DVAs would be an effective countermeasure to address railway induced ground-borne vibration as the total energy flow radiated upwards from the tunnel can be reduced by an amount between 5.3 and 6.6 dB with optimized DVAs depending on the type of the soil and the train speed.

The rest of the chapter is organized as follows: In section 3.2, the vehicle-track-tunnel-soil model is described; section 3.3 is dedicated to details regarding the coupling of DVAs to an underground railway infrastructure model. The optimization method to determine the optimal parameters of the DVAs to minimize energy flow radiated upwards for the case of an underground double-deck tunnel railway infrastructure is presented in section 3.4. The efficiency of a set of DVAs as a vibration countermeasure applied to the specific case studies to minimize the radiated energy flow is discussed in section 3.5.

3.2 Modeling of the vehicle-track-tunnel-soil system

This section starts by recapitulating the considered 2.5D semi-analytical model of a double-deck tunnel embedded in a full-space [2]. This model provides the 2.5D Green's functions of the system due to loads applied on the rails and on the interior floor, which are required to couple the train and the DVAs to the system and to compute the train pass-by response. Then, the considered train-track interaction

model is described, followed by an explanation of how this model is employed to determine the response of the system due to a train pass-by.

3.2.1 Track-tunnel-soil model

A scheme of the model considered for the track-tunnel-soil system is shown in Fig. 3.1. The track consists of two rails connected to the interior floor of the double-deck tunnel structure by means of direct fixation fasteners, and the tunnel is assumed to be embedded in a homogeneous full-space. The system is considered to be invariant in the longitudinal direction, i.e., the direction in which the train circulates.

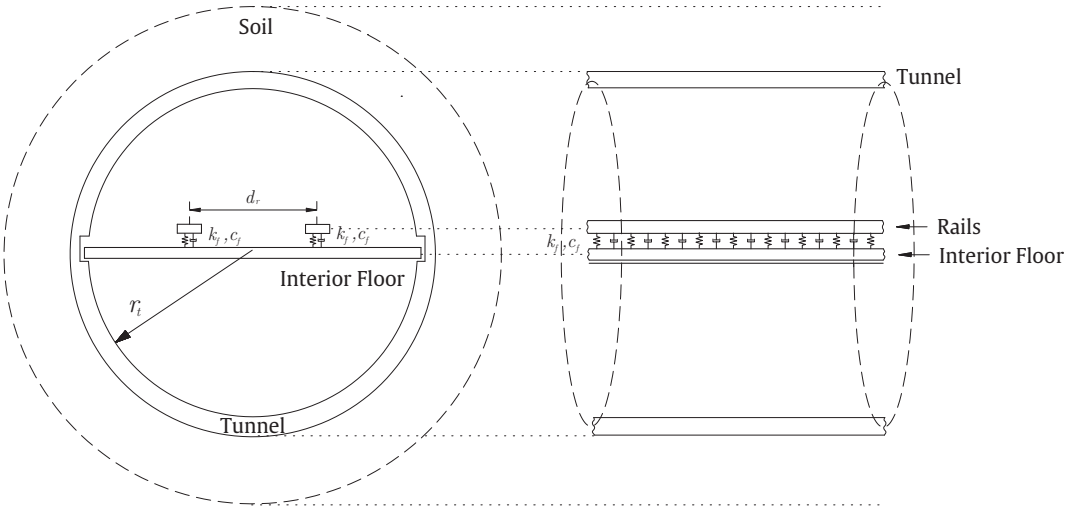

FIG. 3.1: A scheme of a double-deck tunnel and its subsystems embedded in a full-space.

The rails are modeled as Euler-Bernoulli beams of infinite length separated by a distance d_r. The DFF are represented by a continuous mass-less distribution of springs, with a stiffness per unit length k_f, and dashpots, with a viscous damping per meter c_f. The interior floor is modeled as a homogeneous isotropic thin strip plate with a rectangular cross-section. The tunnel and soil subsystems are described using the PiP model, developed by Forrest and Hunt [57], which assumes that they can be represented as an infinite thin cylindrical shell and as an infinite homogeneous elastic medium, respectively.

3.2.2 Vehicle-track coupling

There are two excitation mechanisms that mostly contribute to the vibration induced by railway traffic: i) the quasi-static excitation ii) the dynamic excitation. The former is induced by the static component of the moving loads applied by the train to the track and is of great importance for high-speed trains. The latter can be attributed to various mechanisms [18], mainly the wheel/rail unevenness and the longitudinal variability of the track's mechanical parameters. Since the present investigation is done in the context of urban railway infrastructure, the vertical dynamic excitation caused by the rail unevenness is considered as the main excitation source. It is assumed that the unevenness of the rails is uncorrelated between them [103].

Consider a moving frame of reference associated to a train motion. Due to the Doppler effect, the frequency components of the time signals seen from the perspective of this moving frame of reference ($\tilde{\omega}$) are different from the ones related to a fixed frame of reference (ω) [104]. All the derivation presented in this section is based on the moving coordinate system, thus, all the variables represented in the frequency domain are associated to the frequency $\tilde{\omega}$, except when it is specifically mentioned otherwise. Capital letters notation is used to denote variable in the frequency domain.

The vertical displacements of the two rails in the frequency domain due to the wheel/rail contact forces can be represented by

$$\begin{Bmatrix} \mathbf{Z}_{r_1}^{w/r} \\ \mathbf{Z}_{r_2}^{w/r} \end{Bmatrix} = \begin{Bmatrix} \mathbf{H}_{r_1r_1}^{w/r} & \mathbf{H}_{r_1r_2}^{w/r} \\ \mathbf{H}_{r_2r_1}^{w/r} & \mathbf{H}_{r_2r_2}^{w/r} \end{Bmatrix} \begin{Bmatrix} \mathbf{F}_{r_1}^{w/r} \\ \mathbf{F}_{r_2}^{w/r} \end{Bmatrix}, \tag{3.1}$$

where $\mathbf{Z}_{r_1}^{w/r}$ and $\mathbf{Z}_{r_2}^{w/r}$ are the vertical displacements of the left and right rails, respectively, at all the vehicle axle positions, $\mathbf{H}_{r_1r_1}^{w/r}$ and $\mathbf{H}_{r_2r_2}^{w/r}$ are the direct receptance matrices of the left and right rails, respectively, at all the axles positions, $\mathbf{H}_{r_2r_1}^{w/r} = \mathbf{H}_{r_1r_2}^{w/r}$ is the cross receptance matrix between the left and right rails at all axle positions, $\mathbf{F}_{r_1}^{w/r}$ and $\mathbf{F}_{r_2}^{w/r}$ are the vectors of wheel/rail interaction forces associated to the left and right rails, respectively; and the response of the two half

vehicles can be written by

$$\begin{Bmatrix} \mathbf{Z}_{v_1}^{w/r} \\ \mathbf{Z}_{v_2}^{w/r} \end{Bmatrix} = - \begin{Bmatrix} \mathbf{H}_{v_1}^{w/r} & 0 \\ 0 & \mathbf{H}_{v_2}^{w/r} \end{Bmatrix} \begin{Bmatrix} \mathbf{F}_{r_1}^{w/r} \\ \mathbf{F}_{r_2}^{w/r} \end{Bmatrix}, \tag{3.2}$$

where $\mathbf{Z}_{v_1}^{w/r}$ and $\mathbf{Z}_{v_2}^{w/r}$ are the vertical displacements of vehicle wheels in contact with the left and right rails, respectively, and $\mathbf{H}_{v_1}^{w/r}$ and $\mathbf{H}_{v_2}^{w/r}$ are the receptances of each half vehicle at all the vehicle axle positions. Eqs. (3.1) and (3.2) can easily be compacted to

$$\mathbf{Z}_r^{w/r} = \mathbf{H}_r^{w/r}\mathbf{F}^{w/r}, \qquad \mathbf{Z}_v^{w/r} = -\mathbf{H}_v^{w/r}\mathbf{F}^{w/r}. \tag{3.3}$$

Consider now that the 2.5D Green's functions associated to the studied railway infrastructure system are obtained on the basis of a double Fourier transform (FT) defined by

$$\bar{G}(k_x, \omega) = \int_{-\infty}^{+\infty} \int_{-\infty}^{+\infty} g(x,t) \mathrm{e}^{\mathrm{i}(k_x x - \omega t)} \mathrm{d}x \mathrm{d}t. \tag{3.4}$$

where x, t, k_x and ω represent the longitudinal coordinate, the time, the wavenumber associated to the longitudinal coordinate and the frequency seen from a fixed frame of reference, respectively. Combined bar and capital letters notation is used to denote variables in the wavenumber-frequency domain on a fixed frame of reference. Taking this into account, the elements of the receptance matrices required to construct $\mathbf{H}_r^{w/r}$ can be computed by

$$H_{r_i r_j, nm}^{w/r} = \frac{1}{2\pi} \int_{-\infty}^{+\infty} \tilde{H}_{r_i r_j} \mathrm{e}^{-\mathrm{i}k_x(\tilde{x}_n - \tilde{x}_m)} \mathrm{d}k_x, \tag{3.5}$$

where $H_{r_i r_j, nm}^{w/r}$ is the (n, m) element of the matrix $\mathbf{H}_{r_i r_j}^{w/r}$, $\tilde{x}_n$ and $\tilde{x}_m$ are the longitudinal coordinates of the n-th and m-th axles, respectively, seen from the point of view of the moving frame of reference, and $\tilde{H}_{r_i r_j}$ is the 2.5D Green's function of the system defined in the $(k_x, \tilde{\omega})$ domain that relates the vertical motions of the rails r_i and r_j. A 2.5D Green's function defined in the $(k_x, \tilde{\omega})$ domain can be obtained from the one defined in the (k_x, ω) domain by $\tilde{H}(k_x, \tilde{\omega}) = \bar{H}(k_x, \tilde{\omega} + k_x v_t)$, being v_t the speed of the train. Note that combined $\sim$ and capital letters notation is used to denote variables in the wavenumber-frequency domain on a moving frame of reference. The vehicle receptance matrix is obtained by means of the dynamic model of the vehicle, which in this investigation is considered to be the

two-dimensional (2D) multi-degree-of-freedom rigid body model presented by Lei and Noda [105]. A 3D model of each car consists of two uncoupled 2D models separately applied on each rail. A global train is modeled as a set of N_c identical cars.

Assuming a linearized Hertz contact, the wheel/rail interaction forces can be obtained in the frequency domain by using

$$\mathbf{F}^{w/r} = k_H \left(\mathbf{Z}_v^{w/r} - \mathbf{Z}_r^{w/r} + \mathbf{E}_r \right), \tag{3.6}$$

where k_H is the stiffness of the linearized Hertzian spring, considered to be the same in all the wheel/rail contacts, and $\mathbf{E}_r$ is the vector of complex amplitudes of rails unevenness at all the wheel/rail contacts. Combining Eq. (3.6) with Eq. (3.3) one can obtain a transfer function in the frequency domain between the unevenness of the rails and the dynamic wheel/rail interaction forces, which may be written as

$$\mathbf{F}^{w/r} = \left(\mathbf{H}_v^{w/r} + \mathbf{H}_r^{w/r} + k_H^{-1}\mathbf{I} \right)^{-1} \mathbf{E}_r, \tag{3.7}$$

where $\mathbf{I}$ is the identity matrix.

Once the wheel/rail interaction forces are computed, the response at an arbitrary position l of the railway infrastructure system due to the passage of the train can be found using the expression

$$u_l(\tilde{x}, t) = \sum_{i=1}^{2} \frac{1}{2\pi} \int_{-\infty}^{+\infty} \sum_{n=1}^{N_a} \left[\frac{1}{2\pi} \int_{-\infty}^{+\infty} \tilde{H}_{lr_i} F_{r_i,n}^{w/r} \mathrm{e}^{-\mathrm{i}k_x(\tilde{x}-\tilde{x}_n)} \mathrm{d}k_x \right] \mathrm{e}^{\mathrm{i}\tilde{\omega}t} \mathrm{d}\tilde{\omega}, \tag{3.8}$$

where $u_l(\tilde{x}, t)$ is the displacement response at l position of the railway infrastructure system, $\tilde{H}_{lr_i}$ is the 2.5D Green's function in the wavenumber-frequency domain that relates the displacement response at that arbitrary position l with a force applied in the i-th rail, $\tilde{x}$ is the longitudinal coordinate associated to the moving frame of reference, N_a is the number of axles of the train and $F_{r_i,n}^{w/r}$ is the wheel/rail interaction force associated to the i-th rail and the n-th axle. An equivalent expression for the soil tractions can be obtained by simply replacing the displacement Green's functions with those for the tractions in Eq. (3.8). The

expression of the soil vibration velocity can be written similarly to Eq. (3.8) as

$$v_l(\tilde{x},t)=\sum_{i=1}^{2}\frac{1}{2\pi}\int_{-\infty}^{+\infty}\sum_{n=1}^{N_a}\left[\frac{1}{2\pi}\int_{-\infty}^{+\infty}\mathrm{i}(\tilde{\omega}+k_x v_t)\tilde{H}_{lr_i}F_{r_i,n}^{w/r}\mathrm{e}^{-\mathrm{i}k_x(\tilde{x}-\tilde{x}_n)}\mathrm{d}k_x\right]\mathrm{e}^{\mathrm{i}\tilde{\omega}t}\mathrm{d}\tilde{\omega}, \tag{3.9}$$

3.3 Application of DVAs on an underground railway system

This section starts with the explanation of a methodology which can be used to couple a set of DVAs to any subsystem of a railway infrastructure. Then, the application of this methodology for the case of the double-deck tunnel is explained.

DVAs can be applied on different subsystems of a railway infrastructure, such as the tunnel or the track. For example, Fig. 3.2 shows a cross-section of a track with one longitudinal distribution of DVAs. Consider M longitudinal distributions of DVAs, where each distribution has N_m DVAs, being $m=1,2,\ldots,M$. The total amount of DVAs, then, is $\sum_{m=1}^{M}N_m$. In the following the n-th DVA of the m-th distribution is represented by d_{mn}.

FIG. 3.2: A track system with one longitudinal distribution of DVAs.

Considering each DVA as a SDOF system, as shown in Fig. 3.3, the equation of motion of the n-th DVA of the m-th distribution can be written as

$$-c_{d_{mn}}\left(\dot{z}_{d_{mn}}^{c}-\dot{z}_{d_{mn}}\right)-k_{d_{mn}}\left(z_{d_{mn}}^{c}-z_{d_{mn}}\right)=m_{d_{mn}}\ddot{z}_{d_{mn}}, \tag{3.10}$$

where $z_{d_{mn}}^{c}$ and $z_{d_{mn}}$ are the displacement of the DVA and the displacement of the system at the position of the DVA, respectively, in a direction perpendicular to the surface on which DVAs are applied. $m_{d_{mn}}$, $k_{d_{mn}}$ and $c_{d_{mn}}$ are the mass, stiffness and viscous damping coefficient of d_{mn}.

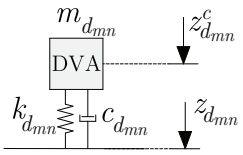

FIG. 3.3: DVAs modeled as a SDOF.

Using a FT, the equation of motion can be transformed to the frequency domain

$$-\omega^2 m_{d_{mn}} Z_{d_{mn}} + \mathrm{i}\omega c_{d_{mn}} \left(Z^c_{d_{mn}} - Z_{d_{mn}}\right) + k_{d_{mn}} \left(Z^c_{d_{mn}} - Z_{d_{mn}}\right) = 0. \tag{3.11}$$

Then, assuming that all DVAs of the m-th distribution have the same mass m_{d_m}, stiffness k_{d_m} and damping coefficient c_{d_m}, the relation between the displacement of the DVA $Z^c_{d_{mn}}$ and the displacement of the system at the position of the DVA $Z_{d_{mn}}$ can be found as

$$Z^c_{d_{mn}} = \frac{k_{d_m} + \mathrm{i}\omega c_{d_m}}{-m_{d_m}\omega^2 + k_{d_m} + \mathrm{i}\omega c_{d_m}} Z_{d_{mn}}. \tag{3.12}$$

The forces applied to the system due to the DVAs of the m-th distribution can be written as

$$f_{d_m}(x,t) = \sum_{n=1}^{N_m} \left(k_{d_m} + c_{d_m}\frac{\partial}{\partial t}\right) \delta(x - x_{d_{mn}}) \left(z^c_{d_{mn}} - z_{d_{mn}}\right), \tag{3.13}$$

where $x_{d_{mn}}$ is the position of d_{mn} in the longitudinal direction. These forces can be transformed to the wavenumber-frequency domain using Eq. (3.4), resulting in

$$\bar{F}_{d_m}(k_x,\omega) = \sum_{n=1}^{N_m} \left(k_{d_m} + \mathrm{i}\omega c_{d_m}\right) \mathrm{e}^{\mathrm{i}k_x x_{d_{mn}}} \left(Z^c_{d_{mn}} - Z_{d_{mn}}\right). \tag{3.14}$$

Finally, by introducing Eq. (3.12) into Eq. (3.14), the forces applied to the interior floor by the DVAs can be rewritten as

$$\bar{F}_{d_m}(k_x,\omega) = \sum_{n=1}^{N_m} k^*_{d_m} \mathrm{e}^{\mathrm{i}k_x x_{d_{mn}}} Z_{d_{mn}}, \tag{3.15}$$

where

$$k^*_{d_m} = \frac{\omega^2 m_{d_m}(k_{d_m} + \mathrm{i}\omega c_{d_m})}{-\omega^2 m_{d_m} + \mathrm{i}\omega c_{d_m} + k_{d_m}}. \tag{3.16}$$

Therefore, the forces applied to the system by all M distributions of DVAs can be written in matrix form as

$$\bar{\mathbf{F}}_d = \mathbf{\Gamma}_d \mathbf{K}_d^* \mathbf{Z}_d, \tag{3.17}$$

where

$$\bar{\mathbf{F}}_d = \begin{Bmatrix} \bar{F}_{d_1} \\ \bar{F}_{d_2} \\ \vdots \\ \bar{F}_{d_m} \\ \vdots \\ \bar{F}_{d_M} \end{Bmatrix}, \qquad \mathbf{Z}_d = \begin{Bmatrix} \mathbf{Z}_{d_1} \\ \mathbf{Z}_{d_2} \\ \vdots \\ \mathbf{Z}_{d_m} \\ \vdots \\ \mathbf{Z}_{d_M} \end{Bmatrix}, \tag{3.18}$$

where $\mathbf{Z}_{d_m}$ is a vector which contains the displacements of the system at the positions of all the DVAs of the m-th distribution. The other matrices are defined as

$$\mathbf{K}_d^* = \begin{bmatrix} \mathbf{K}_{d_1}^* & & & & & \\ & \mathbf{K}_{d_2}^* & & & & \\ & & \ddots & & & \\ & & & \mathbf{K}_{d_m}^* & & \\ & & & & \ddots & \\ & & & & & \mathbf{K}_{d_M}^* \end{bmatrix}, \tag{3.19}$$

where $\mathbf{K}_{d_m}^*$ is a $N_m \times N_m$ matrix defined by $k_{d_m}^* \mathbf{I}$; and

$$\mathbf{\Gamma}_d = \begin{bmatrix} \mathbf{\Gamma}_{d_1} & & & & & \\ & \mathbf{\Gamma}_{d_2} & & & & \\ & & \ddots & & & \\ & & & \mathbf{\Gamma}_{d_m} & & \\ & & & & \ddots & \\ & & & & & \mathbf{\Gamma}_{d_M} \end{bmatrix}, \tag{3.20}$$

where

$$\mathbf{\Gamma}_{d_m} = \left\{ \mathrm{e}^{\mathrm{i}k_x x_{d_{m1}}} \quad \mathrm{e}^{\mathrm{i}k_x x_{d_{m2}}} \quad \cdots \quad \mathrm{e}^{\mathrm{i}k_x x_{d_{mN_m}}} \right\}. \tag{3.21}$$

In the following, it is assumed that the force is applied only on one of the rails. For the case of the two forces applied on the two rails, linear superposition can be held. Moreover, the following derivation is based on the moving frame of reference,

as explained in section 3.2.All the variables represented in the frequency domain in this section are thus associated to the frequency $\tilde{\omega}$. The system's response at the position of the DVAs can be obtained from

$$\tilde{\mathbf{Z}}_d = \tilde{\mathbf{H}}_{dr}\tilde{F}_r + \tilde{\mathbf{H}}_{dd}\tilde{\mathbf{F}}_d, \tag{3.22}$$

where $\tilde{\mathbf{H}}_{dr}$ refers to the 2.5D Green's function for the displacement of the system at the DVAs positions due to a force on the rail seen in the moving frame of reference in the absence of the DVAs; $\tilde{F}_r$ is a force applied on the rails in the moving frame of reference; and $\tilde{\mathbf{H}}_{dd}$ refers to the 2.5D Green's function for displacements of the system at the DVAs positions due to a force applied on the DVAs positions. Replacing $\tilde{\mathbf{F}}_d$ with its equivalent from Eq. (3.17), Eq. (3.22) can be rewritten in the form of 2.5D Green's functions as

$$\tilde{\mathbf{H}}^d_{dr} = \tilde{\mathbf{H}}_{dr} + \tilde{\mathbf{H}}_{dd}\boldsymbol{\Gamma}_d\tilde{\mathbf{K}}^*_d\mathbf{H}^d_{dr}, \tag{3.23}$$

where $\tilde{\mathbf{H}}^d_{dr}$ is the 2.5D Green's function that relates the displacement in the DVAs positions with a force in the rails seen in the moving frame of reference in the presence of the DVAs and $\mathbf{H}^d_{dr}$ is its inverse FT over the defined wavenumber by using the same structure as $\mathbf{Z}_d$ in Eq. (3.18). Transforming Eq. (3.23) to the space-frequency domain by applying an inverse FT over the wavenumber and evaluating the transformed equation at the positions of the DVAs one can obtain the expression

$$\mathbf{H}^d_{dr} = \mathbf{H}_{dr} + \mathbf{H}_{dd}\mathbf{K}^*_d\mathbf{H}^d_{dr}, \tag{3.24}$$

where

$$\mathbf{H}_{dr} = \begin{Bmatrix} \mathbf{H}_{d_1 r} \\ \mathbf{H}_{d_2 r} \\ \vdots \\ \mathbf{H}_{d_m r} \\ \vdots \\ \mathbf{H}_{d_M r} \end{Bmatrix}, \tag{3.25}$$

being $\mathbf{H}_{d_m r}$ the receptances of the system at the DVAs positions of m-th distribution due to the force applied on one of the rails, defined as

$$\mathbf{H}_{d_m r} = \frac{1}{v_t}\bar{\mathbf{H}}_{d_m r}\boldsymbol{\Gamma}^{\mathrm{T}}_{d_m}, \tag{3.26}$$

and where

$$\mathbf{H}_{dd} = \begin{bmatrix} \mathbf{H}_{d_1d_1} & \mathbf{H}_{d_1d_2} & \cdots & \mathbf{H}_{d_1d_p} & \cdots & \mathbf{H}_{d_1d_M} \\ \mathbf{H}_{d_2d_1} & \mathbf{H}_{d_2d_2} & \cdots & \mathbf{H}_{d_2d_p} & \cdots & \mathbf{H}_{d_2d_M} \\ \vdots & \vdots & \ddots & \vdots & \ddots & \vdots \\ \mathbf{H}_{d_md_1} & \mathbf{H}_{d_md_2} & \cdots & \mathbf{H}_{d_md_p} & \cdots & \mathbf{H}_{d_md_M} \\ \vdots & \vdots & \ddots & \vdots & \ddots & \vdots \\ \mathbf{H}_{d_Md_1} & \mathbf{H}_{d_Md_2} & \cdots & \mathbf{H}_{d_Md_p} & \cdots & \mathbf{H}_{d_Md_M} \end{bmatrix}, \tag{3.27}$$

being $\mathbf{H}_{d_md_p}$ a $N_m \times N_p$ matrix which contains receptance matrices of the system at the DVAs positions of the m-th distribution due to the forces applied on the system at the DVAs positions of the p-th distribution. Each element of these matrices can be determined by

$$H_{d_md_p,jq} = \frac{1}{2\pi}\int_{-\infty}^{+\infty} \tilde{H}_{d_md_p,jq} \mathrm{e}^{\mathrm{i}k_x(x^j_{d_m} - x^q_{d_p})} \mathrm{d}k_x, \tag{3.28}$$

$$j = 1, 2, \ldots, N_m, \quad q = 1, 2, \ldots, N_p,$$

where $x^j_{d_m}$ is the position of j-th DVA in the m-th distribution in the longitudinal direction, and $x^q_{d_p}$ is the position of q-th DVA in the p-th distribution in the longitudinal direction.

Finally, operating Eq. (3.24), the receptance of the system at the DVAs positions in the presence of the DVAs can be obtained as

$$\mathbf{H}^d_{dr} = \left(\mathbf{I} - \mathbf{H}_{dd}\mathbf{K}_d\right)^{-1}\mathbf{H}_{dr}. \tag{3.29}$$

Having these receptances, one can obtain the 2.5D Green's functions of the system at any arbitrary position l due to the force applied at the rail in the presence of the DVAs as

$$\tilde{\mathbf{H}}^d_{lr} = \tilde{\mathbf{H}}_{lr} + \tilde{\mathbf{H}}_{ld}\mathbf{\Gamma}_d\tilde{\mathbf{K}}^*_d\mathbf{H}^d_{dr}. \tag{3.30}$$

where the $\tilde{\mathbf{H}}_{lr}$ refers to the 2.5D Green's function of the system in the absence of the DVAs. It is noteworthy that this methodology considers a strong coupling approach, in which the DVAs affect the response of the rails.

In this chapter, the application of the DVAs is studied in the context of a double-deck tunnel. Using the process explained previously, M longitudinal distribution

of DVAs can be coupled to the interior floor of this type of tunnels. Fig. 3.4 shows a cross-section of the double-deck tunnel model with one longitudinal distribution of DVAs, which is the model that will be used in the following sections.

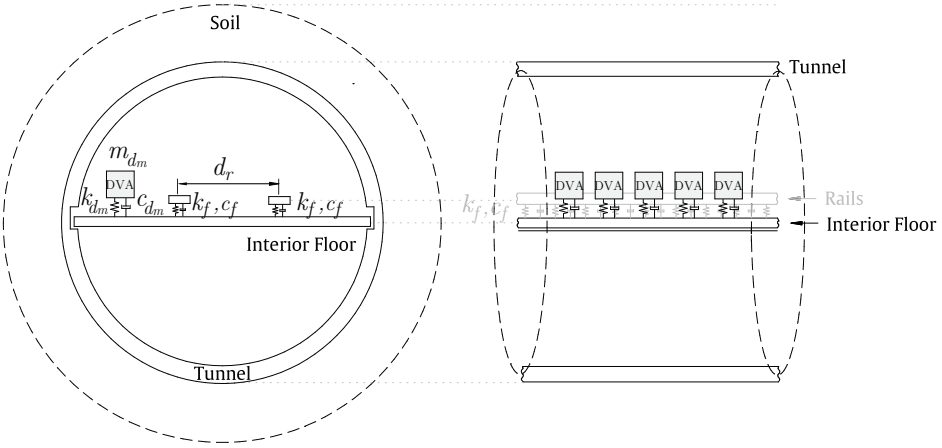

FIG. 3.4: The track-tunnel-soil model in full-space with one distribution of DVAs.

3.4 DVAs optimization approach

A global optimization approach based on GA is used in this chapter to obtain the optimum parameters of DVAs as countermeasures for underground railway-induced ground-borne vibration. Design variables that affect the performance of DVAs are: number of DVAs distributions, position of DVAs distributions, number of DVAs in each distribution, distance between two consecutive DVAs in each distribution, DVAs masses, DVAs natural frequencies and DVAs damping coefficients. In the optimization process, the effectiveness of DVAs is assessed by their performance in minimizing energy flow radiated upwards.

The mean power flow radiated upwards from a tunnel towards nearby buildings was proposed by Hussein and Hunt [106] as a criterion to evaluate the performance of vibration countermeasures. Studies of power flow and energy flow that radiate upwards from a double-deck tunnel are presented by Clot et al. [5] and [80], respectively. The radiated energy flow is the one used in this study to assess the efficiency of DVAs and, in the following, it is explained how to compute it.

For a double-deck tunnel, the vibration energy radiating upwards through a cylindrical strip (shown in Fig. 3.5) at any arbitrary cross section x_e due to the passage

of the train can be determined by integrating the power flow that crosses through the cylindrical strip as

$$E = r_m \, \Delta \mathrm{x} \int_{\theta_1}^{\theta_2} \int_{-\infty}^{+\infty} \mathbf{v}(x_e, \theta, t) \cdot \boldsymbol{\tau}(x_e, \theta, t) \mathrm{d}t \mathrm{d}\theta, \tag{3.31}$$

where $\mathbf{v}$ and $\boldsymbol{\tau}$ are the soil vibration velocity and tractions, respectively, at the strip due to the train pass-by. Tractions here refer to the stresses projected to the cylindrical strip surface.

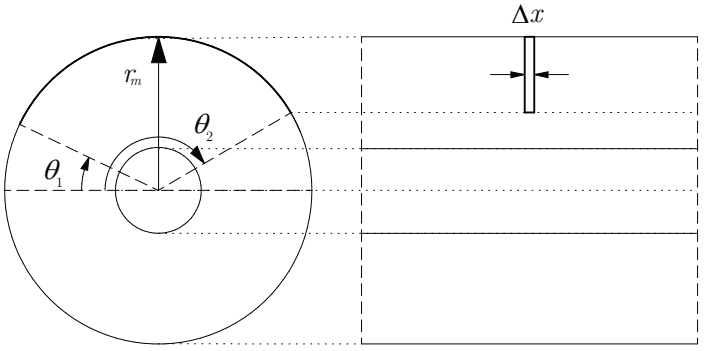

FIG. 3.5: A finite cylindrical strip through which the radiated energy flow is calculated.

To assess the performance of the DVAs by using the energy flow criterion, it is necessary to compute the vibration energy radiating upwards for the cases in which the DVAs are applied to the system and in which they are not. For the case without DVAs, the displacement and traction Green's functions that relates the response on the soil at the cylindrical strip due to a force applied on the i-th rail can be obtained using the model explained in subsection 3.2.1. These Green's functions can be used to obtain the response on the soil at the cylindrical strip due a train pass-by by applying the formulation presented in subsection 3.2.2 and, finally, to obtain the energy flow radiated upwards by the tunnel using Eq. (3.31). For the case in which the DVAs are coupled to the tunnel's interior floor, the same procedure can be followed using the Green's functions that accounts for the DVAs application, which can be found by following section 3.3.

3.5 Application and results

In this section, the efficiency of the application of the optimized DVAs on the interior floor of the double-deck tunnel in minimizing the energy flow radiated upwards by the tunnel is investigated. The considered mechanical properties for the different subsystems are described first in subsection 3.5.1. Then, in subsection 3.5.2, it is explained how the required Green's function have been computed, concerning the position of the receivers, possible position of DVAs and the wavenumber-frequency sampling. The train pass-by response is computed in subsection 3.5.3. In subsection 3.5.4, optimized parameters of DVAs to minimize energy flow radiated upwards are computed by using the previously explained optimization procedure explained previously, and the effects of the optimized DVAs are discussed.

3.5.1 Parameters used to model subsystems

Two types of soil are considered, soft soil and hard soil. Their mechanical parameters are summarized in Table 3.1. The mechanical and geometric parameters of the tunnel and the interior floor can be found in Tables 3.2 and 3.3, respectively. Typical values of reinforced concrete are used to model the tunnel and the interior floor.

TABLE 3.1: Mechanical parameters used to model the soil.

Soil parameters	Values for soft soil	Values for hard soil
Young modulus (MPa)	15	550
Density (kg m^{-3})	1600	2000
Poisson ratio (-)	0.49	0.3
P-wave damping ratio (-)	0.05	0.03
S-wave damping ratio (-)	0.05	0.03

TABLE 3.2: Mechanical parameters used to model the tunnel.

Tunnel parameters	Values
Young modulus (GPa)	50
Density (kg m^{-3})	3000
Poisson ratio (-)	0.175
Thickness (m)	0.4
Interior radius (m)	5.65

TABLE 3.3: Mechanical parameters used to model the interior floor.

Interior floor parameters	Values
Young modulus (GPa)	30
Density (kg m^{-3})	3000
Poisson ratio (-)	0.175
Thickness (m)	0.5
Width (m)	10.9

The track consists of two identical rails separated at a constant distance of 1.5 m and a continuous mass-less distribution of springs-dashpots as a model of the fasteners. Their parameters are given in Tables 3.4 and 3.5.

TABLE 3.4: Mechanical parameters used to model the rail.

Rail parameters	Values
Young modulus (GPa)	207
Density (kg m^{-3})	7850
Cross-section area (m^2)	$6.93 \cdot 10^{-3}$
Second moment of area (m^4)	$23.5 \cdot 10^{-6}$

TABLE 3.5: Mechanical parameters used to model the fastener.

Fasteners parameters	Values
Uniformly distributed stiffness (N m^{-2})	$20 \cdot 10^{6}$
Uniformly distributed viscous damping (N s m^{-2})	$10 \cdot 10^{3}$

The considered train consists of two identical 3D models of the vehicle, shown in Fig. 3.6. The distance between the wheels of a bogie, bogies of a same car and bogies of two consecutive cars are 2.2 m, 15 m and 7 m, respectively. The parameters of the 2D vehicle models referred to in subsection 3.2.2 are: m_w represents the mass of the combined wheel and 1/2-axle system; m_{bog} and J_{bog} represent the mass and mass of inertia of a 1/2-bogie, respectively; k_{ps} and c_{ps} represent the stiffness and viscous damping, respectively, of the primary vehicle suspension system; m_{c} and J_{c} represent the mass and mass of inertia of a 1/2-car body; and k_{ss} and c_{ss} represent the stiffness and viscous damping, respectively, of the secondary vehicle suspension system. The values for these parameters can be found in Table 3.6.

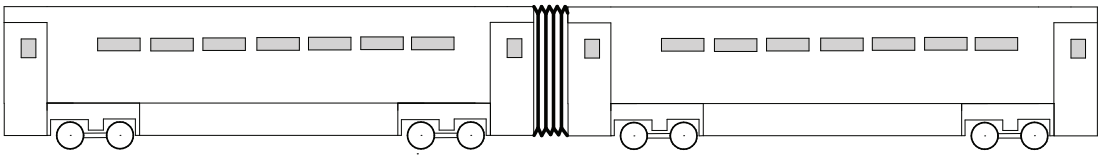

FIG. 3.6: Train configuration.

TABLE 3.6: Mechanical parameters used to model the train.

Vehicle parameters	Values	Vehicle parameters	Values
m_w (kg)	950	k_H (N m^{-1})	10^9
m_{bog} (kg)	4700	k_{ps} (N m^{-1})	$14{\cdot}10^5$
J_{bog} (kg m^2)	1300	c_{ps} (N s m^{-1})	$9{\cdot}10^3$
m_c (kg)	22500	k_{ss} (N m^{-1})	$6{\cdot}10^5$
J_c (kg m^2)	$55{\cdot}10^4$	c_{ss} (N s m^{-1})	$21{\cdot}10^3$

3.5.2 Computation of the Green's functions

The track-tunnel-soil model presented in subsection 3.2.1, along with the parameters of the subsystems given in the previous section, is used to compute the Green's functions required for coupling the vehicle and DVAs to the track and the interior floor, respectively, and for computing the energy flow radiated upwards due to the passage of the train. The computation of the energy flow radiated upwards takes into account a set of receivers on the soil at a semicircle concentric with the tunnel

and with the radius $r_s = 12$ m. A total amount of 21 receivers with an angular resolution of $9\pi/20$ rad are spread out across the semicircle. For the coupling between the DVAs and the interior floor, 20 receivers along the y coordinate over the interior floor are considered. They are the possible DVAs positions that are considered in the optimization process. These receivers are equidistantly spread out across the interior floor considering a space resolution of 0.5 m, and a distance of 0.5 m from each edge of the interior floor. The receivers in the soil and the interior floor, denoted by d_m and s_l, respectively, are shown in Fig. 3.7.

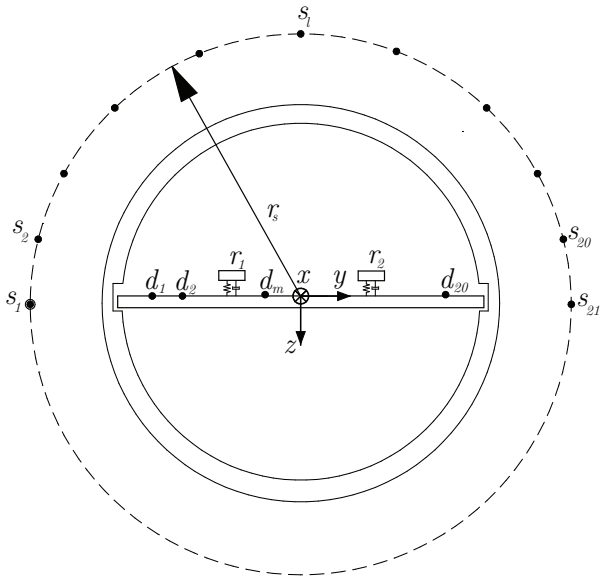

FIG. 3.7: Geometrical scheme of the receivers located at the soil and at the interior floor.

The Green's functions have been computed for the moving loads with the speeds of $v_t = 20$ and 25 m s^{-1}, which represent typical and maximum train speeds for underground urban railways, respectively. The wavenumber-frequency sampling is developed assuming a maximum frequency of interest, seen from a fixed frame of reference, of $\omega_{\max} = 80$ Hz. To compute the corresponding maximum frequency of interest seen from the perspective of the moving frame of reference $\tilde{\omega}_{\max}$, the expression

$$\tilde{\omega}_{\max} = \omega_{\max}\left(1 + \frac{v_t}{\beta}\right), \tag{3.32}$$

from [104] is used here, where β is the speed of S-waves in the soil.

It is proposed to computationally solve Eqs. (3.8) or (3.9) by using a fast Fourier Transform (`fft`) routine. Consider that the train response is computed at $x = 0$.

Taking into account that the moving frame of reference is defined as $\tilde{x} = x - v_t t$, one can define the sampling vectors for $\tilde{x}$ and t in the basis of the `fft` as

$$\tilde{x}_n = -\Delta\tilde{x}\left[-N/2 \quad \dots \quad n-1-N/2 \quad \dots \quad N/2-1\right] \tag{3.33}$$

and

$$t_n = \Delta t\left[-N/2 \quad \dots \quad n-1-N/2 \quad \dots \quad N/2-1\right], \tag{3.34}$$

respectively, where $\Delta\tilde{x} = v_t\Delta t$. Thus, the corresponding sampling for k_x and $\tilde{\omega}$ should be

$$k_{xn} = -\Delta k_x\left[-N/2 \quad \dots \quad n-1-N/2 \quad \dots \quad N/2-1\right], \tag{3.35}$$

and

$$\tilde{\omega}_n = \Delta\tilde{\omega}\left[-N/2 \quad \dots \quad n-1-N/2 \quad \dots \quad N/2-1\right], \tag{3.36}$$

respectively, where $\Delta\tilde{\omega} = v_t\Delta k_x$. Applying a 2D `fft` over this sampling strategy, the diagonal of the resulting 2D matrix for the specific receiver contains the time response at $x = 0$.

The assumption for which the train response is computed at $x = 0$ comes from the fact that, in pure 2.5D models, the time response at any arbitrary x is always the same as the one computed at $x = 0$ but delayed in time. However, when the DVAs are coupled to the system, the resulting model is no longer longitudinally invariant since it includes a periodical system, which induces a periodical behavior on the time response. Therefore, $x = 0$ represents only one of the possible time responses existing within a periodicity. However, the soil response is not significantly affected by this periodical behaviour due to the distance between the track and the receivers in comparison with the longitudinal distance between DVAs. Thus, $x = 0$ is taken as the representative time signal for the train response.

3.5.3 Train pass-by response

In this study, the unevenness profiles of the two rails are held to be uncorrelated. As shown by Ntotsios et al. [103], unevenness spectral content of wavelengths shorter than 3 m should be considered uncorrelated. The train speeds studied in this chapter imply that for frequencies larger than ≈ 8 Hz (most of the frequency

range of interest for railway-induced vibrations), the unevenness profiles of the two rails are deemed to be uncorrelated. They are modeled using a stochastic random process that is characterized by its power spectral density (PSD) [107] which depends on the rail quality. According to the Federal Railroad Administration (FRA), the unevenness of the rails can be grouped into six classes depending on the rail quality. Class 3 track is used in here.

Fig. 3.8 shows the time histories of the vertical rail velocity at $x = 0$ of the left rail, in the absence of DVAs, due to the train passage at speeds of 20 and 25 m s^{-1}. The passage of the train, which has a total of eight axles, can be seen through the eight peaks appearing in the figure. It is apparent that the vertical rail velocity of the rail grows by increasing the train speed. Furthermore, considering the velocity and the length of the train, the time it takes for the train to pass corresponds to the distance between the peaks in time.

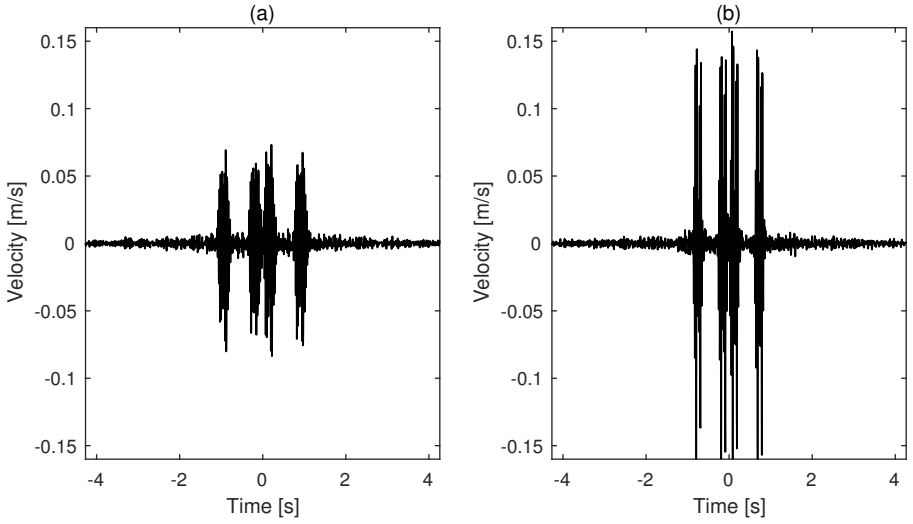

FIG. 3.8: Time history of the vertical velocity of the left rail due to the train passing at speeds of (a) $v_t = 20$ m s^{-1} and (b) $v_t = 25$ m s^{-1}.

Fig. 3.9 shows the time history of the radial velocity of the hard soil at the receiver s_{10}, i.e. located at $\theta = \pi/2$ and $r_s = 12$ m, due to train passing at speeds of 20 and 25 m s^{-1}. In this case, due to the distance between the receiver and the track, the passage of the train axles cannot be clearly identified as compared with the rail response.

Fig. 3.10 shows the frequency spectrum of the radial velocity for the hard and soft soil at the receiver s_{10}, located at $\theta = \pi/2$ rad and $r_s = 12$ m, due to the passage of the train at the speeds of 20 and 25 m s^{-1}. It can be observed that

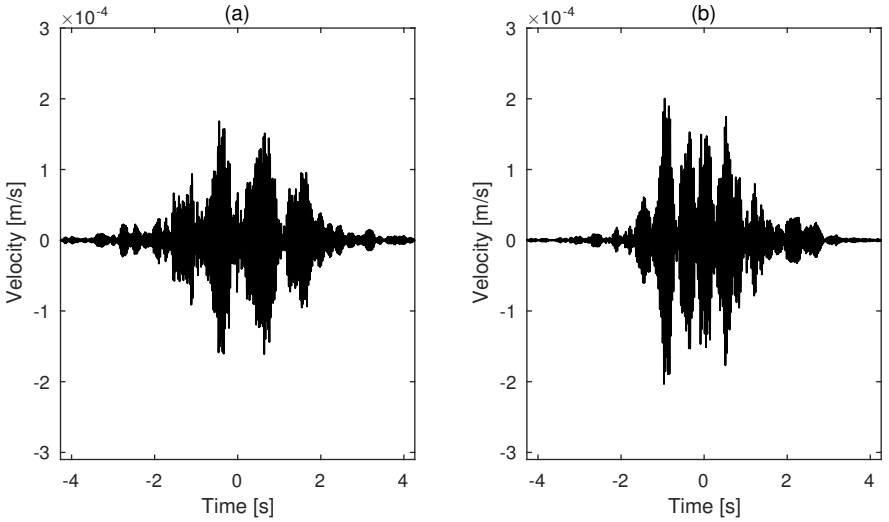

FIG. 3.9: Time history of the radial velocity of the soil at $\theta = \pi/2$ and $r_s = 12$ m due to the train passing at speeds of (a) $v_t = 20$ m s^{-1} and (b) $v_t = 25$ m s^{-1}.

the dominant spectral content is in a narrow frequency band for the four cases. Observing the same behavior at the other receivers implies that DVAs would be suitable vibration isolation measures. However, they would be less efficient for the soft soil cases as the dominant frequency band is wider.

3.5.4 Optimum parameters of DVAs

Only one distribution of DVAs is considered in this study. Moreover, the distance between any two consecutive DVAs in a distribution is assumed to be the same. The DVAs in a distribution are considered to have the same mass. Its value, together with the minimum distance between the DVAs and the number of them, are defined in the pre-design stage (common practice in designing DVAs [108]) by ensuring that the static tensions to which the interior floor is subjected would stay approximately unchanged after adding DVAs. Thus, the transverse position of DVAs distribution at the interior floor, the distance between two consecutive DVAs, the natural frequency of the DVAs and viscous damping of the DVAs are defined as variables in the optimization process in which the Matlab Global Optimization Toolbox [109] is employed. GA searches for the optimal values of these parameters that can minimize the energy flow radiated upwards from the cylindrical strip due to the passage of the train. The upper and lower bounds of these

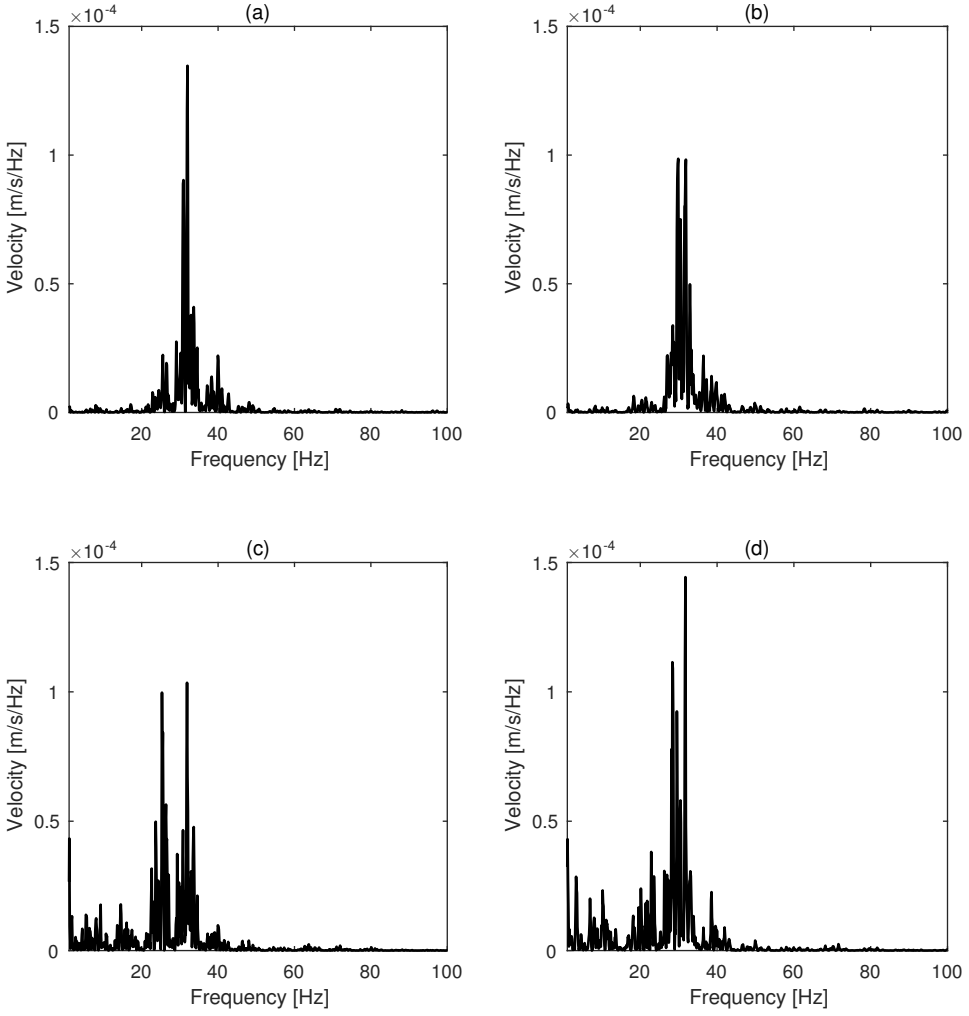

FIG. 3.10: Frequency spectrum of the radial velocity for the hard soil (top) and soft soil (bottom) at $\theta = \pi/2$ rad and $r_s = 12$ m due to the train passing at speeds of (a,c) $v_t = 20$ m s^{-1} and (b,d) $v_t = 25$ m s^{-1}.

design variables and the value of the parameters defined in the pre-design stage are given in the following:

1. Number of DVAs distributions M: Only one longitudinal distribution of DVAs is considered.

2. Transverse position of DVAs distribution y_d. It can be chosen from 20 possible positions defined previously in subsection 3.5.2.

3. Distance between two consecutive DVAs l_d: It is defined as a discrete variable, which can be chosen from 1 m to 8 m as the lower and upper bounds of this design variable, respectively, with a space step of 0.5 m. The space step has been restricted to 0.5 m because of the size of the DVAs to be used.

4. The mass of the DVAs m_d: It is defined in the pre-design stage. All DVAs in a distribution are assumed to have the same mass of 800 kg.

5. Number of DVAs in a distribution N: It is also defined in the pre-design stage, taking a value of 15 DVAs.

6. The natural frequency of the DVAs f_d: It is defined as a discrete variable that can be chosen from the values of the fixed frame frequency (i.e. seen from the fixed frame of reference) given by the wavenumber-frequency sampling defined in subsection 3.5.2.

7. The viscous damping of the DVAs c_d: It is defined as a discrete variable with lower and upper bounds of 5 kN s m^{-1} and 500 kN s m^{-1}, respectively. It is considered to be a total amount of 316 possible values linearly distributed between the defined bounds.

An optimization process based on GA has been carried out to minimize the energy flow radiated upwards due to the application of a distribution of DVAs. The following four cases have been studied: Case H25: hard soil and train speed of $v_t = 25$ m s^{-1}; Case H20: hard soil and train speed of $v_t = 20$ m s^{-1}; Case S20: soft soil and train speed of $v_t = 20$ m s^{-1} and Case S25: soft soil and train speed of $v_t = 25$ m s^{-1}. The resulting optimum values of the DVAs parameters and the associated insertion loss (IL) on the radiated energy flow are presented in Table 3.7. The IL was computed as

$$\mathrm{IL} = 10 \log_{10} \left(\frac{E}{E'} \right), \tag{3.37}$$

where E and E' represent the radiated energy without and with the application of the DVAs.

TABLE 3.7: The optimum values of DVAs parameters and resulting IL.

Case	y_d (m)	l_d (m)	f_d (Hz)	c_d (kN s m^{-1})	IL (dB)
H20	3.55	7.5	31.52	14.09	6.2
H25	-2.45	4.5	28.83	27.07	6.6
S20	1.05	7	31.17	20.65	5.3
S25	-3.45	6	31.6	27.76	5.8

Fig. 3.11 shows the mean power flow radiated upwards from the cylindrical strip with and without DVAs in the time domain for the four studied cases. The total radiated energy with and without DVAs is also given for each case. This mean power flow has been computed using the velocities and tractions over the cylindrical strip at $x_e = 0$, which is defined in accordance with the space-time sampling previously defined in subsection 3.5.2. The expression to compute the mean power flow can be derived from Eq. (3.31) and it is

$$P(t) = r_m \, \Delta x \int_{\theta_1}^{\theta_2} \mathbf{v}(x_e, \theta, t) \cdot \boldsymbol{\tau}(x_e, \theta, t) \mathrm{d}\theta. \tag{3.38}$$

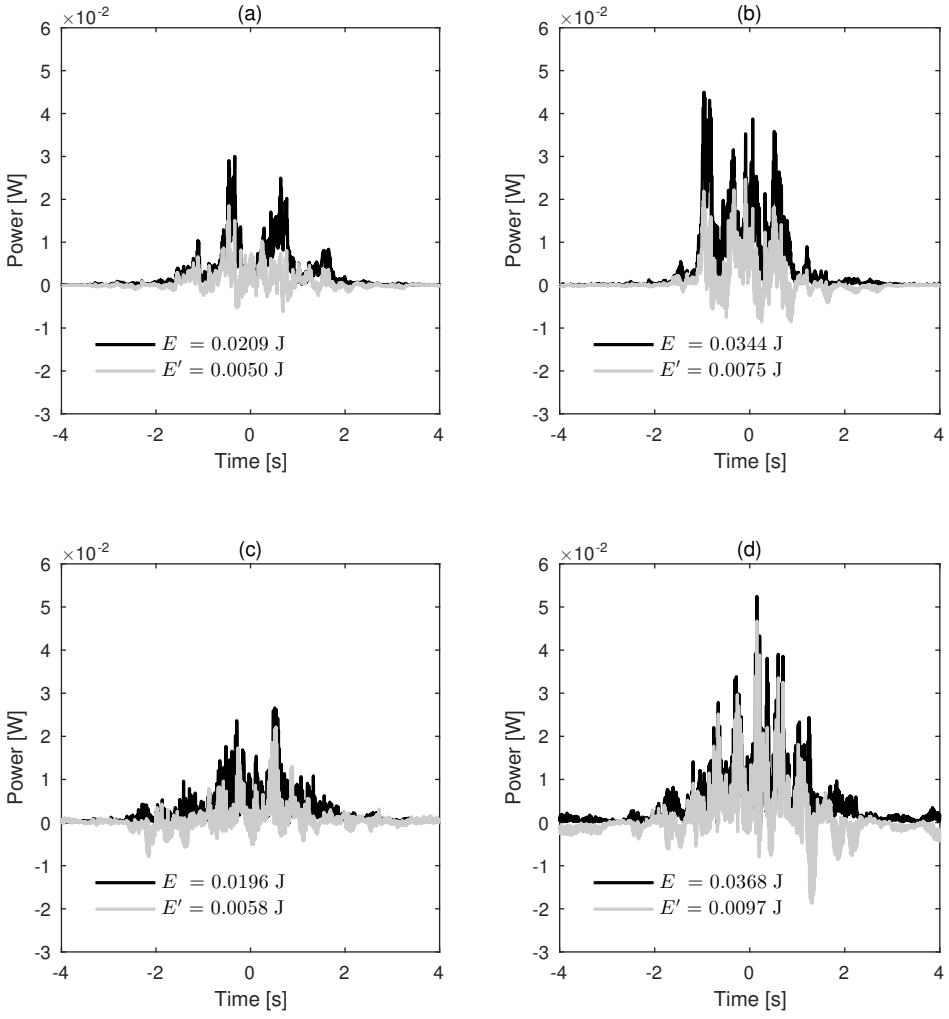

FIG. 3.11: Mean power flow radiated upwards over the cylindrical strip in the time domain for the cases (a) H20, (b) H25, (c) S20 and (d) S25. The grey and black lines represent the results with and without DVAs, respectively. The total radiated energy is presented for each case.

As generally expected, the radiated energy increases for both soft and hard soil when the speed of the train increases. The comparison of the radiated power flow or the total radiated energy with and without the application of DVAs indicates that using DVAs results in a notable decrease in radiated power flow or total radiated energy for all studied cases. For all the studied cases, Fig. 3.11 shows that the mean power flow becomes negative-valued at specific instants of time. This behavior of the mean power flow radiated upwards by a double-deck tunnel was previously observed by Clot [6] for the case of a quasi-static point load. A meaningful explanation of this phenomenon is that the elastic surface waves that travel along the tunnel cavity exhibit a particle motion very similar to the one presented by Rayleigh surface waves [110].

Fig. 3.12 shows the energy spectral density (ESD) of the previously computed mean power flow, with and without DVAs, for the four studied cases. As expected, the results of computing the total radiated energy using ESD is the same value previously achieved from the mean power flow in the time domain. It can be observed in Fig. 3.12 that the most significant energy content is concentrated in a frequency range between 25 to 35 Hz. It is noteworthy that the optimized natural frequencies of DVAs have been obtained in this range of frequency, which makes them effective in minimizing the radiated energy. The range of frequency in which most of the energy content is found and at which the DVAs are effective can be seen more clearly in Fig. 3.13, which represents ESD in one-third octave band for the considered cases with and without application of DVAs. The presented octave bands are normalized with the length of the time signal, which is 8.54 seconds.

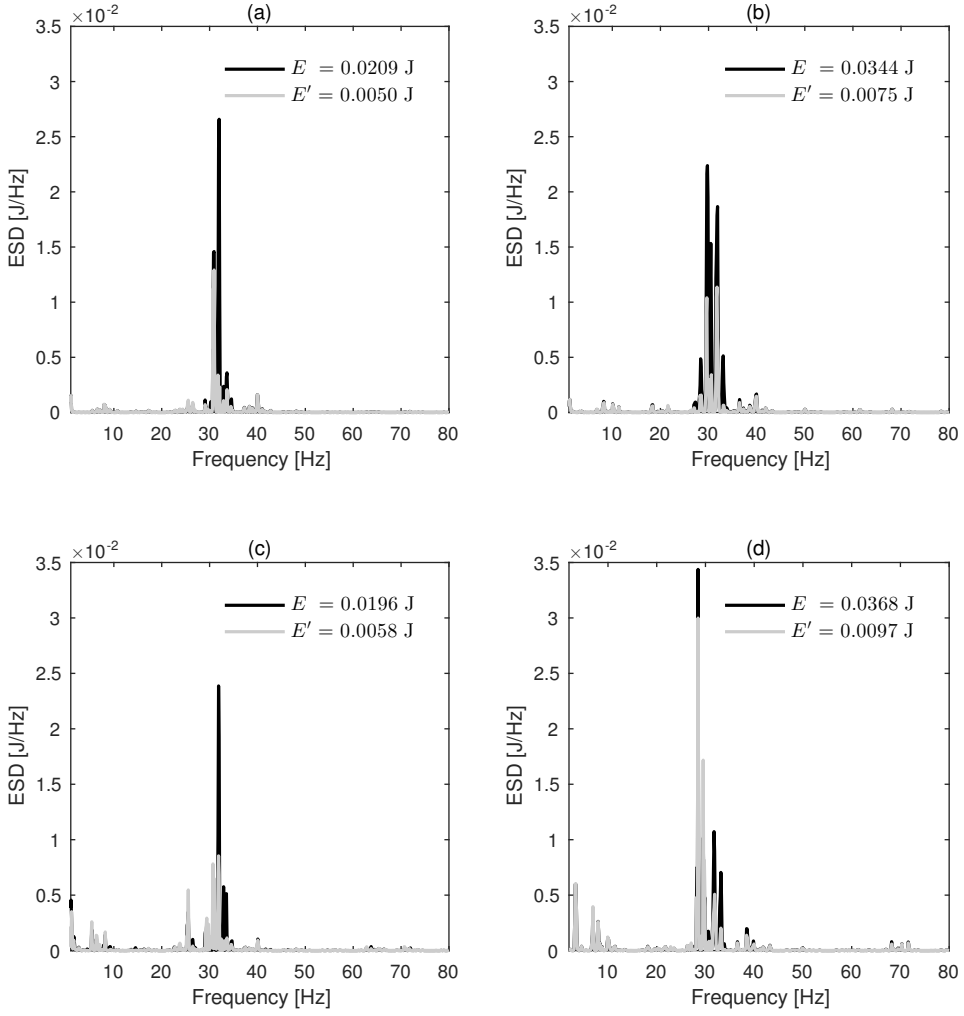

FIG. 3.12: ESD for cases (a) H20, (b) H25, (c) S20 and (d) S25. The grey and black lines represent the results with and without DVAs, respectively. The total radiated energy is also presented for each case.

In order to study the radiation pattern of the energy flow, the energy radiated through the cylindrical strip has been computed as a function of θ, for all studied cases and with and without the application of DVAs, using

$$E(\theta) = r_m \, \Delta \mathrm{x} \int_{-\infty}^{+\infty} \mathbf{v}(0,\theta,t) \cdot \boldsymbol{\tau}(0,\theta,t) \mathrm{d}t. \tag{3.39}$$

The results are shown in Fig. 3.14. One thing to note is that depending on the type of the soil, the energy flow radiation pattern would differ. For hard soil cases, the energy mostly radiates over the center of the strip, however, for the soft soil cases, it radiates mostly over the sides of the strip. For both cases, DVAs are significantly affecting the θ distribution of the radiation pattern. This is because

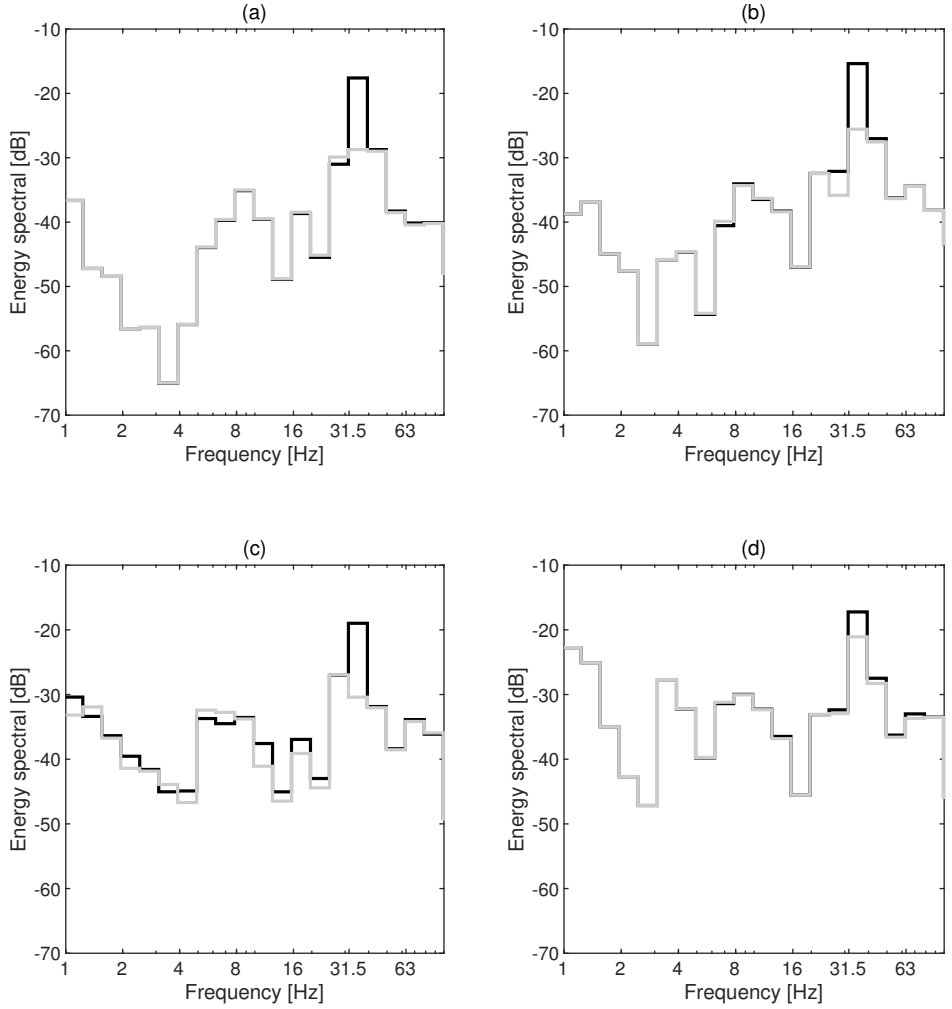

FIG. 3.13: One-third octave bands for cases (a) H20, (b) H25, (c) S20 and (d) S25. The grey and black lines represent the results with and without DVAs, respectively.

the mode shapes of the interior floor, which are modified by the application of the DVAs, are strongly related with the radiation pattern distribution, as discussed previously by Clot et al. [5] in a 2D power flow analysis of the double-deck tunnel subjected to a harmonic line load.

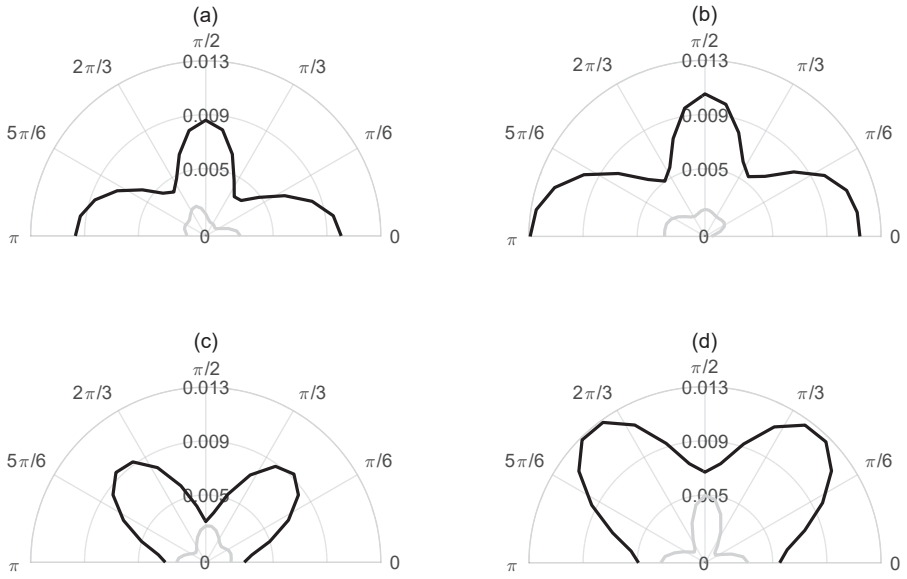

FIG. 3.14: Energy radiated over cylindrical strip in J as a function of θ for cases (a) H20, (b) H25, (c) S20 and (d) S25. The grey and black lines represent the results with and without DVAs, respectively.

In order to investigate the relation between the natural frequency of the optimal DVAs and the dynamical behavior of the original system, two figures are presented. On the one hand, Fig. 3.15 shows the radial velocity Green's functions of the hard soil case at three receivers located at $\theta = 0$, $\theta = \pi/2$ and $\theta = \pi$ rad, and at a radius of 12 m due to the force applied on the right rail. The red areas show local maximums of the velocity Green's functions and they represent an approximation to the dispersion curves of the system. From this approximation, three propagation modes of the interior floor coupled to the tunnel-soil system can be observed: the first and the third are anti-symmetric (not observed at $\theta = \pi/2$) and the second is symmetric (the only one appearing at $\theta = \pi/2$). The inclined dashed black lines plotted in Fig. 3.15 represent combinations of k_x and ω of constant $\tilde{\omega}$ for the specific speed of 25 m s^{-1}. On the other hand, Fig. 3.16 shows dynamic wheel-rail interaction forces for the same case study but considering 20 m s^{-1} and 25 m s^{-1}. For both figures, the computations have been done without considering coupled DVAs. Comparing these two figures with the results shown in Table 3.7, where the natural frequency of the optimal DVAs for the hard soil case is 31.52 Hz for $v_t = 20$ m s^{-1} and 28.83 Hz for $v_t = 25$ m s^{-1}, one can observe that the DVAs are targeting the second propagation mode of the track-interior floor-tunnel-soil system. This can be deduced because of two reasons: firstly, the inclined black lines of constant $\tilde{\omega}$ have a slope far from the tangents to the dispersion curves

except for wavenumbers close to zero, resulting in that the frequency associated to these propagation modes is mostly the one of the 2D problem; secondly, the contact forces have a significant amount of spectral energy close to the resonance frequency associated to the second propagation mode for the 2D case.

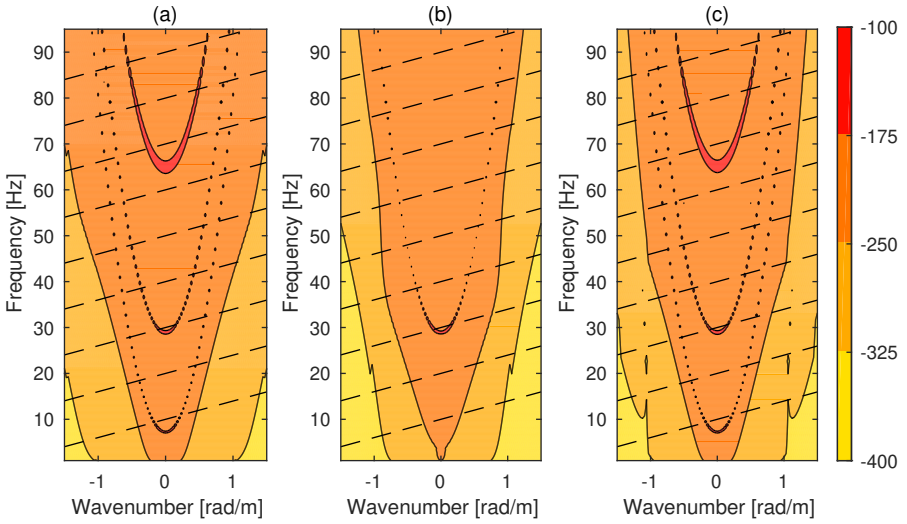

FIG. 3.15: The radial velocity Green's functions of the hard soil in dB (dB reference 1 m $N^{-1}s^{-1}$) at the receivers located at $r_s = 12$ m and (a) $\theta = 0$, (b) $\theta = \pi/2$ rad and (c) $\theta = \pi$ rad for $v_t = 25$ m s^{-1}. Inclined dashed black lines denote points of constant $\tilde{\omega}$ for the specific speed of 25 m s^{-1}.

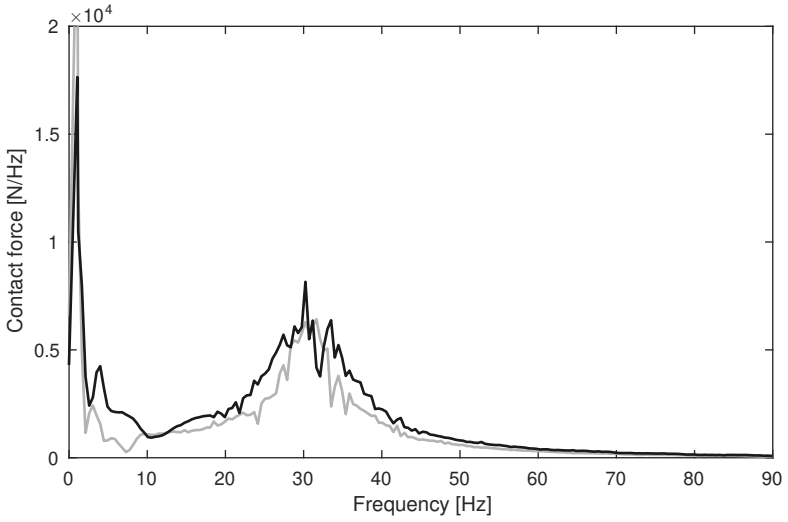

FIG. 3.16: Contact forces caused by wheel-rail interaction associated to $v_t = 20$ m s^{-1} (grey) and $v_t = 25$ m s^{-1} (black).

The effect of the DVAs on the dynamic response of the rails is also studied. Fig. 3.17 shows the one-third octave band spectrum of the vertical velocity of the left

rail with and without DVAs, for two different train speeds. It can be seen from the figures that the application of DVAs on the interior floor of the tunnel has little effect on the dynamic response of the track. Because of that, the train-track dynamic forces can be computed before the optimization process, only once. If the track is already constructed, these forces can be obtained using a hybrid approach [52] that enhance the accuracy of the DVAs efficiency prediction. However, it is important to highlight that this result is only associated to the present problem parameters. In cases where the DVAs natural frequency is similar to the rail/fasteners natural frequency, this conclusion is no longer valid.

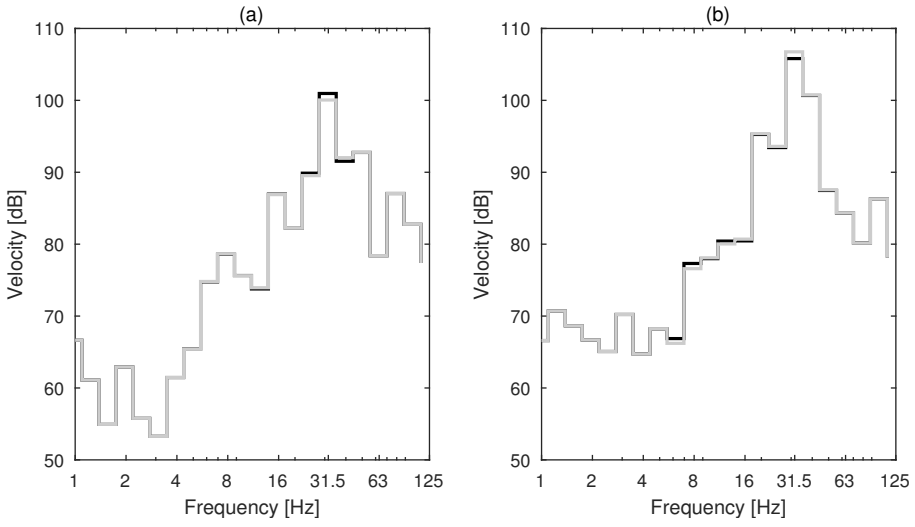

FIG. 3.17: One-third octave band spectrum of the vertical velocity of the left rail in dB (dB reference 10^{-8} m s^{-1}) for the train speeds of (a) $v_t = 20$ m s^{-1} and (b) $v_t = 25$ m s^{-1}. The grey and black lines represent the results with and without DVAs, respectively.

Chapter 4

Application of DVAs as vibration countermeasures: Case study of L9 Barcelona metro

4.1 Introduction

This chapter is concerned with investigating the application of DVAs in a double-deck tunnel as measures to mitigate ground-borne vibrations in a building, which are induced by the railway traffic of the double-deck tunnel underneath the building. For this purpose, a hybrid experimental-numerical model of a train-track-tunnel-soil-building system is used. In this hybrid model, a numerical model of the track-tunnel system based on a 2.5D coupled FE-BE approach along with a dynamic rigid multi-body model of the vehicle is used to compute the response in the tunnel wall. Then, the response in the building is computed using experimentally obtained transfer functions between the tunnel wall and the building floor. The optimum design parameters of the DVAs are obtained using an optimization process based on the GA. The effectiveness of the DVAs is assessed by a response parameter, MTVV in the building near the tunnel, which is used as an objective function to be minimized in the optimization process. The triaxial response in the building is used to compute the MTVV. The natural frequency, the viscous damping and the positions of the DVAs are considered as design parameters in the optimization procedure. DVAs are found to be efficient vibration countermeasures in the framework of the double-deck tunnel infrastructures as a reduction of 3.3 dB in the MTVV in the building is achieved due to the application of the DVAs on the interior floor of the tunnel.

The rest of the chapter is organized as follows. In section 4.2, the hybrid numerical-experimental model is described. The optimization process and design parameters of the DVAs are detailed in section 4.3. The performance of optimized DVAs in minimizing MTVV in the building is presented in section 4.4. Noteworthy, the methodology proposed in section 3.3 is employed here to couple DVAs to the interior floor.

4.2 Hybrid vibration prediction model

A hybrid model of the train-track-tunnel-soil-building system is used to calculate the response of the system in the building due to train pass-by. In this model, the vibration response of the tunnel wall is computed using a theoretical prediction model of the train-track-tunnel-soil system. Then, the response at the building

first floor is computed using experimentally obtained transfer functions between the tunnel wall and the building. The theoretical prediction model of the train-track-tunnel-soil system includes numerical model of the tunnel-soil subsystem based on a 2.5D FE-BE approach [111] (briefly explained in subsection 4.2.1), a semi-analytical model of the track coupled to the interior floor of the tunnel (outlined in subsection 4.2.2) and a train-induced response model (summarized in subsection 4.2.3).

4.2.1 Modeling of tunnel-soil system

A coupled 2.5D FE-BE formulation approach is used to model tunnel-soil system. The particular 2.5D FE-BE approach used in this work is the one presented by Ghangale et al. [111]. In this method, the 2.5D boundary element method (BEM) and the 2.5D finite element method (FEM) are used to model the soil and the tunnel, respectively. Then, the subsystems are coupled by enforcing continuity of displacements and stresses on the interface between them. This model is used to obtain the response of a set of evaluators located in the tunnel/soil system. On one hand, the evaluators that should be selected for the simulations explained in this chapter are the FE nodes that should be in contact with the rails, the FE nodes considered to be candidates for a DVA placement and the FE nodes where the final response of the simulation is required. On the other hand, the forces that should be applied at the model are vertical forces at the FE nodes that should be in contact with the rails and vertical forces in the FE nodes considered to be candidates for a DVA placement.

4.2.2 Modeling of track-interior floor system

A semi-analytical model of a track system consisting of two rails supported by the fasteners is derived in this section. The rails are modeled as two identical Euler-Bernoulli beams of infinite length and the fasteners are modeled as continuously distributed linear massless viscous springs. The equations that define the dynamic behavior of the rails excited by moving harmonic vertical point loads with the same

excitation frequency $\tilde{\omega}$ and the same speed v_t can be expressed in the wavenumber-frequency domain as [112]

$$\left(E_r I_r k_x^4 - \rho_r S_r \omega^2\right) \bar{\mathbf{Z}}_r + \left(k_f + \mathrm{i}\omega c_f\right)\left(\bar{\mathbf{Z}}_r - \bar{\mathbf{Z}}_{f_r}\right) = 2\pi\delta\left(\tilde{\omega} - (\omega - k_x v_t)\right)\mathbf{F}_r, \quad (4.1)$$

where

$$\bar{\mathbf{Z}}_r = \begin{Bmatrix} \bar{Z}_{r_1} \\ \bar{Z}_{r_2} \end{Bmatrix}, \quad \bar{\mathbf{Z}}_{f_r} = \begin{Bmatrix} \bar{Z}_{f_{r_1}} \\ \bar{Z}_{f_{r_2}} \end{Bmatrix}, \quad \mathbf{F}_r = \begin{Bmatrix} F_{r_1} \\ F_{r_2} \end{Bmatrix},$$

and where E_r is the Young's modulus of the rail material, I_r is the second moment of inertia of the rail cross section, ρ_r is the density of the rail material, S_r is the rail cross-sectional area and k_f and c_f are the stiffness and viscous damping of the fasteners, respectively. For $i = 1, 2$, F_{r_i} is the amplitude of the vertical load applied on the i-th rail and $\bar{Z}_{r_i}$ and $\bar{Z}_{f_{r_i}}$ are the vertical displacement of the i-th rail and the equivalent vertical displacement of the interior floor below the i-th rail, respectively. This equivalent vertical displacement is obtained by averaging the responses at the FE nodes of the interior floor that should be in contact with the rails induced by the set of vertical forces applied at these nodes.

Thus, the equivalent response of the interior floor below the rails due to the equivalent forces applied by the fasteners of the first rail ($\bar{F}_{f_{r_1}}$) and second rail ($\bar{F}_{f_{r_2}}$) is given by

$$\bar{\mathbf{Z}}_{f_r} = \bar{\mathbf{H}}_{f_r f_r} \bar{\mathbf{F}}_{f_r}, \quad (4.2)$$

where

$$\bar{\mathbf{F}}_{f_r} = \begin{Bmatrix} \bar{F}_{f_{r_1}} \\ \bar{F}_{f_{r_2}} \end{Bmatrix} \quad \text{and} \quad \bar{\mathbf{H}}_{f_r f_r} = \begin{bmatrix} \bar{H}_{f_{r_1} f_{r_1}} & \bar{H}_{f_{r_1} f_{r_2}} \\ \bar{H}_{f_{r_2} f_{r_1}} & \bar{H}_{f_{r_2} f_{r_2}} \end{bmatrix}, \quad (4.3)$$

being $\bar{H}_{f_{r_i} f_{r_j}}$, for $i, j = 1, 2$, the Green's functions of the interior floor below the i-th rail due a force applied on the interior floor below the j-th rail. The 2.5D numerical model of the soil-tunnel system explained in the previous subsection is used to compute the Green's functions $\bar{\mathbf{H}}_{f_r f_r}$.

The equivalent forces applied by the fasteners on the interior floor below the rails can be obtained by

$$\bar{\mathbf{F}}_{f_r} = \left(k_f + \mathrm{i}\omega c_f\right)\left(\bar{\mathbf{Z}}_r - \bar{\mathbf{Z}}_{f_r}\right). \quad (4.4)$$

By replacing the equivalent fastener forces in Eq. (4.2) with the ones from Eq.

(4.4) and rearranging the resulting equation, the relation between the displacements of the interior floor below the rails and the displacements of the rails can be obtained as

$$\bar{\mathbf{Z}}_{f_r} = \bar{\mathbf{T}}_{f_r r}\bar{\mathbf{Z}}_r \tag{4.5}$$

where

$$\bar{\mathbf{T}}_{f_r r} = \left(\frac{1}{k_f + \mathrm{i}\omega c_f}\mathbf{I} + \bar{\mathbf{H}}_{f_r f_r}\right)^{-1}\bar{\mathbf{H}}_{f_r f_r}, \tag{4.6}$$

being $\mathbf{I}$ the identity matrix.

By substituting Eq. (4.5) into Eq. (4.1), then equation of motion of the rails in the wavenumber-frequency domain can be written as

$$\left[\left(E_r I_r k_x^4 - \rho_r S_r \omega^2\right)\mathbf{I} + \bar{\mathbf{K}}_{rf}\right]\bar{\mathbf{Z}}_r = 2\pi\delta\left(\tilde{\omega} - (\omega - k_x v_t)\right)\mathbf{F}_r, \tag{4.7}$$

where

$$\bar{\mathbf{K}}_{rf} = \left(k_f + \mathrm{i}\omega c_f\right)\left(\mathbf{I} - \bar{\mathbf{T}}_{f_r r}\right), \tag{4.8}$$

Thus, the Green's function of the rails on the moving frame of reference due to a force applied on the rails can be defined as

$$\tilde{\mathbf{H}}_{rr} = \left[\left(E_r I_r k_x^4 - \rho_r S_r\left(\tilde{\omega} + k_x v_t\right)^2\right)\mathbf{I} + \tilde{\mathbf{K}}_{rf}\right]^{-1}, \tag{4.9}$$

where $\tilde{\mathbf{K}}_{rf} = \tilde{\mathbf{K}}_{rf}(k_x, \tilde{\omega}) = \bar{\mathbf{K}}_{rf}(k_x, \tilde{\omega} + k_x v_t)$.

On one hand, the Green's function of the system at any arbitrary position of the tunnel due to a force applied on the rails can be obtained by

$$\tilde{\mathbf{H}}_{tr} = \tilde{\mathbf{H}}_{tf_r}\tilde{\mathbf{K}}_{rf}\tilde{\mathbf{H}}_{rr}, \tag{4.10}$$

being

$$\tilde{\mathbf{H}}_{tr} = \left\{\tilde{\mathbf{H}}^r_{tr_1} \quad \tilde{\mathbf{H}}^r_{tr_2}\right\}, \quad \tilde{\mathbf{H}}_{tf_r} = \left\{\tilde{\mathbf{H}}_{tf_{r_1}} \quad \tilde{\mathbf{H}}_{tf_{r_2}}\right\}, \tag{4.11}$$

where $\tilde{\mathbf{H}}_{tf_r}$ are the Green's functions of the tunnel structure due to forces applied on the interior floor below the rails. On the other hand, the Green's functions of the system at any arbitrary position due to external forces applied at any arbitrary position of the tunnel in the presence of the rails can be written as

$$\bar{\mathbf{H}}^r_{te} = \bar{\mathbf{H}}_{te} + k_{rt}\bar{\mathbf{H}}_{tf_r}\bar{\mathbf{H}}_{f_r e} \tag{4.12}$$

where the sub-index e represents the external loading and

$$k_{rt} = \left(k_f + \mathrm{i}\omega c_f\right)\left(\frac{k_f + \mathrm{i}\omega c_f}{E_r I_r k_x^4 - \rho_r S_r \omega^2 + k_f + \mathrm{i}\omega c_f} - 1\right), \tag{4.13}$$

and where $\bar{\mathbf{H}}_{te}$ are the Green's functions of the system at the tunnel due to external forces in the absence of the rails, $\bar{\mathbf{H}}_{tf_r}$ are the Green's functions of the system at the tunnel due to the force applied on the interior floor below the rails and $\bar{\mathbf{H}}_{f_re}$ are the Green's functions of the system at the interior floor below the rails due to the external loads in the absence of the rails. Finally, the Green's functions associated to the response of the rails due to external loading can be written as

$$\bar{\mathbf{H}}^r_{re} = k_{rr}\bar{\mathbf{H}}_{f_re}, \tag{4.14}$$

where

$$k_{rr} = \frac{k_f + \mathrm{i}\omega c_f}{E_r I_r k_x^4 - \rho_r S_r \omega^2 + k_f + \mathrm{i}\omega c_f}. \tag{4.15}$$

Eqs. (4.12) and (4.14) are not defined in the moving frame of reference because the external loads, in this case applied by the DVAs, are not moving with the train. The Green's functions $\bar{\mathbf{H}}_{tf_r}$, $\bar{\mathbf{H}}_{te}$ and $\bar{\mathbf{H}}_{f_re}$ can be computed using the 2.5D numerical model of the tunnel-soil system based on FE-BE formulation explained in subsection 4.2.1.

4.2.3 Modeling of train-track interaction

In the context of the urban railway infrastructures, the dynamic excitation due to dynamic train-track interaction is the mechanism which contributes the most in the railway-induced vibration. It can be generated by several mechanisms, such as variation of the track's mechanical parameters and the wheel and track unevenness. The latter is considered as main excitation mechanism in this section. A detailed derivation of the train-track interaction model employed can be found in the section 3.2.2.

4.2.4 Building response prediction

The vibration transmission between the tunnel wall and the building can be modeled using experimentally obtained vibration transfer functions [113, 114]. This transfer function is based on the ratio between cross-power spectrum and power spectrum [114].

To generate the transfer functions, the response of the tunnel wall and the building floor due to the train pass-by need to be measured simultaneously using triaxial accelerometers (or a set of three single-axial accelerometers that gives triaxial vibration). Then, a single input spectrum in the frequency domain $\ddot{U}_t(\omega)$ can be approximately obtained using triaxial information at the tunnel wall as

$$\ddot{U}_t = \sqrt{|\ddot{U}_{t_x}|^2 + |\ddot{U}_{t_y}|^2 + |\ddot{U}_{t_z}|^2}, \tag{4.16}$$

being $\ddot{U}_{t_x}$, $\ddot{U}_{t_y}$ and $\ddot{U}_{t_z}$ the spectra of the vibration acceleration measured at the tunnel wall in x, y and z directions, respectively, in the frequency domain. A single output signal in the frequency domain $\ddot{U}_b(\omega)$ can also be approximately obtained using triaxial information measured at the building floor as

$$\ddot{U}_b = \sqrt{|\ddot{U}_{b_x}|^2 + |\ddot{U}_{b_y}|^2 + |\ddot{U}_{b_z}|^2}, \tag{4.17}$$

being $\ddot{U}_{b_x}$, $\ddot{U}_{b_y}$ and $\ddot{U}_{b_z}$ the spectra of the vibration acceleration measured at the building floor in x, y and z directions, respectively, in the frequency domain. As both input and output signals are transient signals, the transfer function between the tunnel wall and the building can be obtained by

$$T_{tb}(\omega) = \frac{E_{tb}(\omega)}{E_{tt}(\omega)} \tag{4.18}$$

where $E_{tb}(\omega)$ is the cross-energy spectrum between $\ddot{U}_t$ and $\ddot{U}_b$, and E_{tt} is the energy spectrum of $\ddot{U}_t$.

Noteworthy, it is assumed here that the application of DVAs would not affect the transfer function between tunnel wall and the building. So, the transfer function, obtained in the absence of DVAs, could be also used after the application of DVAs. This assumption is considered based on the work of Arcos et al. [112], in which a similar hybrid model approach was used to compute the optimal rail fastener

stiffness. It was shown that the transfer functions between tunnel wall and the building are not significantly affected by changing the stiffness of the fasteners.

4.3 DVAs optimization approach

A global optimization approach similar to the one explained in section 3.4 is used here to obtain the optimum parameters of DVAs. The only difference with that approach is that the objective function to be minimized in the optimization process is the MTVV in the building near the tunnel. As before, the number of DVAs distributions, the position of DVAs distributions, number of DVAs in each distribution, distance between two consecutive DVAs in each distribution, DVAs masses, DVAs natural frequencies and DVAs damping coefficients are design variables. Computing the MTVV in the building for the system with DVAs, MTVV_{iso}, consists of the following calculations:

1. The Green's function of the system at the tunnel wall due to a force applied on the rails, by means of Eq. (4.10);
2. The response of the system at the tunnel wall due to train pass-by, using the Green's function computed in step 1 and Eq. (3.8);
3. The response of the building due to the train pass-by using the experimentally obtained transfer function between the tunnel wall and the building floor and the response at the tunnel wall obtained in step 2;
4. The MTVV in accordance with [14].

The optimization process used in this work minimizes the MTVV_{iso}. Minimizing the MTVV_{iso} results on a maximization of the IL associated to the MTVV in the building, as it is stated by

$$\text{IL} = 20 \log_{10} \left(\frac{\text{MTVV}_{\text{uniso}}}{\text{MTVV}_{\text{iso}}} \right), \tag{4.19}$$

where $\text{MTVV}_{\text{uniso}}$ is the MTVV in the building floor in the absence of DVAs. Its calculation consist of the following computations:

1. The Green's function of the system at the tunnel wall due to a force applied on the rails, by means of Eq. (4.10);

2. The response of the system at the tunnel wall due to train pass-by, using the Green's function computed in step 1 and Eq. (3.8);

3. The response of the building due to the train pass-by using the experimentally obtained transfer function between the tunnel wall and the building floor and the response at the tunnel wall obtained in step 2;

4. The MTVV in accordance with [14].

4.4 Application and results

The proposed methodology is employed to investigate the efficiency of application of optimized DVAs in minimizing the ground-borne vibrations in the case study of L9 Barcelona metro. The study is done in particular building nearby to a L9 stretch where the existing level of vibration due to common train traffic is severe. In that L9 section, the tunnel is double-decked and the circulations that are inducing high vibration levels are the ones running over the upper floor of the tunnel.

4.4.1 Computation of the Green's functions of the tunnel/soil system

The 2.5D FE-BE model of the particular section of double-deck tunnel used for 2.5D numerical studies is shown in Fig. 4.1. The model consists of the tunnel and the soil discretized by linear triangular finite elements and linear elastodynamic boundary elements, respectively. The criteria of minimum of six elements per wavelength is considered, assuming that the wavelength is the one associated to the S-waves of each medium. The tunnel has an inner radius and thickness of 5.65 m and 0.4 m, respectively, and the thickness of the interior floor is 0.5 m. The mechanical parameters used for the tunnel and the interior floor are the ones associated to reinforced concrete. They are summarized in Table 4.1. The mechanical parameters associated to the soil can also be found in Table 4.1.

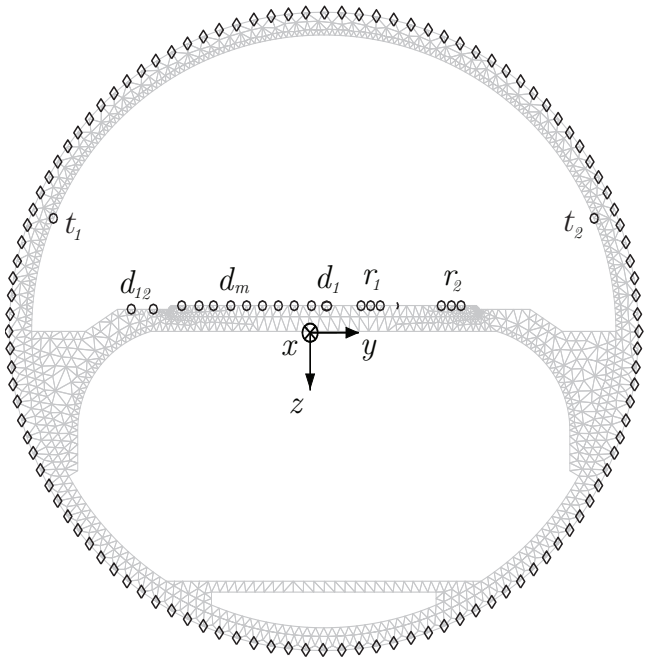

FIG. 4.1: Mesh of the 2.5D FE-BE model of the double-deck tunnel for the specific section studied. The boundary element nodes are shown by diamonds. The FE nodes used to couple the rails (three nodes for each rail, r_1 and r_2), the ones used to evaluate the response of the system at the tunnel wall (t_1 and t_2), and the ones considered as possible positions of DVAs (d_1 to d_{12}) are shown by circles.

TABLE 4.1: Mechanical parameters used to model the tunnel/interior floor system and soil.

Parameters	Tunnel/interior floor	Soil
Young's modulus (GPa)	31	0.18
Density (kg m^{-3})	2500	2100
Poisson's ratio (-)	0.2	0.3
P-wave damping ratio (-)	0.01	0.025
S-wave damping ratio (-)	0.01	0.025

This model has been used to compute the Green's functions required to couple the rails and the DVAs to the interior floor, as well as the Green's functions required to compute the response of the system due to train pass-by. In order to couple the rails to the interior floor, the Green's function of the system at the position of the fasteners due to the force applied at those positions are needed, as explained in subsection 4.2.2. For each rail, three nodes have been considered to couple

the rails to the interior floor. They are shown by circles in Fig. 4.1, as r_1 and r_2. Then, equivalent responses and applied forces are computed for each rail by averaging the obtained Green's functions. The fasteners are modelled as uniformly distributed viscous springs with stiffness and viscous damping of $20{\cdot}10^6$ N m^{-2} and $10{\cdot}10^3$ N s m^{-2}, respectively. The parameters used to model the rails can be found in Table 4.2. To compute the response of the system due to train pass-by, two FE nodes at each side of the tunnel wall has been considered, shown by circles in Fig. 4.1 as t_1 and t_2. The rest of the FE nodes shown by the circles in Fig. 4.1 represent the nodes used to couple DVAs to the interior floor. These are the 12 possible transverse positions of the DVAs that are considered in the optimization process.

TABLE 4.2: Parameters used to model the rails.

Rail parameters	Values
Young's modulus (GPa)	207
Density (kg m^{-3})	7850
Cross-section area (m^2)	$6.93{\cdot}10^{-3}$
Second moment of area (m^4)	$23.5{\cdot}10^{-6}$

The Green's functions have been computed for a train speed of $v_t = 16.67$ m s^{-1}, which is the speed of the train in L9 Barcelona metro at the section where the efficiency of DVAs is being studied. Regarding the wavenumber-frequency sampling, the maximum frequency of interest seen from a fixed frame of reference is considered to be $f_{\max} = 80$ Hz. The corresponding maximum frequency of interest seen from the perspective of the moving frame of reference $\tilde{\omega}_{\max}$ is obtained using expression proposed in [104] as $\tilde{\omega}_{\max} = \omega_{\max}\left(1 + v_t/\beta\right)$, where β is S-wave speed in the soil. Uniformly distributed samples of 2^{11} points from 0 to $\tilde{\omega}_{\max}$ have been used as a sampling vector of the frequency, and the sampling vector for wavenumber has been obtained according to the relation $\Delta\tilde{\omega} = v_t \Delta k_x$, where $\Delta\tilde{\omega}$ and Δk_x are the frequency and wavenumber steps of the selected sampling, respectively. More details about the sampling strategy can be found at section 3.5.2.

4.4.2 Train pass-by response prediction

The vertical dynamic excitation caused by rail unevenness is considered as the main source of the excitation. The unevenness profiles of the two rails are held to be uncorrelated here, as proposed in previous chapter. The unevenness profiles of the rails are modeled using stochastic random processes characterized by its power spectral density (PSD) [107]. According to the Federal Railroad Administration (FRA), the unevenness of the rails can be grouped in six classes depending on the rail quality [115]. Class 3 track is used in this study.

After the computation of the Green's functions and the wheel-rail interaction forces, the response of the system due to the train pass-by can be computed. The considered train consists of five identical cars. Each car is represented as two uncoupled 2D models independently applied on each rail, as shown in Fig. 4.2. The distance between the wheels of a bogie, bogies of the same car and bogies of two consecutive cars are 2 m, 11.37 m and 4.9 m, respectively. The other parameters of the 2D vehicle models are: m_w, which represents the mass of the combined wheel and 1/4-axle system; m_{bog} and J_{bog}, that represent the mass and the moment of inertia of a 1/2-bogie, respectively; k_{ps} and c_{ps}, which represent the stiffness and viscous damping, respectively, of the primary vehicle suspension system; m_{c} and J_{c}, which represent the mass and moment of inertia of a 1/2-car body; and k_{ss} and c_{ss}, which represent the stiffness and viscous damping, respectively, of the secondary vehicle suspension system. The values for these parameters can be found in Table 4.3.

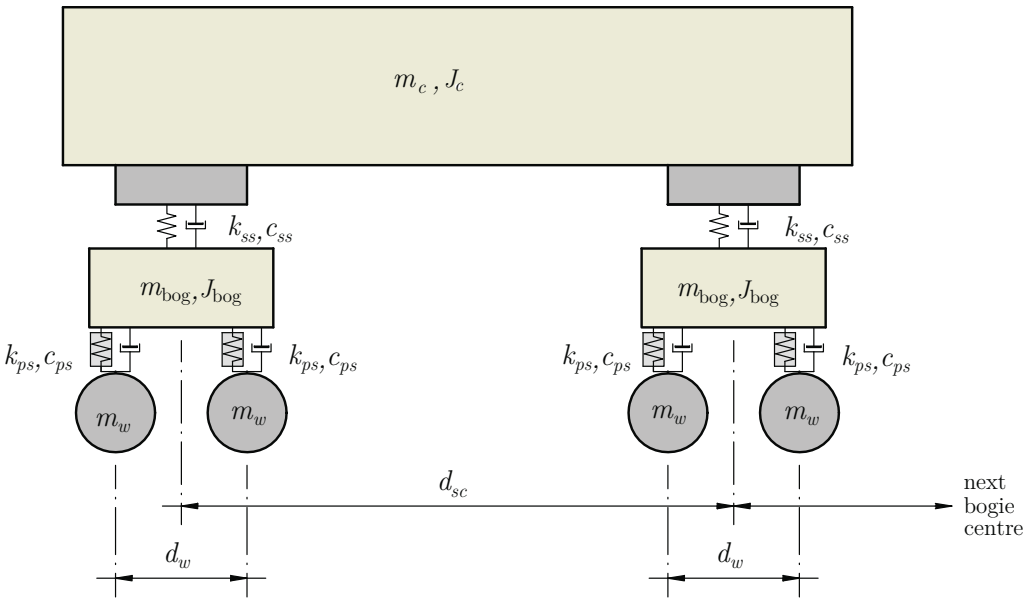

FIG. 4.2: Schematic of 2D MDOF rigid body model of each car.

TABLE 4.3: Mechanical parameters used to model the train.

Train parameters	Values	Train parameters	Values
m_w (kg)	705	k_H (N m^{-1})	10^9
m_{bog} (kg)	1730	k_{ps} (N m^{-1})	$12.4{\cdot}10^5$
J_{bog} (kg m^2)	824	c_{ps} (N s m^{-1})	$10{\cdot}10^3$
m_c (kg)	20961	k_{ss} (N m^{-1})	$8.12{\cdot}10^5$
J_c (kg m^2)	$45.85{\cdot}10^4$	c_{ss} (N s m^{-1})	$15{\cdot}10^3$

The time history of the vertical velocity of both rails at $x = 0$ due to train pass-by is shown in Fig. 4.3 for case where the DVAs are not applied. The passage of the train can be seen through the peaks associated to the 20 axles that are appearing in the figure. As the geometry of the system is not symmetric (as shown in Fig. 4.1), the responses of the rails are different between them.

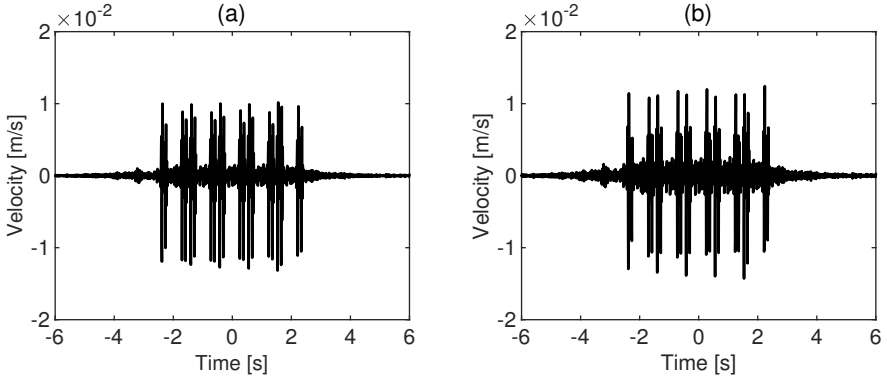

FIG. 4.3: Time history of the vertical velocity of the rail r_1 (a) and the rail r_2 (b), at $x = 0$, in the absence of DVAs.

Fig. 4.4 shows the frequency spectrum and time history of the vertical velocity due to train passage evaluated at the position d_3 on the interior floor, which is located at $(x, y, z) = (0, -0.2, -0.5)$ m with respect to the coordinates presented in Fig. 4.1, in the absence of the DVAs. It can be seen from the frequency spectrum that the frequency content is mostly concentrated in the frequency range between 20 Hz to 40 Hz.

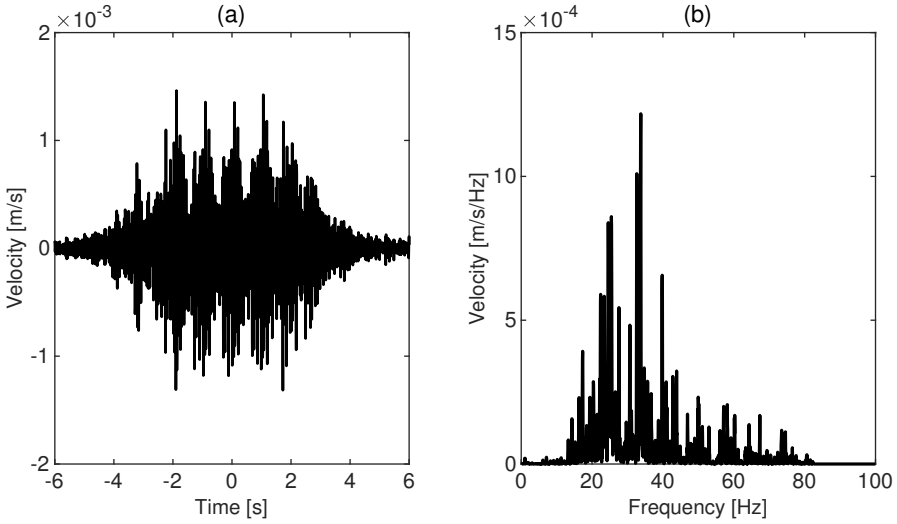

FIG. 4.4: Time history (a) and frequency spectrum (b) of the vertical velocity of the interior floor d_3.

Fig. 4.5 shows the time history and the frequency spectrum of the vertical and horizontal velocity due to the train passage evaluated at the position t_1 on the tunnel wall, which is located at $(x, y, z) = (0, -5, -2.1)$ m, in the absence of the DVAs. It can be observed again that the frequency content is mostly concentrated in the frequency range of 20 Hz to 40 Hz. This should be attributed to the

frequency spectrum of the dynamic wheel-rail interaction forces, since it has most of the spectral energy concentrated in that frequency range, as can be observed in Fig. 4.6. Moreover, as discussed in section 3.5.4, the presence of a propagation mode of the interior floor within this range of frequency could even magnify the concentration of spectral energy at the mentioned frequency range.

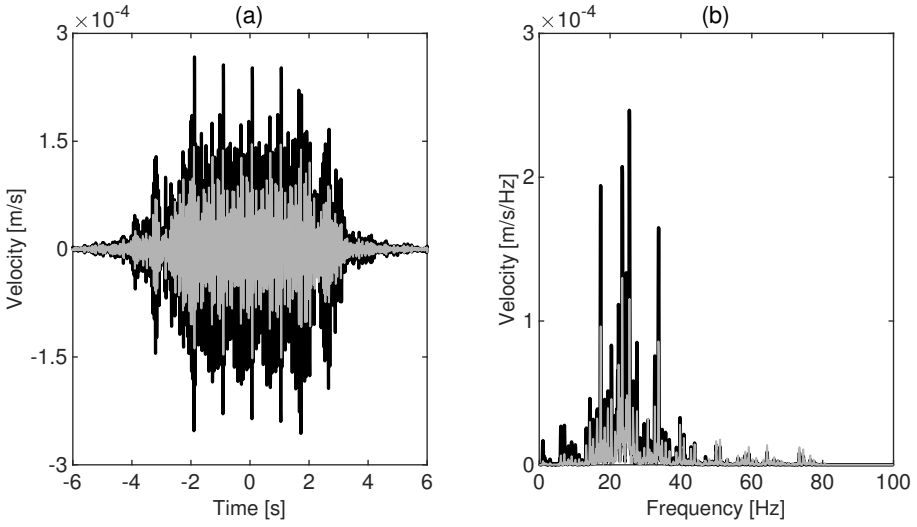

FIG. 4.5: Time history (a) and frequency spectrum (b) of the velocity of the tunnel wall at t_1 associated to y direction. Superimposed (in gray) time history and frequency spectrum of the vertical velocity at t_1.

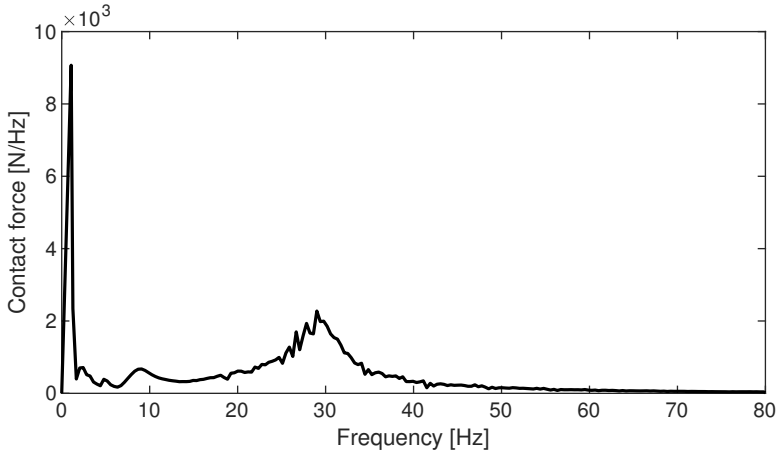

FIG. 4.6: Wheel-rail interaction contact force at the first wheel.

4.4.3 Experimental measurements required for the hybrid model

Vibration measurements have been performed in the building where the vibrations intended to be reduced (targeted building) and inside the double-deck tunnel underneath the building. The in-situ vibration measurements have been used in the following to substantiate the numerical results obtained previously in subsection 4.4.2 and to determine the tunnel-building transfer function to model the vibration propagation between the tunnel wall and the targeted building.

The configuration of the accelerometers for the vibration measurements inside the tunnel and the building is shown in Fig. 4.7. The measurement setup consists of three accelerometers on the interior floor (a_1, a_2 and a_3), two accelerometers on the tunnel wall (a_4 and a_5) and three accelerometers on the floor of the targeted building (b_1, b_2 and b_3). They have been used to simultaneously record the time history of the vibrations of the interior floor, tunnel wall and the building, respectively, caused by train pass-by. A 12-channel Siemens LMS XS Scadas is the data acquisition system used for measurements inside the tunnel and the building. The time history vibrations at the interior floor, at the tunnel wall and at the building have been simultaneously recorded for five train passes with a speed of 16.67 m/s. During the measurements, no train was circulating over the lower section of the double-deck tunnel and the road traffic in the vicinity of the building was light.

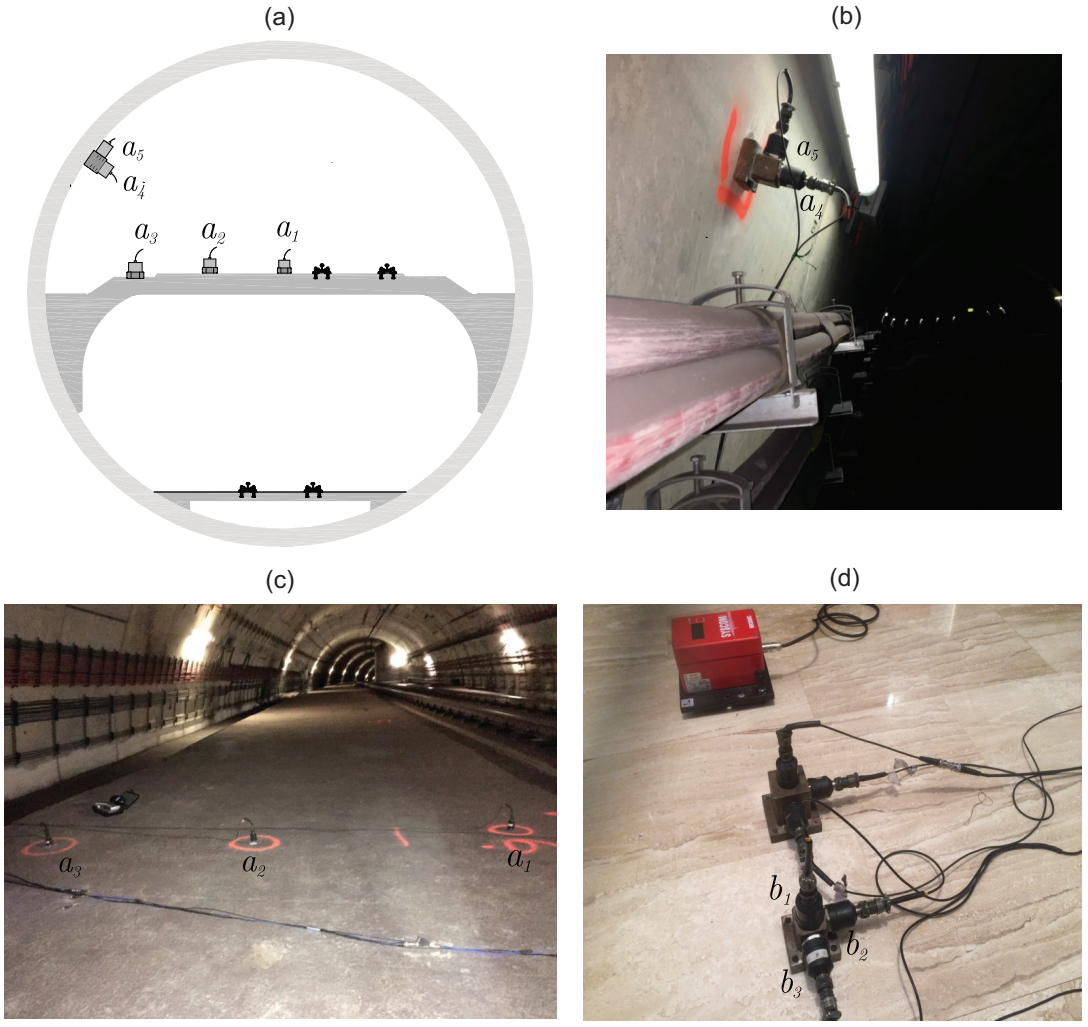

FIG. 4.7: Schematic representation of the setup of accelerometers used for the vibration measurements inside the tunnel (a). Accelerometers used to record time history of the tunnel wall (b), the interior floor (c) and the building (d) due to train pass-by.

Fig. 4.8 shows the vertical vibration acceleration spectra of the interior floor obtained using the proposed numerical prediction model at the points d_3 and d_{12} and the vibration measurements at the points a_1 and a_3. The points a_1 and d_3 represent the same location for both theoretical and experimental cases: $(x, y, z) = (0, -0.2, -0.5)$ m. In the same way, the points a_3 and d_{12} represent an evaluator at $(x, y, z) = (0, -3.5, -0.5)$ m. For both positions, the approximate agreement between the experimental and numerical results is observed for the frequency range between 25 Hz to 63 Hz, where the agreement between the results is generally within 8 dB. The numerical model prediction does not show good agreements with the experimental one for the frequencies above 63 Hz and below 20 Hz. The lack

of information about actual rail roughness profile and the soil parameters, along with the assumption that the model is longitudinally invariant (the interior floor consists on precast finite slabs and the particular coupling conditions between them cannot be neglected) are some of the parameters which are affecting the accuracy of the results of the numerical model.

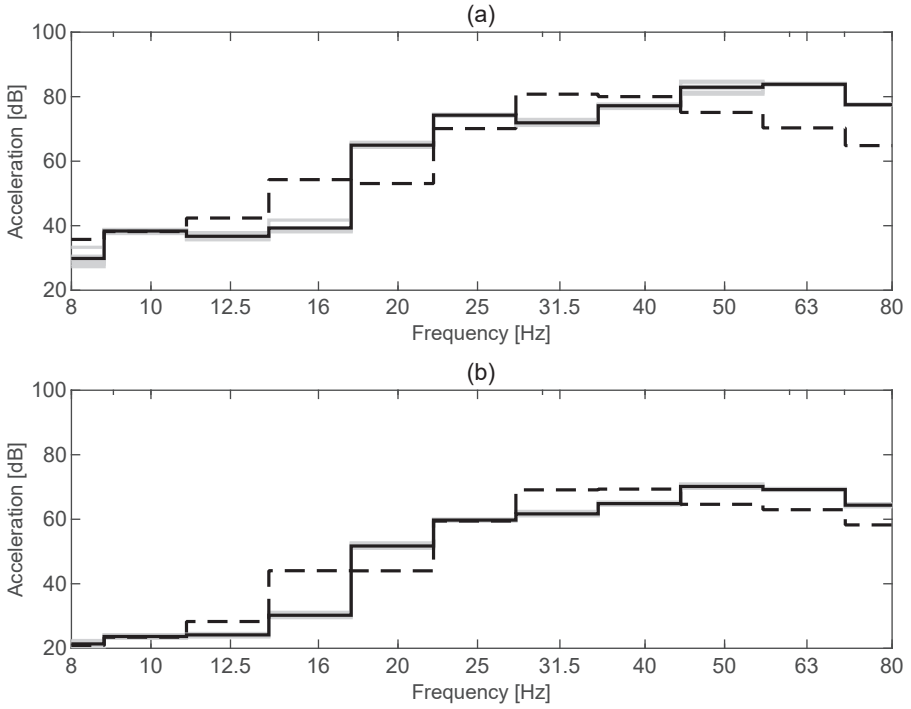

FIG. 4.8: One-third octave band spectra of the vertical vibration acceleration of the interior floor for the passage of the train in dB (dB reference 10^{-6} m s^{-2}): (a) Numerical prediction response (dashed black line) at d_3, five measured responses (gray lines) and the average of measured responses (dashed black line) at a_1; (b) Numerical prediction response (dashed black line) at d_{12}, five measured response (gray lines) and the average of measured responses (dashed black line) at a_3.

Fig. 4.9 shows the computed and the measured vibration acceleration spectra of the tunnel wall in y direction due to train pass-by. At some frequencies, a reasonable agreement between the computed and measured results have been observed. However, at the frequency of 31.5 Hz, the simulation is clearly overestimating the vibration acceleration level. In general, the level of the agreement for the tunnel wall evaluator is less than the one for the case of the interior floor. This can be attributed to the fact that the soil properties are much more significant for the response of the tunnel wall rather than for the interior floor. Therefore, a better

agreement would be achieved by defining soil properties more accurately, since in the the present model, the soil data is obtained from general geotechnical studies used in the L9 project. To solve this issue, in this thesis it is proposed to apply a correction factor on the numerically obtained response of the tunnel wall to fit the real response of the system. This correction factor would be the ratio between the measured and the computed response on the tunnel wall in the frequency domain (narrow band). Following the assumption explained in section 4.2.4, it is also assumed that the application of DVAs would not affect significantly the correction factor.

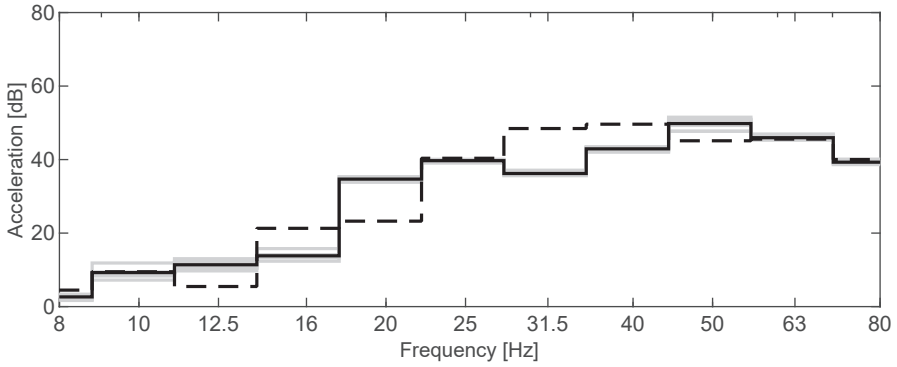

FIG. 4.9: One-third octave band spectra of the vibration acceleration of the tunnel wall in y direction in dB (dB reference 10^{-6} m s^{-2}). Dashed black line, gray lines and solid black line represent numerical prediction response, five measured responses and the average of measured responses, respectively.

In the hybrid model presented in this section, the vibration propagation between the tunnel wall and the targeted building is modeled using experimentally obtained transfer functions. These transfer functions can be computed based on the methodology explained in subsection 4.2.4, which requires the simultaneous vibration measurements in the tunnel wall and the targeted building. Using the proposed methodology, the transfer function has been computed for five train pass-by measurements, and their average is used as the main transfer function. These transfer functions and their average are shown in Fig. 4.10, where a frequency resolution of 0.5 Hz is used.

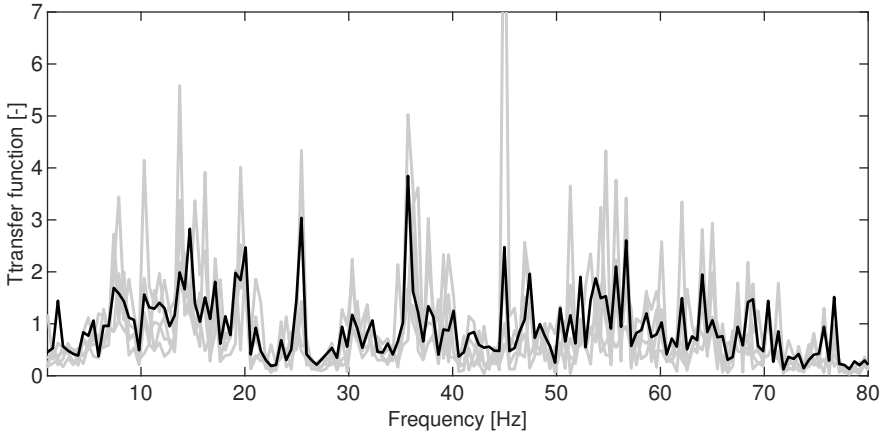

FIG. 4.10: Experimentally obtained transfer functions between the tunnel wall and the targeted building (gray lines) and average of all transfer functions (black line).

In order to compare the response on the building floor obtained experimentally and using the hybrid method, the following steps should be accounted for:

- Experimental response in the building: A single vibration acceleration spectrum of the targeted building floor can be obtained by Eq. (4.17) using the triaxial response of the building through experimental measurements.
- Response in the building by using the hybrid model: To obtain a single acceleration spectrum in the building by using the hybrid mode, four steps should be followoed:
    1. The triaxial response at the tunnel is computed by means of the 2.5D FE-BE approach;
    2. The correction factor is applied to fit the simulated response with the experimental one at the tunnel wall;
    3. The single acceleration spectrum at the tunnel wall should be computed using Eq. (4.16);
    4. The computed transfer function between the tunnel wall and the building is applied to obtain the vibration acceleration spectrum at the building floor.

Fig. 4.11 shows the predicted vibration acceleration spectrum of the targeted building obtained by following this methodology and the ones obtained using the

vibration measurements. As expected, a good agreement between the results can be observed because of the application of the correction factor previously presented.

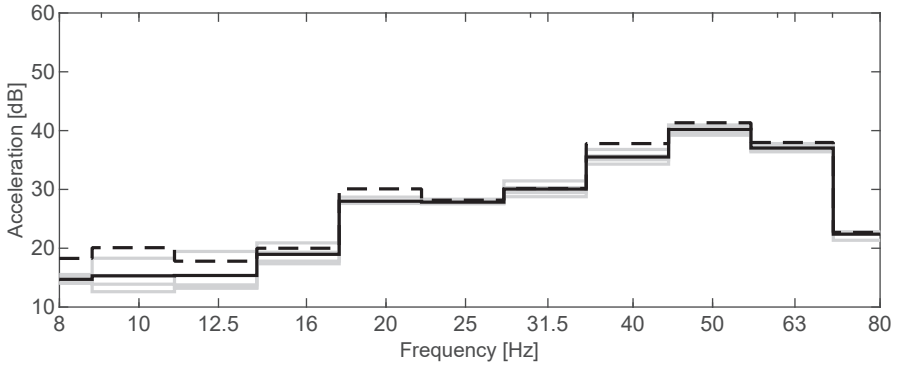

FIG. 4.11: One-third octave band spectra of the vibration acceleration at the targeted building floor in dB (dB reference 10^{-6} m s^{-2}). Dashed black line, gray lines, and solid black line represent numerical prediction response, five measured responses and the average of measured responses, respectively.

4.4.4 Application of DVAs

Only one distribution of DVAs is considered in this study. Among design variables, the mass of the DVAs and the number of DVAs in the distribution are defined in the pre-design stage (a common practice in designing DVAs [108]), ensuring that the static tensions to which the interior floor is subjected would stay approximately unchanged after adding DVAs. The remaining design variables, which are the transverse position of the DVAs distribution at the interior floor y_d, the distance between two consecutive DVAs l_d, the natural frequency of the DVAs f_d and viscous damping of the DVAs c_d are defined in the optimization process, based on GA, aiming to minimize the MTVV in the targeted building due to the passage of the train. For the optimization purpose, the Matlab Global Optimization Toolbox [109] has been used. The upper and lower bounds of these design variables and the value of the parameters defined in the pre-design stage are given in the following:

- y_d can be chosen from 12 possible positions, shown in Fig. 4.1.
- l_d is defined as a discrete variable, which can be chosen from 1 m to 8 m at intervals of 0.5 m. The space step has been restricted to 0.5 m because of

the size of the DVAs to be used. The distance between any two consecutive DVAs in distribution is assumed to be similar.

- m_d is defined in the pre-design stage. All DVAs are assumed to have the same mass of 800 kg.
- Number of DVAs per distribution is also defined in the pre-design stage, taking a value of 10 DVAs.
- f_d is defined as a discrete variable that can be chosen from 1 Hz to 80 Hz at intervals of 0.2 Hz.
- c_d is defined as a discrete variable that can be chosen from 31 kN s m^{-1} and 800 kN s m^{-1} at intervals of 12 kN s m^{-1}.

An optimization process has been performed to minimize the MTVV in the targeted building due to the application of a distribution of DVAs in the interior floor of the double-deck tunnel. A reduction of 3.3 dB in the MTVV at the targeted building has been achieved by applying one distribution of 10 DVAs with the parameters presented in Table 4.4.

TABLE 4.4: The optimum values of DVAs parameters and resulting IL.

y_d (m)	l_d (m)	f_d (Hz)	c_d (kN s m^{-1})	IL (dB)
-3.1	6	56.8	91.8	3.3

The vibration acceleration spectrum of the targeted building due to the train pass-by over the upper section of the tunnel has been computed before and after the application of optimal DVAs. The results are shown in Fig. 4.12.

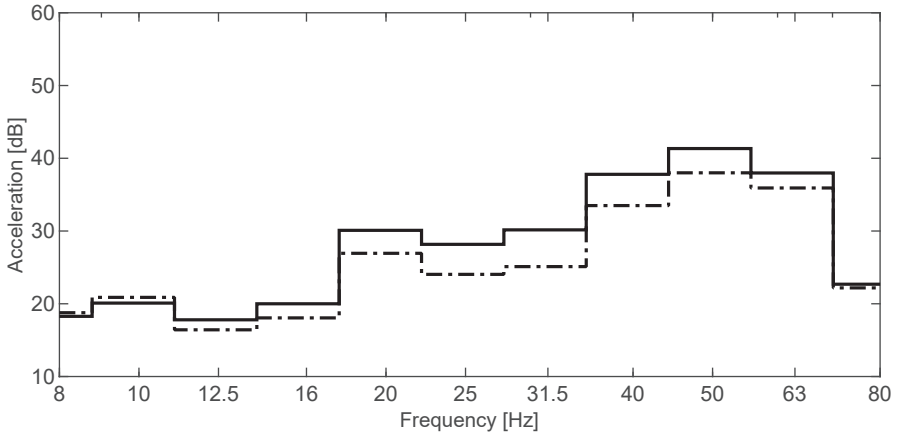

FIG. 4.12: One-third octave band spectra of the vibration acceleration of the targeted building in dB (dB reference 10^{-6} m s^{-2}) before (solid black line) and after (dashed black line) the application of the DVAs in the tunnel.

Chapter 5

Fast computation of 2.5D elastodynamic Green's functions in half-spaces

5.1 Introduction

A computationally efficient method to calculate Green's functions for 2.5D elastodynamic problems in homogeneous and horizontally layered half-spaces subjected to a harmonic load is presented in this section [116]. Exact expressions of the 3D stiffness matrix method for isotropic layered media in Cartesian coordinates are used to determine stiffness matrices for a horizontal layer and a half-space. In the absence of interfaces, virtual interfaces are considered at the positions of external loads. The analytic continuation is used to find the displacements at any receiver point placed within a layer. The responses of a horizontally layered half-space subjected to a unit harmonic load obtained using the present method are compared with those calculated using a well-established methodology, achieving good agreement. In addition, this Green's functions are used to present an extension for the fictitious force method [22]; and the results obtained using the new extension of the method and the original one is compared.

The remainder of the chapter is organized as follows. First, the derivation of the 3D stiffness matrices for the cases of a single layer and a lower/upper half-space is outlined in section 5.2. Afterwards, it is explained how to employ the stiffness matrices to compute 2.5D Green's functions in section 5.3. The 2.5D Green's functions for homogeneous and layered half-spaces calculated by employing the present method are compared with those obtained by using the method developed by Tadeu *et al.* [19] and calculated by following the methodology based on stiffness matrix method described in [3], respectively, in section 5.4. Moreover, an extension of the fictitious force method is explained in section 5.4.

5.2 3D Stiffness matrices in Cartesian coordinates

A brief explanation of the derivation of the expressions for the 3D stiffness matrices of a single layer and a lower half-space is presented in this section. Kausel presented the elements of the stiffness matrices for the plane strain case [117]. The same process is followed for the case of 3D wave propagation, resulting in the closed-form expressions for the elements of stiffness metrics in the wavenumber-frequency domain in Cartesian coordinates (x, y, z).

The motion within a 3D, homogeneous, isotropic and elastic medium can be written as [118]

$$(\lambda+\mu)\,\nabla\nabla\cdot\mathbf{u}-\mu\nabla\times\nabla\times\mathbf{u}+\rho\mathbf{f}=\rho\frac{\partial^2\mathbf{u}}{\partial t^2}, \tag{5.1}$$

where $\mathbf{u}$ and $\mathbf{f}$ are the vectors of the displacements and the body forces, respectively, ρ is the density of the medium, λ and μ are Lamé's first and second parameters, ∇ represents the Nabla operator and t stands for the time. Assuming the gravity as only body forces, it can be neglected by describing the motion about an equilibrium position. The displacement field in terms of the scalar (Φ) and vector ($\mathbf{\Psi}$) potentials can be written as

$$\mathbf{u}=\nabla\Phi+\nabla\times\mathbf{\Psi}, \tag{5.2}$$

in which the gauge condition is assumed to be $\nabla\cdot\mathbf{\Psi}=0$, for convenience. So, the elastic wave equation can be written as

$$\nabla^2\Phi=\frac{1}{\alpha^2}\frac{\partial^2\Phi}{\partial t^2}\quad\text{and}\quad\nabla^2\mathbf{\Psi}=\frac{1}{\beta^2}\frac{\partial^2\mathbf{\Psi}}{\partial t^2}, \tag{5.3}$$

where α and β represent the phase velocities of the P- and S-waves, respectively. By transforming Eq. (5.3) to the wavenumber-frequency domain (k_x,k_y,ω) through applying a 3D Fourier transform of the form

$$\hat{F}(k_x,k_y,z,\omega)=\int_{-\infty}^{+\infty}\int_{-\infty}^{+\infty}\int_{-\infty}^{+\infty}f(x,y,z,t)\mathrm{e}^{\mathrm{i}(k_xx+k_yy-\omega t)}\mathrm{d}x\mathrm{d}y\mathrm{d}t, \tag{5.4}$$

where k_x and k_y are the wavenumbers associated to the x and y coordinates, the scalar and vector Helmholtz equations can be found as

$$\frac{\mathrm{d}^2\hat{\Phi}}{\mathrm{d}z^2}+\upsilon_\alpha^2\hat{\Phi}=0,\quad\frac{\mathrm{d}^2\hat{\mathbf{\Psi}}}{\mathrm{d}z^2}+\upsilon_\beta^2\hat{\mathbf{\Psi}}=0 \tag{5.5}$$

respectively, where

$$\upsilon_\alpha=\sqrt{k_{xy}^2-k_\alpha^2},\qquad\upsilon_\beta=\sqrt{k_{xy}^2-k_\beta^2}, \tag{5.6}$$

and

$$k_{xy}=\sqrt{k_x^2+k_y^2},\qquad k_\alpha=\frac{\omega}{\alpha},\qquad k_\beta=\frac{\omega}{\beta}. \tag{5.7}$$

The general solution of Eq. (5.5) is

$$\hat{\Phi} = A_{\alpha_1} \mathrm{e}^{\upsilon_\alpha z} + A_{\alpha_2} \mathrm{e}^{-\upsilon_\alpha z}, \qquad \hat{\mathbf{\Psi}} = \begin{Bmatrix} A_{\beta_1} \mathrm{e}^{\upsilon_\beta z} + A_{\beta_2} \mathrm{e}^{-\upsilon_\beta z} \\ A_{\beta_3} \mathrm{e}^{\upsilon_\beta z} + A_{\beta_4} \mathrm{e}^{-\upsilon_\beta z} \\ A_{\beta_5} \mathrm{e}^{\upsilon_\beta z} + A_{\beta_6} \mathrm{e}^{-\upsilon_\beta z} \end{Bmatrix}, \tag{5.8}$$

being A_{α_1}, A_{α_2}, A_{β_1}, A_{β_2}, A_{β_3}, A_{β_4}, A_{β_5} and A_{β_6} unknown constants. Substituting the general solutions of the Helmholtz equations into the transformed form of Eq. (5.2) in the wavenumber-frequency domain results in general displacements as

$$\hat{\mathbf{U}} = \mathbf{R}_1 \mathbf{E}_z^{-1} \mathbf{a}_1 + \mathbf{R}_2 \mathbf{E}_z \mathbf{a}_2. \tag{5.9}$$

Capital letters and ˆdenote that the variables are defined in the (k_x, k_y, ω) domain, where ω is the angular frequency and k_x and k_y are the wavenumbers along the x and y directions, respectively. $\mathbf{a}_1$ and $\mathbf{a}_2$ are vectors of unknown arbitrary constants. $\mathbf{R}_1$, $\mathbf{R}_2$, $\mathbf{E}_z$ and $\mathbf{E}_z^{-1}$ are calculated from

$$\mathbf{R}_1 = \begin{bmatrix} 1 & -\dfrac{k_y}{k_x} & -\dfrac{\upsilon_\beta}{k_x} \\ \dfrac{k_y}{k_x} & 1 & 0 \\ -\dfrac{\upsilon_\alpha}{k_x} & 0 & 1 \end{bmatrix}, \tag{5.10}$$

$$\mathbf{R}_2 = \begin{bmatrix} 1 & -\dfrac{k_y}{k_x} & \dfrac{\upsilon_\beta}{k_x} \\ \dfrac{k_y}{k_x} & 1 & 0 \\ \dfrac{\upsilon_\alpha}{k_x} & 0 & 1 \end{bmatrix}, \tag{5.11}$$

$$\mathbf{E}_z = \begin{bmatrix} \mathrm{e}^{\upsilon_\alpha z} & & \\ & \mathrm{e}^{\upsilon_\beta z} & \\ & & \mathrm{e}^{\upsilon_\beta z} \end{bmatrix} \tag{5.12}$$

and

$$\mathbf{E}_z^{-1} = \begin{bmatrix} \mathrm{e}^{-\upsilon_\alpha z} & & \\ & \mathrm{e}^{-\upsilon_\beta z} & \\ & & \mathrm{e}^{-\upsilon_\beta z} \end{bmatrix} \tag{5.13}$$

respectively.

The stresses in horizontal planes can be written as a function of the displacements [117]. Using the displacements defined in Eq. (5.9), the solution for the stresses can be written as

$$\hat{\mathbf{T}}_z = \mu \left(-\mathbf{Q}_1 \mathbf{E}_z^{-1} \mathbf{a}_1 + \mathbf{Q}_2 \mathbf{E}_z \mathbf{a}_2 \right), \tag{5.14}$$

where $\mathbf{Q}_1$ and $\mathbf{Q}_2$ are defined as

$$\mathbf{Q}_1 = \begin{bmatrix} 2\upsilon_\alpha & -\dfrac{\upsilon_\beta k_y}{k_x} & -k_x - \dfrac{\upsilon_\beta^2}{k_x} \\ \dfrac{2\upsilon_\alpha k_y}{k_x} & \upsilon_\beta & -k_y \\ -\dfrac{k_{xy}^2}{k_x} - \dfrac{\upsilon_\beta^2}{k_x} & 0 & 2\upsilon_\beta \end{bmatrix} \tag{5.15}$$

and

$$\mathbf{Q}_2 = \begin{bmatrix} 2\upsilon_\alpha & -\dfrac{\upsilon_\beta k_y}{k_x} & k_x + \dfrac{\upsilon_\beta^2}{k_x} \\ \dfrac{2\upsilon_\alpha k_y}{k_x} & \upsilon_\beta & k_y \\ \dfrac{k_{xy}^2}{k_x} + \dfrac{\upsilon_\beta^2}{k_x} & 0 & 2\upsilon_\beta \end{bmatrix} \tag{5.16}$$

respectively.

5.2.1 Stiffness matrix of a layer

Consider Fig. 5.1, a free horizontal homogeneous, isotropic and elastic layer with arbitrary thickness h is subjected to arbitrary distributed tractions $\mathbf{P}_u$ and $\mathbf{P}_l$ on the upper and lower interfaces, respectively.

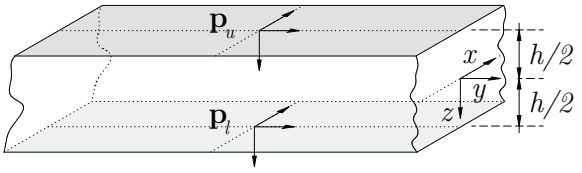

FIG. 5.1: Free body diagram of a layer without body forces.

The displacements and tractions at the upper and lower interfaces can be found by evaluating Eqs. (5.9) and (5.14) at these interfaces as

$$\begin{Bmatrix} \hat{\mathbf{U}}_u \\ \hat{\mathbf{U}}_l \end{Bmatrix} = \begin{bmatrix} \mathbf{R}_1\mathbf{E}_{h/2} & \mathbf{R}_2\mathbf{E}_{h/2}^{-1} \\ \mathbf{R}_1\mathbf{E}_{h/2}^{-1} & \mathbf{R}_2\mathbf{E}_{h/2} \end{bmatrix} \begin{Bmatrix} \mathbf{a}_1 \\ \mathbf{a}_2 \end{Bmatrix} \tag{5.17}$$

and

$$\begin{Bmatrix} \hat{\mathbf{P}}_u \\ \hat{\mathbf{P}}_l \end{Bmatrix} = \mu \begin{bmatrix} \mathbf{Q}_1\mathbf{E}_{h/2} & -\mathbf{Q}_2\mathbf{E}_{h/2}^{-1} \\ -\mathbf{Q}_1\mathbf{E}_{h/2}^{-1} & \mathbf{Q}_2\mathbf{E}_{h/2} \end{bmatrix} \begin{Bmatrix} \mathbf{a}_1 \\ \mathbf{a}_2 \end{Bmatrix}. \tag{5.18}$$

respectively.

Combining the displacements and tractions by eliminating the constants and performing the matrix operations analytically, the stiffness matrix of the layer can be written in closed-form expressions as

$$\begin{Bmatrix} \hat{\mathbf{P}}_u \\ \hat{\mathbf{P}}_l \end{Bmatrix} = \begin{bmatrix} \hat{\mathbf{K}}_{11} & \hat{\mathbf{K}}_{12} \\ \hat{\mathbf{K}}_{21} & \hat{\mathbf{K}}_{22} \end{bmatrix} \begin{Bmatrix} \hat{\mathbf{U}}_u \\ \hat{\mathbf{U}}_l \end{Bmatrix}, \tag{5.19}$$

where closed-form expressions for the elements of this stiffness matrix are

$$\hat{\mathbf{K}}_{11} = \frac{\mu}{D}\frac{k_\beta^2}{k_{xy}^2}\mathbf{A}_1 + \mu\mathbf{A}_2, \tag{5.20}$$

$$\hat{\mathbf{K}}_{12} = \frac{\mu}{D}\frac{k_\beta^2}{k_{xy}^2}\mathbf{A}_3 + \mu\mathbf{A}_4, \qquad \hat{\mathbf{K}}_{21} = \hat{\mathbf{K}}_{12}^{\mathrm{T}}, \tag{5.21}$$

$$\hat{\mathbf{K}}_{22} = \hat{\mathbf{K}}_{11} \circ \begin{bmatrix} 1 & 1 & -1 \\ 1 & 1 & -1 \\ -1 & -1 & 1 \end{bmatrix}. \tag{5.22}$$

In the above equations, μ is Lamé's second parameter, the superscript T denotes the transpose operator, $\circ$ is the Hadamard product and coefficient D is calculated from:

$$D = 2\mathrm{e}^{(\upsilon_\beta - \upsilon_\alpha)h} - 2C_\alpha C_\beta + \left(\frac{k_{xy}^2}{\upsilon_\alpha \upsilon_\beta} + \frac{\upsilon_\alpha \upsilon_\beta}{k_{xy}^2} \right) B_\alpha B_\beta, \tag{5.23}$$

$$B_\alpha = \frac{1 - \mathrm{e}^{-2\upsilon_\alpha h}}{2}, \qquad B_\beta = \frac{1 - \mathrm{e}^{-2\upsilon_\beta h}}{2}, \tag{5.24}$$

$$C_\alpha = \frac{1 + \mathrm{e}^{-2\upsilon_\alpha h}}{2}, \qquad C_\beta = \frac{1 + \mathrm{e}^{-2\upsilon_\beta h}}{2}. \tag{5.25}$$

Matrices A_1, A_2, A_3 and A_4 are obtained from:

$$\mathbf{A}_1 = \begin{bmatrix} \frac{k_x^2}{\upsilon_\beta} D_1 & \frac{k_x k_y}{\upsilon_\beta} D_1 & k_x D_3 \\ \frac{k_x k_y}{\upsilon_\beta} D_1 & \frac{k_y^2}{\upsilon_\beta} D_1 & k_y D_3 \\ k_x D_3 & k_y D_3 & \frac{k_{xy}^2}{\upsilon_\alpha} D_2 \end{bmatrix}, \tag{5.26}$$

$$D_1 = B_\beta C_\alpha - \frac{\upsilon_\alpha \upsilon_\beta}{k_{xy}^2} B_\alpha C_\beta, \qquad D_2 = B_\alpha C_\beta - \frac{\upsilon_\alpha \upsilon_\beta}{k_{xy}^2} B_\beta C_\alpha, \tag{5.27}$$

$$D_3 = \mathrm{e}^{-(\upsilon_\alpha + \upsilon_\beta)h} - C_\alpha C_\beta + \left(\frac{k_{xy}^2}{\upsilon_\alpha \upsilon_\beta} \right) B_\alpha B_\beta, \tag{5.28}$$

$$\mathbf{A}_2 = \begin{bmatrix} \upsilon_\beta \frac{k_y^2}{k_{xy}^2} \frac{C_\beta}{B_\beta} & -\upsilon_\beta \frac{k_x k_y}{k_{xy}^2} \frac{C_\beta}{B_\beta} & -2k_x \\ -\upsilon_\beta \frac{k_x k_y}{k_{xy}^2} \frac{C_\beta}{B_\beta} & \upsilon_\beta \frac{k_x^2}{k_{xy}^2} \frac{C_\beta}{B_\beta} & -2k_y \\ -2k_x & -2k_y & 0 \end{bmatrix}, \tag{5.29}$$

$$\mathbf{A}_3 = \begin{bmatrix} -\dfrac{k_x^2}{\upsilon_\beta} D_4 & -\dfrac{k_x k_y}{\upsilon_\beta} D_4 & k_x D_6 \\ -\dfrac{k_x k_y}{\upsilon_\beta} D_4 & -\dfrac{k_y^2}{\upsilon_\beta} D_4 & k_y D_6 \\ -k_x D_6 & -k_y D_6 & -\dfrac{k_{xy}^2}{\upsilon_\alpha} D_5 \end{bmatrix}, \tag{5.30}$$

$$D_4 = B_\beta \mathrm{e}^{-\upsilon_\alpha h} - \frac{\upsilon_\alpha \upsilon_\beta}{k_{xy}^2} B_\alpha \mathrm{e}^{-\upsilon_\beta h}, \quad D_5 = B_\alpha \mathrm{e}^{-\upsilon_\beta h} - \frac{\upsilon_\alpha \upsilon_\beta}{k_{xy}^2} B_\beta \mathrm{e}^{-\upsilon_\alpha h}, \tag{5.31}$$

$$D_5 = B_\alpha \mathrm{e}^{-\upsilon_\beta h} - \frac{\upsilon_\alpha \upsilon_\beta}{k_{xy}^2} B_\beta \mathrm{e}^{-\upsilon_\alpha h}, \tag{5.32}$$

$$D_6 = C_\beta \mathrm{e}^{-\upsilon_\alpha h} - C_\alpha \mathrm{e}^{-\upsilon_\beta h}, \tag{5.33}$$

and

$$\mathbf{A}_4 = \begin{bmatrix} -\upsilon_\beta \dfrac{k_y^2}{k_{xy}^2} \dfrac{\mathrm{e}^{-\upsilon_\beta h}}{B_\beta} & \upsilon_\beta \dfrac{k_x k_y}{k_{xy}^2} \dfrac{\mathrm{e}^{-\upsilon_\beta h}}{B_\beta} & 0 \\ \upsilon_\beta \dfrac{k_x k_y}{k_{xy}^2} \dfrac{\mathrm{e}^{-\upsilon_\beta h}}{B_\beta} & -\upsilon_\beta \dfrac{k_x^2}{k_{xy}^2} \dfrac{\mathrm{e}^{-\upsilon_\beta h}}{B_\beta} & 0 \\ 0 & 0 & 0 \end{bmatrix}. \tag{5.34}$$

5.2.2 Stiffness matrix of a lower half-space

Consider a homogeneous, isotropic and elastic lower half-space, Fig. 5.2, subjected to an arbitrarily distributed traction $\mathbf{P}_u$. As Sommerfeld radiation condition has

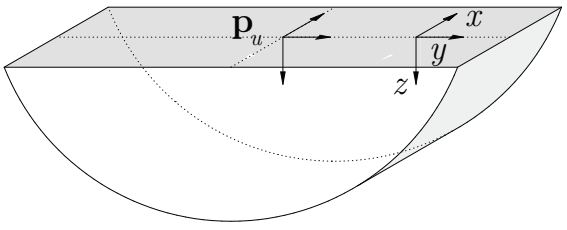

FIG. 5.2: Free body diagram of a lower half-space without body forces.

to be satisfied ($\Phi \to 0$ and $\mathbf{\Psi} \to 0$ when $z \to \infty$), the displacement and the

traction can be written, respectively, as

$$\hat{\mathbf{U}}_u = \mathbf{R}_1\mathbf{a}_1 \quad \text{and} \quad \hat{\mathbf{P}}_u = \mu\mathbf{Q}_1\mathbf{a}_1. \tag{5.35}$$

By eliminating the arbitrary constants vector, $\mathbf{a}_1$, the displacements and traction at the upper interface can be related by means of the stiffness matrix which can be found from

$$\hat{\mathbf{K}}_h = \mu\mathbf{Q}_1\mathbf{R}_1^{-1}. \tag{5.36}$$

Closed-form expressions for the elements of the stiffness matrix of a lower half-space, $\hat{\mathbf{K}}_h$, are

$$\hat{\mathbf{K}}_h = \frac{\mu}{k_{xy}^2 - \upsilon_\alpha\upsilon_\beta}\begin{bmatrix} k_y^2\upsilon_{\beta\alpha} + k_\beta^2\upsilon_\alpha & -k_xk_y\upsilon_{\beta\alpha} & k_xD_H \\ -k_xk_y\upsilon_{\beta\alpha} & k_x^2\upsilon_{\beta\alpha} + k_\beta^2\upsilon_\alpha & k_yD_H \\ k_xD_H & k_yD_H & k_\beta^2\upsilon_\beta \end{bmatrix}, \tag{5.37}$$

where

$$\upsilon_{\beta\alpha} = \upsilon_\beta - \upsilon_\alpha, \quad D_H = 2\upsilon_\alpha\upsilon_\beta - {\upsilon_\beta}^2 - k_{xy}^2. \tag{5.38}$$

5.3 2.5D Green's functions for homogeneous and layered half-spaces

Consider an arbitrarily layered half-space with an arbitrary distribution of receiver points and sources located within the half-space. Based on the methodology proposed in this chapter, the following steps must be taken to obtain the 2.5D Green's functions that relate all the desired receiver points and sources:

1. Add a virtual interface for every source that has not been placed on any of the physical layer interfaces.

2. Follow the same approach used in the finite element method to assemble the global stiffness matrix for the layered media, $\hat{\mathbf{K}}$ in Eq. (5.39), while considering physical and virtual interfaces.

3. Use the concept of analytic continuation, as described by Kausel [117], to obtain the displacements at receiver points within a layer, i.e. those not located at physical or virtual interfaces, in terms of the layers' interface displacements. Then, by means of the inverse of the global stiffness matrix, $\hat{\mathbf{H}}(k_x, k_y, \omega)$ which defines the displacements of all the receiver points as a function of the tractions at the sources' location can be constructed.

4. Compute the 2.5D Green's functions of the system $\bar{\mathbf{H}}$, in the (k_x, y, ω) domain, accounting for all the selected receiver points and sources by applying an inverse Fourier transform (FT) in the y direction on $\hat{\mathbf{H}}(k_x, k_y, \omega)$.

$$\begin{Bmatrix} \hat{\mathbf{P}}_1 \\ \hat{\mathbf{P}}_2 \\ \vdots \\ \hat{\mathbf{P}}_j \\ \vdots \\ \hat{\mathbf{P}}_N \end{Bmatrix} = \underbrace{\begin{bmatrix} \hat{\mathbf{K}}_{11}^{l_1} & \hat{\mathbf{K}}_{12}^{l_1} & \mathbf{0} & \dots & \mathbf{0} \\ \hat{\mathbf{K}}_{21}^{l_1} & \hat{\mathbf{K}}_{22}^{l_1} + \hat{\mathbf{K}}_{11}^{l_2} & \hat{\mathbf{K}}_{12}^{l_2} & \dots & \mathbf{0} \\ \mathbf{0} & \hat{\mathbf{K}}_{21}^{l_2} & \hat{\mathbf{K}}_{22}^{l_2} + \hat{\mathbf{K}}_{11}^{l_3} & \ddots & \vdots \\ \vdots & \vdots & \ddots & \ddots & \hat{\mathbf{K}}_{12}^{l_{(N-1)}} \\ \mathbf{0} & \mathbf{0} & \dots & \hat{\mathbf{K}}_{21}^{l_{(N-1)}} & \hat{\mathbf{K}}_{22}^{l_{(N-1)}} + \hat{\mathbf{K}}_h \end{bmatrix}}_{\hat{\mathbf{K}}} \begin{Bmatrix} \hat{\mathbf{U}}_1 \\ \hat{\mathbf{U}}_1 \\ \vdots \\ \hat{\mathbf{U}}_i \\ \vdots \\ \hat{\mathbf{U}}_N \end{Bmatrix} \tag{5.39}$$

Eq. (5.39) governs the tractions-displacements relation in all interfaces of a N-layered half-space. $\hat{\mathbf{U}}_i$ represents the three components (ordered according to x, y and z) of displacements and $\hat{\mathbf{P}}_j$ represents the three components of forces on the i and j interfaces, respectively, considering the surface as the first interface. In the global stiffness matrix $\hat{\mathbf{K}}$, where each element is a 3×3 matrix, stiffness matrix elements of the n^{th} layer are denoted by the superindex l_n and $\hat{\mathbf{K}}_h$ is the stiffness matrix of a lower half-space.

In the following, 2.5D Green's functions for a homogeneous and layered half-space subjected to a buried harmonic load are determined by using the proposed method and they are compared, in terms of accuracy and computational efficiency, with those calculated by using well-established solutions. For the case of a homogeneous half-space, the Green's functions are compared with the ones obtained using a semi-analytical solution developed by Tadeu *et al.* [19]; the actual formulation of this semi-analytical solution can compute 2.5D Greens' functions between only two positions in the soil. However, the present method can find the Greens' functions

between multiple positions in the soil. For the case of a layered half-space, the results are compared with the ones obtained using cylindrical formulation of the stiffness matrix method [39] which needs more numerical operation in comparison with the present method.

5.4 Results and discussion

As noted previously, different methods have been proposed in the literature to compute the 2.5D Green's functions of homogeneous and layered half-spaces. In this section, it is explained how the present method can decrease the computational costs of calculating the 2.5D Greens' functions, besides its accuracy is evaluated through comparisons between the Greens' functions obtained using the proposed method and previously derived methodologies for the following cases:

Case 1: Surface response of a homogeneous half-space subjected to a buried load;

Case 2: Buried response of a homogeneous half-space subjected to a buried load;

Case 3: Buried response of a layered half-space subjected to a buried load;

Case 4: An extension of the fictitious force method.

For the cases 1 and 2, both associated to a homogeneous half-space, the 2.5D Green's functions calculated by employing the proposed method have been compared with the ones obtained using a semi-analytical solution, developed by Tadeu *et al.* [19]. In Tadeu's method, a set of 2.5D imaginary forces is considered to simulate the free surface on a homogeneous full-space. These imaginary sources can be found by imposing the free surface boundary condition of zero stresses on the surface. The summation of the 2.5D Green's functions for a homogeneous full-space [20] with the motions resulting from the imaginary sources lead to the 2.5D Green's functions of a homogeneous half-space.

For the case of a layered half-space, the 2.5D Green's functions computed by using the present method are compared with the ones obtained by means of the stiffness matrix method in cylindrical coordinates [39]. From a computational point of view, the two methods follow different schemes. In the proposed method, the computational steps are: i) inversion of the global matrix based on 6×6 elementary

matrices; ii) an inverse FT along k_y; and iii) a one-dimensional (1D) interpolation. On the other hand, the method based on stiffness matrices in cylindrical coordinates was developed according to the following steps: i) inversion of the global matrices associated with P-SV and SH waves, separately, to obtain the Green's functions in the (k_r, ω) domain; ii) computation of the Green's functions in the (r, θ, ω) domain by means of an inverse Hankel transform and an inverse Fourier series expansion in the radial and circumferential directions, respectively; iii) a 2D interpolation process to find the Green's functions in the (x, y, ω) domain; and iv) a numerical FT along x to obtain the 2.5D Green's functions in the (k_x, y, ω) domain.

In order to compare the accuracy of the computed 2.5D Green's functions with the new method against previous well-established methodologies, an almost exact solution of the 2.5D Green's functions have to be computed for each case of first three cases. This almost exact solution (reference solution from here on) is computed using Tadeu's method [19] for homogeneous half-spaces and the one described in [3] for layered half-spaces. The reference solution is obtained by subsequently increasing the sampling points and reducing the spacing between them until the solution converges to a sufficiently accurate value. Then, to quantify the accuracy of an arbitrary 2.5D Green's function, an averaged relative error against the reference solution is used. This relative error is computed for each frequency by averaging the results along the wavenumber using the root mean square.

5.4.1 Case 1: Surface response of a homogeneous half-space subjected to a buried load

In Fig. 5.3 an example of the case 1 is shown. As there is only one applied load, only one virtual interface, shown as a dashed line, is added at where the buried load is placed. Therefore, the homogeneous half-space is divided into a homogeneous layer and a lower half-space with the same mechanical parameters. The 2.5D Green's functions can be obtained using the process described in section 5.3. For this example, the global stiffness matrix of the system can be written as

$$\hat{\mathbf{K}} = \begin{bmatrix} \hat{\mathbf{K}}_{11}^{l_1} & \hat{\mathbf{K}}_{12}^{l_1} \\ \hat{\mathbf{K}}_{21}^{l_1} & \hat{\mathbf{K}}_{22}^{l_1} + \hat{\mathbf{K}}_h \end{bmatrix}. \tag{5.40}$$

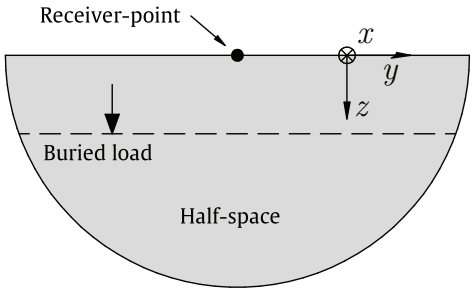

FIG. 5.3: A homogeneous half-space with a virtual interface (dashed lines) placed at the position of the buried load; the receiver-point placed on the surface.

In the following, the numerical parameters used in the computation of the Greens functions are presented. The frequency sampling vector have the range of $[1, 100]$ Hz, with the increments of 1 Hz. The receiver-point and the load are located at $(y_r, z_r) = (4, 0)$ m and $(y_f, z_f) = (2, 10)$ m, respectively. The selected sampling vector for k_x has 2^9 points with increments of 0.01 rad/m. The inverse Fourier transform used for moving from the (k_x, k_y, ω) domain to the 2.5D domain, (k_x, y, ω), is computed using the fast Fourier transform. The mechanical parameters of the soil used in the calculations are given in Table 5.1. Noteworthy, complex-valued Lamé parameters are used to transform the elastic media into a viscoelastic one, being D_p and D_s in Table 5.1 the hysteretic damping ratios for P- and S-waves.

TABLE 5.1: Mechanical parameters used to model the soil in sections 5.4.1 and 5.4.2

Soil parameters	Values
E (MPa)	300
ρ (kg m^{-3})	2000
ν (-)	0.2
D_p (-)	0.03
D_s (-)	0.03

In Fig. 5.4, a comparison between the results obtained using Tadeu's method and the new one for the parameters previously defined is shown. For this comparison, the k_y sampling used in the new method is based on increments of 0.04 rad/m and 2^{10} points. For Tadeu's method, a set of imaginary sources is used which represents the same sampling used for the new method, taking 2^{10} points and a distance between imaginary sources of 0.1534 m. The results presented in this

figure are the ones obtained at 30 Hz. As shown, both methods have a good agreement on the results.

To check the accuracy of the 2.5D Green's functions computed using the new method for a range of frequencies, a reference solution, calculated based on a convergence error of 10^{-8}, is used. For the reference solution, this relative error is ensured for each frequency and wavenumber. The relative errors of the new method and Tadeu's method against this reference solution are shown in Fig. 5.5. The errors obtained with both methods are similar, which implies that the new method is as accurate as the Tadeu's methodology.

5.4.2 Case 2: Buried response of a homogeneous half-space subjected to a buried load

An example of the case 2 is shown in Fig. 5.6. There are no interfaces at positions of the receiver-point and applied load. A virtual interface, shown as dashed line, is added at where the load is placed. Therefore, like case 1, the homogeneous half-space is divided into a homogeneous layer and a lower half-space; the global stiffness matrix is the same as the one of the case 1, Eq. 5.40. However, the elements of the stiffness matrix are not the same as case 1, because the position of the force has been changed.

The 2.5D Green's functions for case 2 can be obtained through using analytic continuation and the inverse of the global stiffness matrix, following the process explained in section 5.3.

The numerical parameters used in the computation of the Green's functions are presented in the following. The selected frequency sampling vector have the range of $[1, 100]$ Hz, with the increments of 1 Hz. The receiver-point and load are placed at $(y_r, z_r) = (4, 3)$ m and $(y_f, z_f) = (2, 10)$ m, respectively. 2^9 points with the increments of 0.01 rad/m are used to sample k_x. The inverse Fourier transform used for moving from the (k_x, k_y, ω) domain to the 2.5D domain, (k_x, y, ω), is computed using the fast Fourier transform. The mechanical parameters of the soil used in the calculations are given in Table 5.1. Noteworthy, complex-valued Lamé parameters are used in order to transform the elastic media into a viscoelastic one, being D_p and D_s in Table 5.1 the hysteretic damping ratios for P- and S-waves.

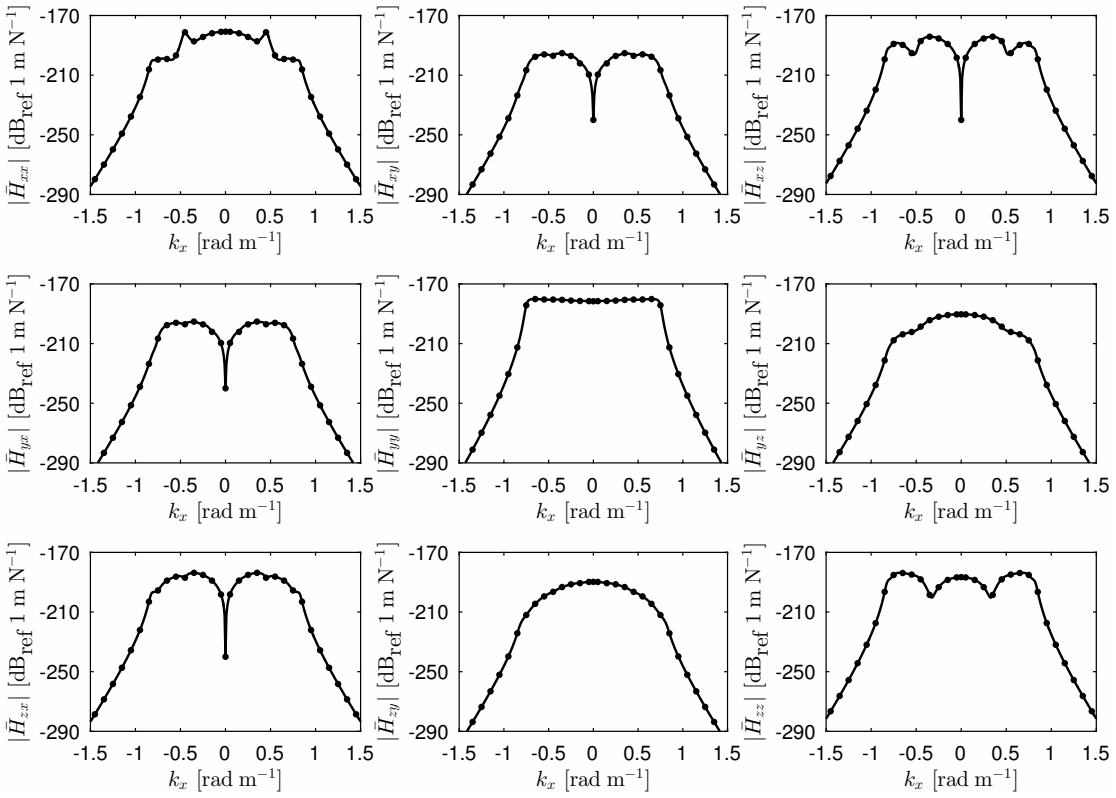

(a)

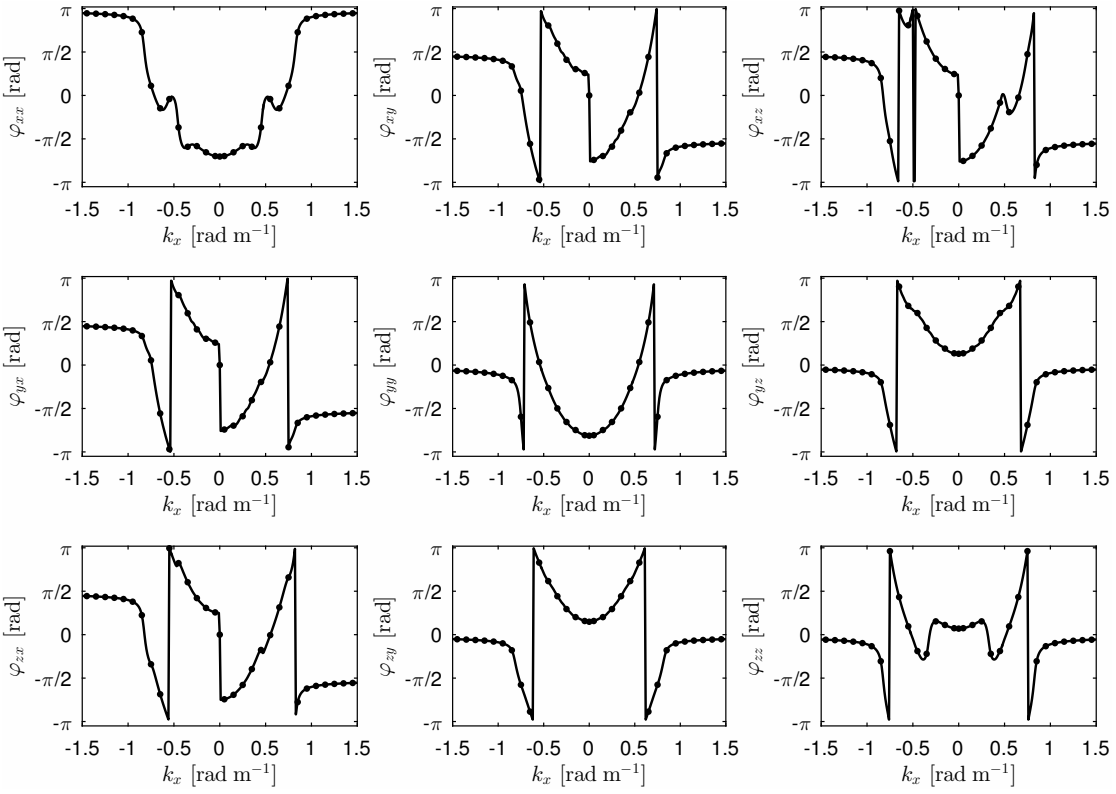

(b)

FIG. 5.4: Amplitude (a) and phase values (b) of the 2.5D Green's functions at 30 Hz for case 1. Solid and dotted lines are used to represent the results obtained using Tadeu's method and the new one, respectively.

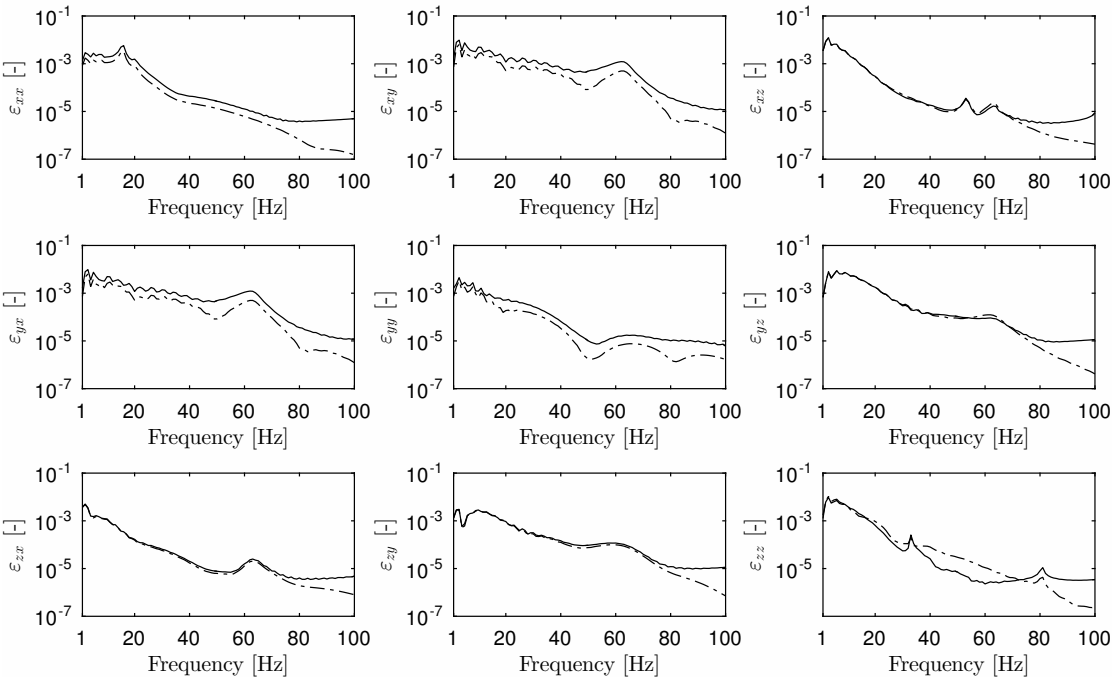

FIG. 5.5: Relative errors of the 2.5D Green's functions with respect to the reference solution for new method (solid lines) and for Tadeu's method (dashed lines) for case 1.

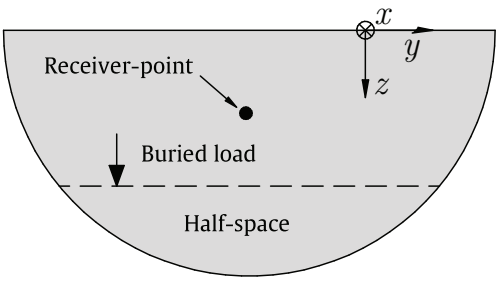

FIG. 5.6: A homogeneous half-space with buried receiver-point and buried load; the virtual interface (dashed lines) placed at the position of the buried load.

A comparison between the results calculated using Tadeu's method and the new one for the parameters defined previously is shown in Fig. 5.7. The results presented in this figure are the ones obtained at 30 Hz. For this comparison, the k_y sampling used in the new method is based on increments of 0.04 rad/m and 2^{10} points. For Tadeu's method, a set of imaginary sources is used which represents the same sampling used for the new method, taking 2^{10} points and a distance between imaginary sources of 0.1534 m. As shown, a good agreement is obtained between the results of the two methods.

To check the accuracy of the 2.5D Green's functions computed using the new

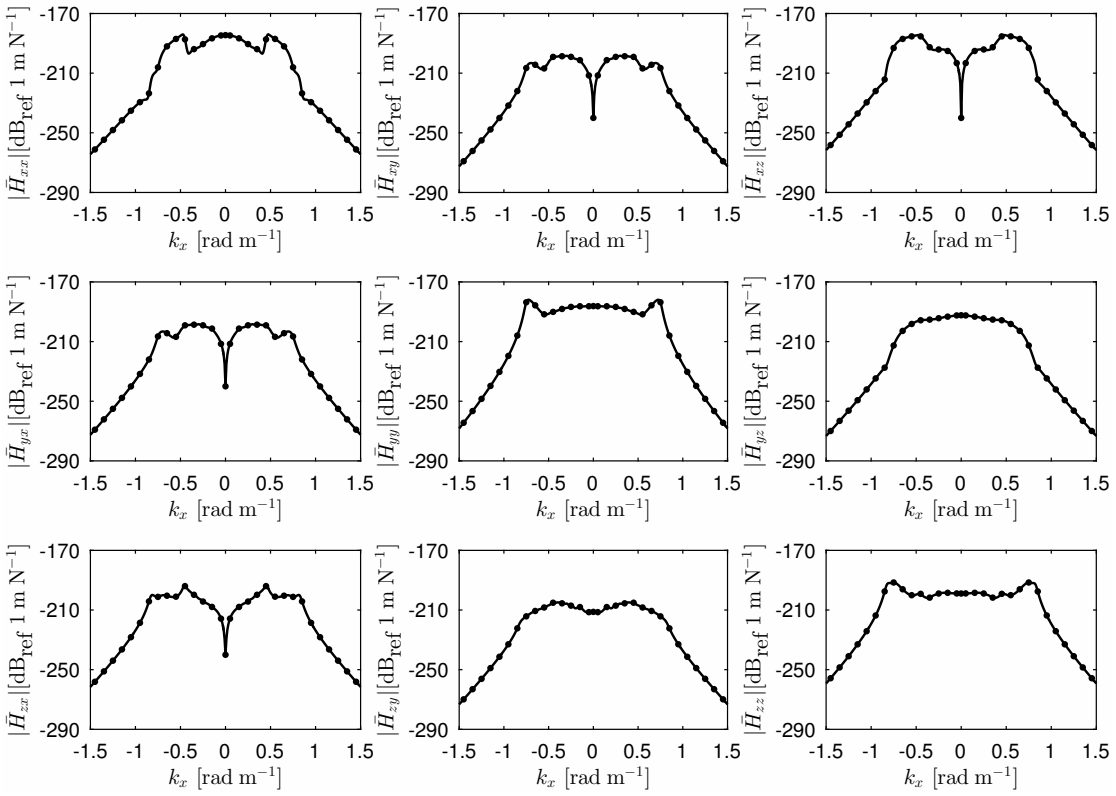

(a)

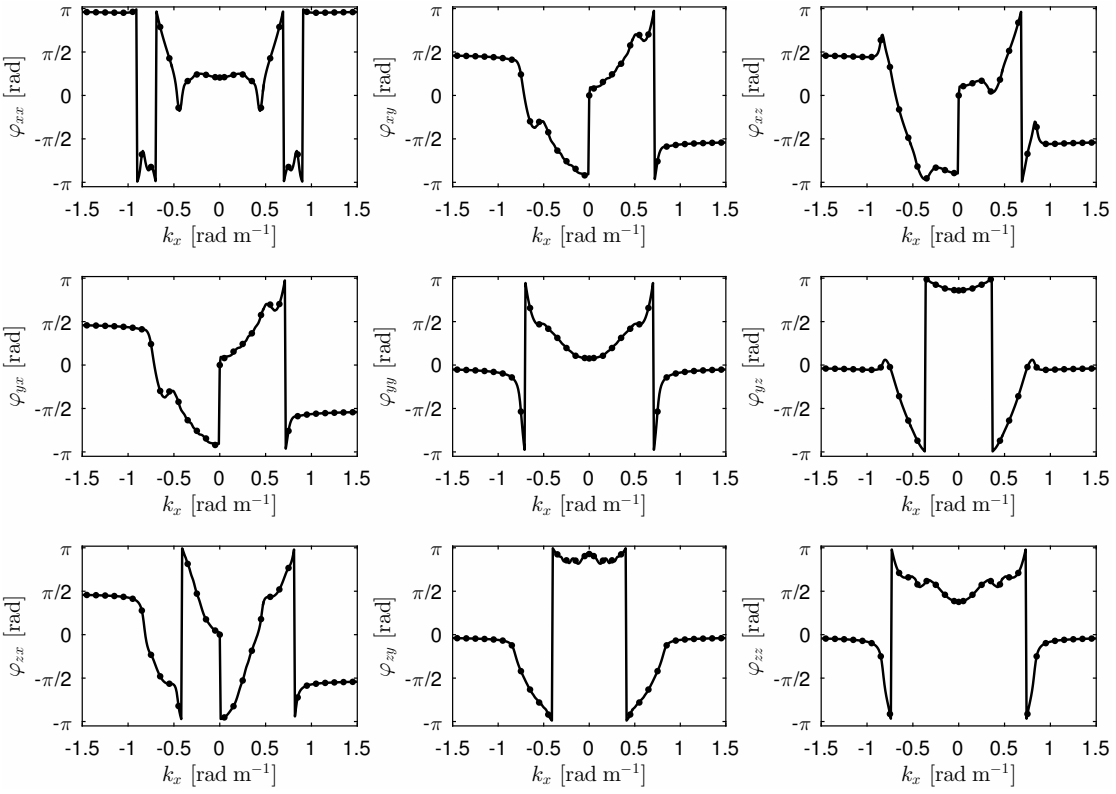

(b)

FIG. 5.7: Amplitude (a) and phase values (b) of the 2.5D Green's functions at 30 Hz for case 2. Solid and dotted lines are used to represent the results obtained using Tadeu's method and the new one, respectively.

method for a range of frequencies, a reference solution, calculated based on a convergence error of 10^{-8}, is used. For the reference solution, this relative error is ensured for each frequency and wavenumber. The relative errors of the new method and Tadeu's method against this reference solution are shown in Fig. 5.8. The errors obtained with both methods are similar, which implies that the new method is as accurate as the Tadeu's methodology.

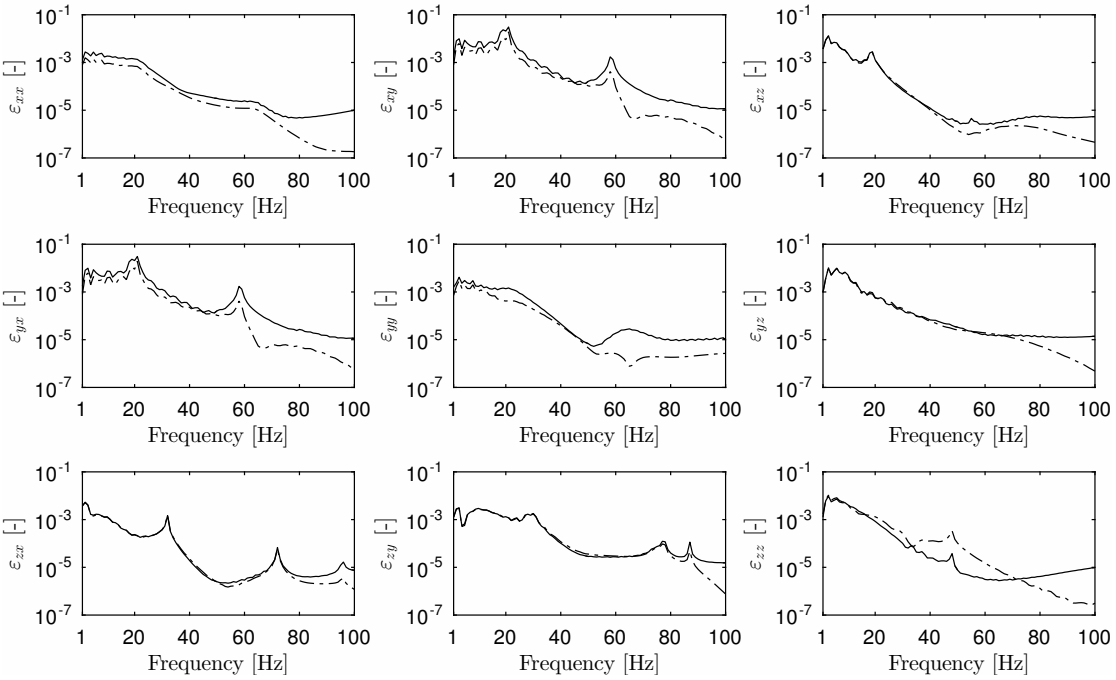

FIG. 5.8: Relative errors of the 2.5D Green's functions with respect to the reference solution for new method (solid lines) and for Tadeu's method (dashed lines) for case 2.

5.4.3 Case 3: Buried response of a layered half-space subjected to a buried load.

An example of case 3 is shown in Fig. 5.9. A virtual interface, represented by the dashed line, is added where the load is applied. A receiver-point is located within the first physical layer of the layered half-space. Therefore, the three-layered half-space is divided into the one with three homogeneous layers and a lower half-space.

In the following, the numerical parameters used in the computation of the Green's function are presented. The receiver point and the source were placed at $(y_r, z_r) =$

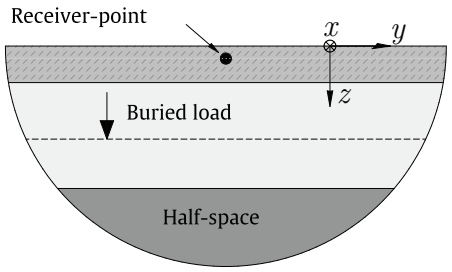

FIG. 5.9: A three-layered half-space with the virtual interfaces, dashed lines, considered for buried load and receiver-point.

$(6, 8)$ m and $(y_f, z_f) = (2, 23)$ m, respectively. We calculated the 2.5D Green's functions for this particular case. A sampling vector with 2^9 points and increments of 0.01 rad/m was selected for k_x. To transform the Green's functions from (k_x, k_y, ω) domain to the 2.5D domain (k_x, y, ω), the inverse fast Fourier transform (FFT) is carried out over a set of 2^{10} values of k_y with increments of 0.04 rad/m. The mechanical parameters of the soil used in the calculations are given in Table 5.2. Hysteretic damping ratios D_p and D_s corresponding to P- and S-waves, respectively, were used to account for viscoelasticity. The selected frequency sampling vector have the range of $[1, 100]$ Hz, with the increments of 1 Hz.

TABLE 5.2: Mechanical parameters used to model the soil in section 5.4.3.

Soil parameters	1st layer values	2nd layer values	3rd layer values
E (MPa)	366	390	420
ρ (kg m^{-3})	2000	2200	2500
ν (-)	0.3	0.25	0.2
D_p (-)	0.03	0.03	0.03
D_s (-)	0.03	0.03	0.03

Fig. 5.10 features a comparison between the results obtained using the new method and the ones computed by means of the stiffness matrix method in cylindrical coordinates [39] for the parameters previously defined is shown. For this comparison, the k_y sampling used in the new method is based on increments of 0.04 rad/m and 2^{10} points. The values presented in the figure correspond to a frequency of 30 Hz. As can be noted, this is good agreement between two sets of results.

Fig. 5.11 shows an example of a sampling grid for computing the 2.5D Green's function with the proposed method. The y axis could be linear or logarithmic, depending on the sampling used for the FT. Interpolation is only needed along

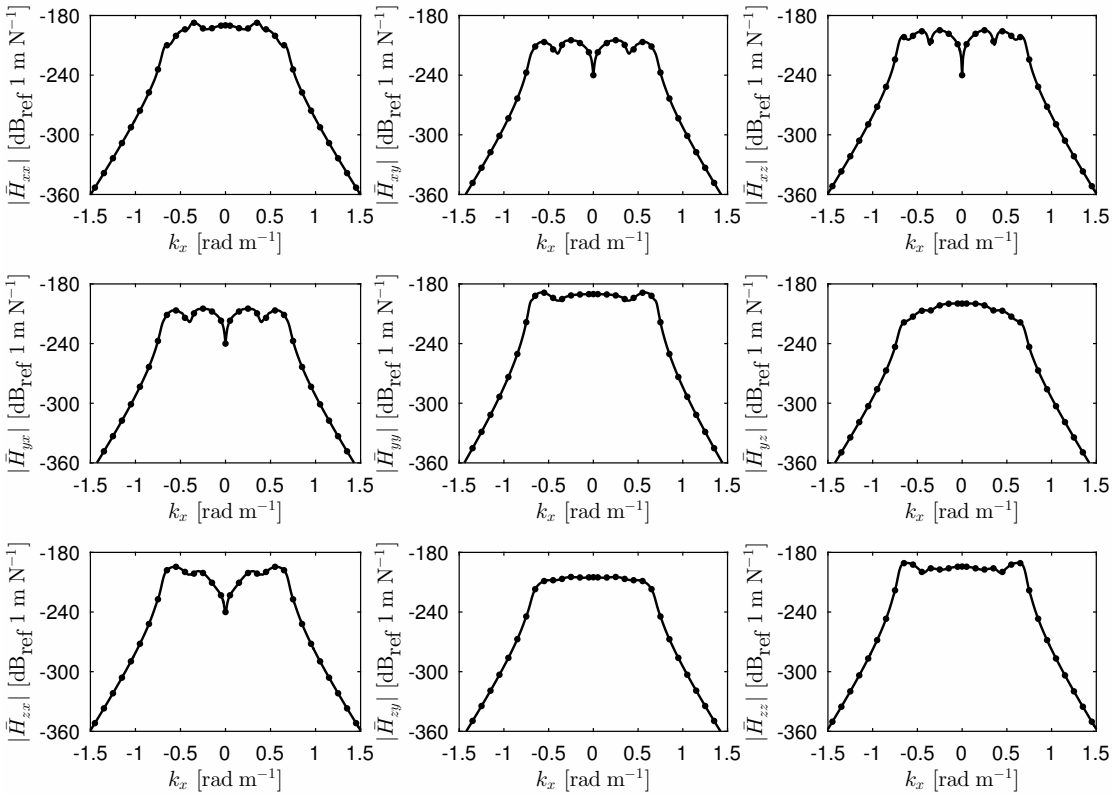

FIG. 5.10: Amplitude (a) and phase values (b) of the 2.5D Green's functions at 30 Hz for case 3. Solid and dotted lines are used to represent the results obtained using the stiffness matrix method in cylindrical coordinate [3] and the new one, respectively.

the y direction, since the required positions may not coincide with the sampling associated with the FT.

Fig. 5.12 is an example of a sampling grid for the method based on stiffness matrices in cylindrical coordinates. Black solid points represent the sampling associated with the direct output of the method. Grey circles correspond to the required sampling points. This example considers the same sampling along x for any required y value. The data obtained directly from this method must be translated from a cylindrical to a Cartesian sampling grid using 2D interpolation. This process will generally induce larger numerical errors than the proposed method, particularly for large values of y, due to the geometrical relationship between cylindrical and Cartesian coordinate systems.

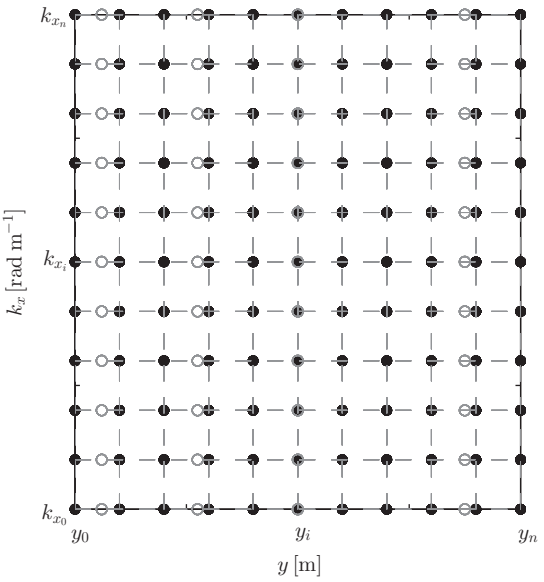

FIG. 5.11: Sampling grid obtained directly using the proposed method (black solid points). The required points are denoted by grey circles.

5.4.4 Case 4: An extension of the fictitious force method

The fictitious force method is an extension of the PiP model to calculate the vibration induced by a tunnel embedded in a layered half-space. In the following, the fictitious force method is explained briefly; A detailed overview of the methodology can be found in [22]. Consider a tunnel embedded in a layered half-space. The near-field dynamic behavior of a tunnel-soil system can be assumed to be the one

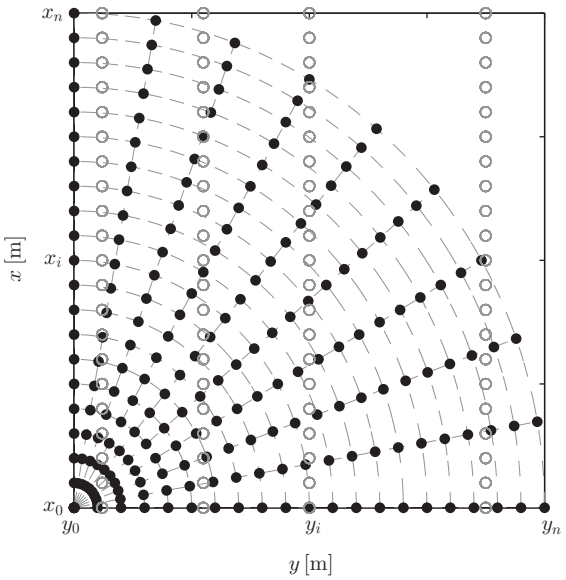

FIG. 5.12: Sampling grid obtained directly from the method based on the stiffness matrices in cylindrical coordinates (black solid points). The required points are denoted by grey circles.

associated to a tunnel embedded in a full-space with the mechanical parameters of the layer that contains the tunnel in the original model. Besides, the model is defined in the basis of a 2.5D approach, which means that the system is assumed to be invariant along the longitudinal direction, therefore, the 3D problem can be decomposed into a set of 2D models which depend on the wavenumber along the invariant direction. The fictitious force method consists of the following three steps:

1. Calculating tunnel-soil interface displacements: The tunnel-soil interface displacements due to a point load on the tunnel invert is calculated using the PiP model [57]. It is assumed that the tunnel is embedded in a homogeneous full-space with the mechanical parameters of the layer that contains the tunnel;

2. Calculating equivalent forces: A set of equivalent forces which are able to reproduce the tunnel-soil interface displacements in a full-space (without the embedded tunnel) are determined. 2.5D Green's functions for a homogeneous full-space, developed by Tadeu and Kausel [20], are employed;

3. Calculating responses at receivers due to the equivalent forces: The response at the receivers can be computed through multiplying the equivalent forces by the required 2.5D Green's functions of the layered half-space.

Fig. 5.13 shows a schematic representation of these steps. The third step is computationally more expensive than the two first steps. In the fictitious force method, these 2.5D Green's functions of the half-space, i.e. third step, are evaluated by means of the stiffness matrix method in cylindrical coordinates [39, 117]. The computational efficiency and accuracy of this method can be increased using new 2.5D Green's functions for a layered half-space, presented in this section, in the third step.

Consider Fig. 5.14, in which a tunnel with outer radius and thickness of 3 m and 0.25 m, respectively, buried in a layered half-space is presented. an algorithm that computes the 2.5D Green's functions of a layered half-space based on the

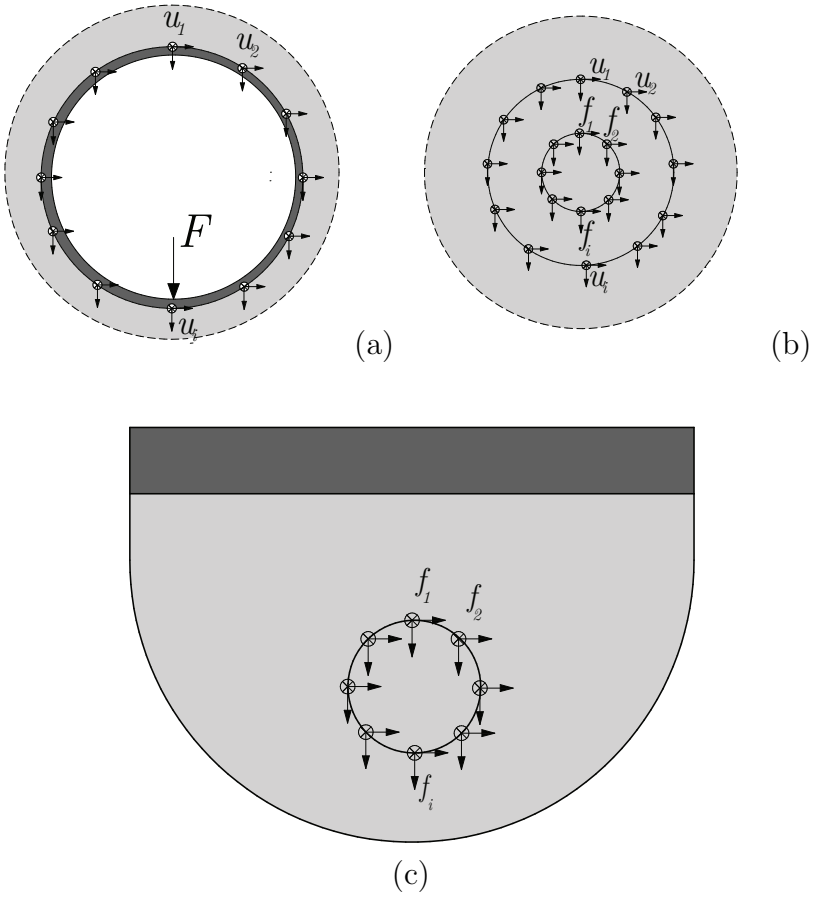

FIG. 5.13: Schematic representation of (a) first (b) second and (c) third step of the fictitious force method.

new presented method is used in the third step of the fictitious force method to calculate far-field displacements of a tunnel buried in a layered half-space. After this, the results are compared with the ones obtained through the methodology that uses the stiffness matrix method in cylindrical coordinates.

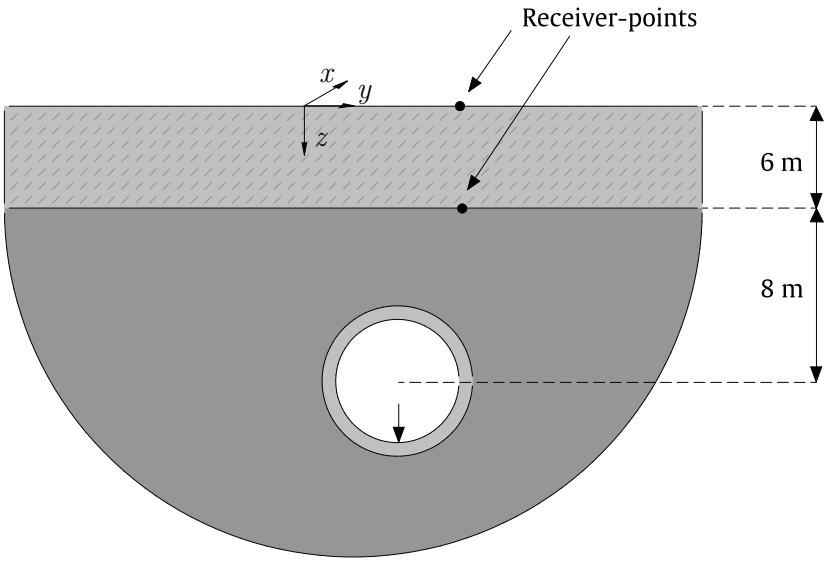

FIG. 5.14: A circular tunnel embedded in a layered half-space.

The mechanical parameters of the soil and the tunnel are given in Tables 5.3 and 5.4. A numerical example has been carried out in the basis of this system. The PiP model has been employed to calculate the displacement fields at 20 positions at tunnel-soil interface due to a load applied at the tunnel invert. The tunnel is assumed to be embedded in a full-space with mechanical parameters of the 2$^{\text{nd}}$ layer. Then, the virtual forces have been computed at r =1 m at 20 positions by means of 2.5D Green's functions for the full-space [20]. Finally, the responses at the receiver-points due to the virtual forces have been computed using the 2.5D Green's functions for the layered half-space evaluated by means of the stiffness matrix method in Cartesian and cylindrical coordinates. The latter has been computed using the ElastoDynamics Toolbox (EDT) [4].

The amplitudes of the three displacement fields at the receiver-point, placed at $(y_{rp}, z_{rp}) = (10, 6)$ m, are plotted versus k_x in Fig 5.15-a for a frequency of 60 Hz. $|H_{ij}|$ represents the response in the i direction due to the force acting along the j direction. Their related phase values, φ_{ij}, are plotted in Fig 5.15-b. As it can be seen, the H_{xz} is antisymmetric but H_{yz} and H_{zz} are symmetric with respect to the k_x. The same comparisons has been provided for the receiver-point placed

TABLE 5.3: Mechanical parameters used to model the soil in section 5.4.4.

Soil parameters	1st layer values	2nd layer values
E (MPa)	446	286
ρ (kg m^{-3})	1980	1980
ν (-)	0.49	0.49
D_p (-)	0.06	0.06
D_s (-)	0.06	0.06

TABLE 5.4: Mechanical parameters used to model the tunnel in sections 5.4.4.

Tunnel parameters	Values
E (GPa)	50
ρ (kg m^{-3})	2500
ν (-)	0.3
D_p (-)	0.03
D_s (-)	0.03

at $(y_{rp}, z_{rp}) = (10, 0)$ m. The results are shown in Fig 5.16. As it was expected, increasing the y results in disagreement between the results of the two methods.

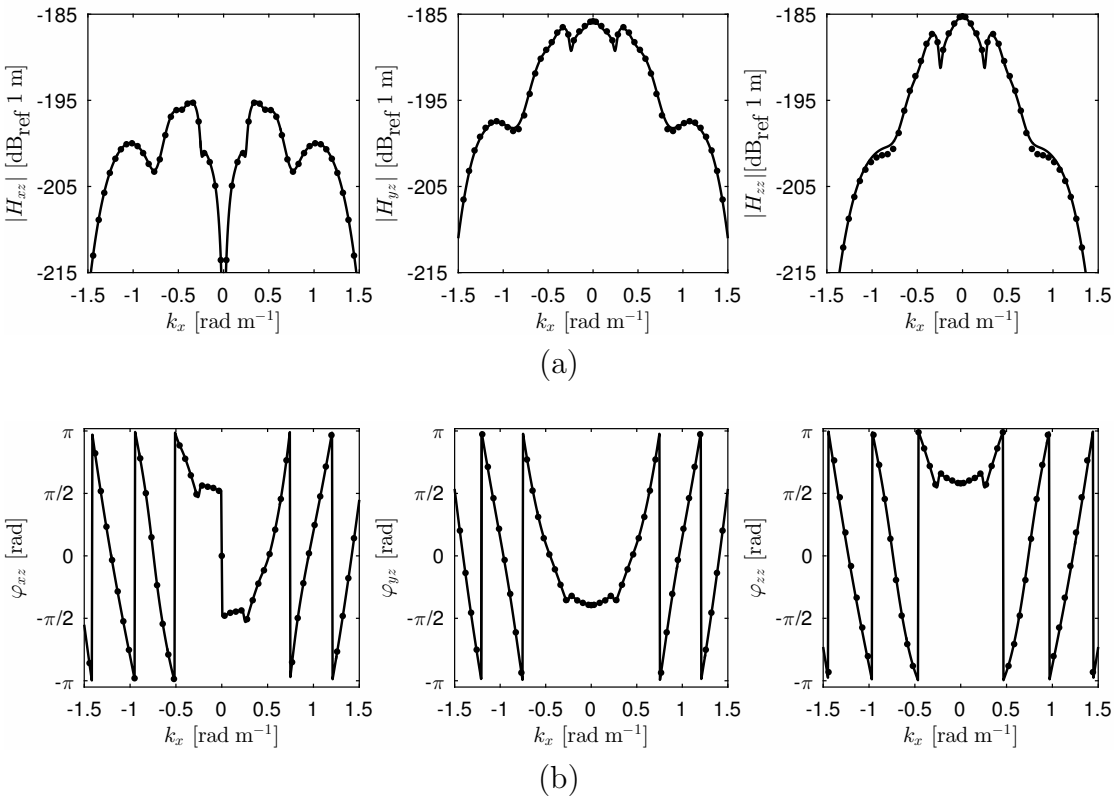

FIG. 5.15: Amplitude (a) and phase values (b) at $(y_{rp}, z_{rp}) = (10, 6)$ at 60 Hz. Solid and dotted lines are used to represent the results obtained using the present method and using EDT [4], respectively.

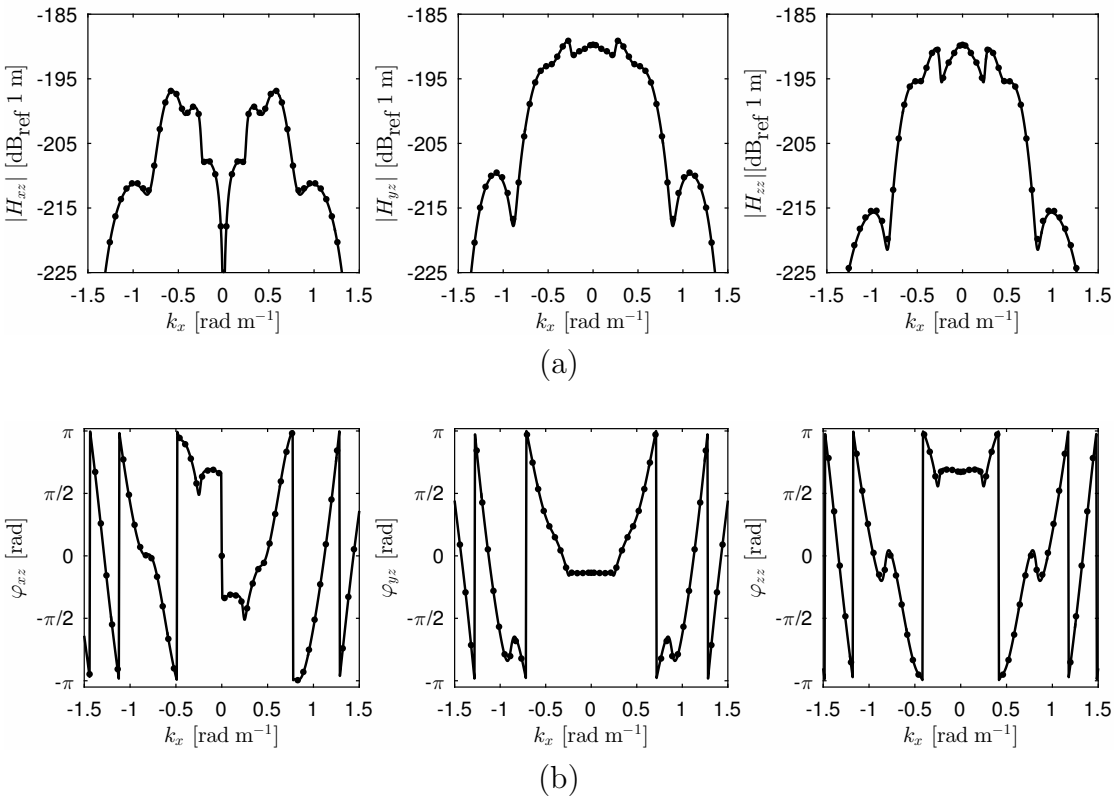

FIG. 5.16: Amplitude (a) and phase values (b) at $(y_{rp}, z_{rp}) = (10, 0)$ at 60 Hz. Solid and dotted lines are used to represent the results obtained using the present method and using EDT [4], respectively.

Chapter 6

Conclusions and further work

In this chapter, the summary of the main findings of this research is presented. Moreover, a number of recommendations for further research on the topic is proposed.

6.1 Conclusions

In this dissertation, the potential of DVAs as a measure to address underground railway-induced ground-borne vibration problems in the context of double-deck tunnels is investigated. For this purpose, first, a methodology for coupling a set of longitudinal distributions of DVAs to any railway subsystem in the context of a theoretical dynamic model of a railway infrastructure is developed. Then, this methodology is used to couple a set of DVAs to the interior floor of a double-deck tunnel. Afterward, the response of this coupled system due to train traffic is computed and the optimum design parameters of the DVAs are obtained using an optimization process based on a genetic algorithm to minimize this response.

Two approaches have been followed to assess the performance of DVAs as vibration countermeasures: i) Evaluation the efficiency of DVAs in mitigation of the energy flow radiated upwards by the tunnel; ii) Assessment of the capability of the DVAs in minimizing MTVV in a building near an underground railway infrastructure. Results obtained regarding each approach is summed up in the following.

Regarding the first approach, a 2.5D semi-analytical model of a train-track-tunnel-soil system that considers a full-space soil model is used. The performance of one longitudinal distribution of optimized DVAs has been evaluated for two different types of soil and two different train speeds. In all of the four cases, they have been found to be efficient in reducing the total energy flow radiated by the tunnel. The obtained ILs of the total radiated energy flow due to the application of DVAs for the four cases show that the harder the soil is and the faster the train is, the more effective the optimized DVAs are. In the best scenario, a reduction of 6.6 dB in the total radiated energy flow has been achieved. The results show that DVAs provide significant vibration attenuation benefits by tuning their optimum natural frequencies to be set down in the range of frequency where most of the spectral energy content is concentrated. It is also found that the mode shapes of the interior floor are modified after the application of DVAs. The affectation on the mode shapes can strongly modify the energy flow radiation pattern from the

tunnel. In contrast, this does not considerably affects the dynamic response of the rails.

For the second approach, a hybrid experimental-numerical model of a train-track-tunnel-soil-building system is employed. In the hybrid model, a numerical model of the tunnel-soil system based on 2.5D coupled FE-BE approach, a semi-analytical model for the track and a dynamic rigid multi-body model of the vehicle are used to compute the response in the tunnel wall. Then, the response in the building is computed using experimentally obtained transfer functions between the tunnel wall and the building floor. This hybrid model provides sufficient level of accuracy in the response prediction of the building only if the parameters of the system are accurately known. In case that high accuracy in the input parameters can be achieved, it is proposed to use a correction factor of the tunnel wall vibration spectrum which has been assumed to be not very dependent of the DVAs application. It is found that using one distribution of ten optimal DVAs results in a reduction of 3.3 dB in MTVV inside the building.

It is expected that using more than one longitudinal distribution of DVAs would result in a greater reduction either in the total radiated energy flow or the MTVV inside the building. It should be noted that DVAs would be a more cost-effective solution for existing underground railway networks than, for example, vibration isolation screens, building base isolation or fasteners retrofitting, as the implementation and manufacturing of DVAs would be cheaper than other vibration countermeasures.

In this dissertation, a computationally efficient method for calculating 2.5D Green's functions in the wavenumber-frequency domain for a homogeneous and layered half-spaces has been also presented. This method is based on explicit expressions of the 3D stiffness matrices for layered isotropic media in Cartesian coordinates defined in the (k_x, k_y, ω) domain. If there is no receiver-point within the layers, the 2.5D Green's functions in the (k_x, y, ω) domain can be found by applying an inverse Fourier transform in the y direction on the inverse of the global stiffness matrix, calculated with the mentioned 3D stiffness matrices in the (k_x, k_y, ω) domain. If there are receiver-points within the layers, the analytic continuation, described by Kausel [117], need to be employed to obtain the 2.5D Green's functions.

For the case of a homogeneous half-space, the 2.5D Green's functions calculated

using the proposed method are compared with the semi-analytical solution developed by Tadeu *et al.* [19]. A very good agreement between the results has been achieved. The new method can be used to compute the Green's functions at multiple receiver-points due to multiple loads by using fast Fourier transform algorithms, which is a more computationally efficient procedure than Tadeu's method. However, Tadeu's method could also be implemented using fast Fourier transform algorithms, although this implementation would still be less simple and efficient than the proposed method implementation because of the complexity of the Tadeu's formulation.

For the case of a layered half-space, the results obtained through the present method are in good agreement with those obtained using the method based on stiffness matrices in cylindrical coordinates. The present method can be used to improve the accuracy of the required interpolations, especially for large values of y. In addition, this method requires fewer numerical steps to obtain the 2.5D Green's functions of the system. In general, this more streamlined process should result in a more computationally accurate method. The proposed Green's functions for the layered half-space has been employed to present an extension of the fictitious force method. In a general point of view, the new methodology is more computationally efficient than the previous one because of the fewer numerical integral transformations. The results of applying the fictitious force method using both methodologies are compared and a very good agreement is obtained.

As a general conclusion for the present thesis, the potential of DVAs a countermeasures for ground-borne vibrations induced by underground railway traffic is proved at least for the case of double-deck tunnel infrastructre. Reductions up to 6.6 dB in total energy flow radiated by the tunnel and up to 3.3 dB in the vibration inside a nearby building demonstrate this statement.

6.2 Further work

In the following, some further researches on the present topic are proposed:

1. Considering the results obtained from this investigation, the foremost action would be the application of DVAs prototypes in a real case study in order to evaluate their efficiency practically. This study is currently in progress for the L9 of Barcelona metro. For this purpose, first, the limitation of the numerical model is going to be addressed aiming of getting a better agreement between prediction and experimental results. Model updating techniques will be used in this regard.

2. In this context, an study of the validity of the correction factor used for the practical application of the DVAs in L9 Barcelona metro is another future work that it is intended to perform.

3. In this study, the application of only one distribution of DVAs has been studied. However, it is expected that using more than one longitudinal distribution of DVAs would result in a greater vibration reduction. Noteworthy, determining the optimal value for more than one distribution of DVAs require a more computationally efficient optimization algorithm.

4. As the objective function defined in the optimization process plays a crucial role in defining the optimal parameters of DVAs and their efficiency, other objective functions rather than the ones used in this investigation would be considered to evaluate the efficiency of DVAs.

5. As this study is the first of its kind, a general approach in optimization process has been employed. However, a deeper investigation on the relation between the propagation modes of the interior floor and the DVAs natural frequency can be developed. An analytical optimization approach to control these propagation modes would be an interesting topic to follow.

6. In terms of computational efficiency, the present methodology can be improved in various directions. This should be an important research line in the future in order to simplify the DVAs effectiveness predictions.

7. Preliminary studies showed that DVAs also could be an effective countermeasures to control underground railway-induced ground-borne vibration

from simple tunnel. However, basic models have been used in these previous studies. Using a more accurate model to evaluate the efficiency of DVAs for simple tunnel, as the ones presented in this thesis for double-deck tunnels, is another interesting topic to follow.

8. Studying the application of DVAs to control ground-borne vibration caused by surface railway traffic can be taken into consideration for further studies.

Bibliography

[1] El Pla Estratègic Metropolità de Barcelona (PEMB), Construction line 9 of the metro, https://pemb.cat/ca/projectes-estrategics/construccio_linia_9_de_metro/2/, 2015.

[2] A. Clot, R. Arcos, J. Romeu, T. Pàmies, Dynamic response of a double-deck circular tunnel embedded in a full-space, Tunnelling and Underground Space Technology 59 (2016) 146–156.

[3] M. Hussein, H. Hunt, L. Rikse, S. Gupta, G. Degrande, J. Talbot, S. François, M. Schevenels, Using the pip model for fast calculation of vibration from a railway tunnel in a multi-layered half-space, in: Noise and Vibration Mitigation for Rail transportation systems, Springer, 2008, pp. 136–142.

[4] M. Schevenels, S. François, G. Degrande, EDT: an ElastoDynamics Toolbox for MATLAB, Computers & Geosciences 35 (2009) 1752–1754.

[5] A. Clot, J. Romeu, R. Arcos, S. R. Martín, A power flow analysis of a double-deck circular tunnel embedded in a full-space, Soil Dynamics and Earthquake Engineering 57 (2014) 1–9.

[6] A. Clot, A dynamical model of a double-deck circular tunnel embedded in a full-space, Ph.D. thesis, Universitat Politècnica de Catalunya, 2014.

[7] A. Clot, R. Arcos, J. Romeu, B. Noori, Prediction of the isolation efficiency of vibration countermeasures for a double-deck tunnel, in: Proceedings of EuroRegio 2016, 2016.

[8] A. Clot, R. Arcos, B. Noori, J. Romeu, Isolation of vibrations induced by railway traffic in double-deck tunnels using elastomeric mats, in: 24th International Congress on Sound and Vibration, ICSV 2017, 2017.

[9] Q. Wang, J. Zeng, L. Wei, C. Zhou, B. Zhu, Reduction of vertical abnormal vibration in carbodies of low-floor railway trains by using a dynamic vibration absorber, Proceedings of the Institution of Mechanical Engineers, Part F: Journal of Rail and Rapid Transit (2017) 0954409717731234.

[10] D. Thompson, C. Jones, T. Waters, D. Farrington, A tuned damping device for reducing noise from railway track, Applied acoustics 68 (2007) 43–57.

[11] T. Wu, Effects on short pitch rail corrugation growth of a rail vibration absorber/damper, Wear 271 (2011) 339–348.

[12] ISO 14837-1:2005 Mechanical vibration. Ground-borne noise and vibration arising from rail systems. Part 1: General Guidance, International Organization for Standardization, 2005.

[13] ISO 2631-1:1997 Mechanical vibration and shock. Evaluation of human exposure to whole-body vibration. Part 1: General requirements, International Organization for Standardization, 1997.

[14] ISO 2631-2:2003 Mechanical vibration and shock. Evaluation of human exposure to whole-body vibration. Part 2: Vibration in buildings (1 Hz to 80 Hz), International Organization for Standardization, 2003.

[15] R. Hood, R. Greer, M. Breslin, P. Williams, The calculation and assessment of ground-borne noise and perceptible vibration from trains in tunnels, Journal of sound and vibration 193 (1996) 215–225.

[16] H. E. von Gierke, A. J. Brammer, Effects of shock and vibration on humans, 2002.

[17] C. G. Gordon, Generic vibration criteria for vibration-sensitive equipment, in: Optomechanical Engineering and Vibration Control, volume 3786, International Society for Optics and Photonics, 1999, pp. 22–34.

[18] M. Heckl, G. Hauck, R. Wettschureck, Structure-borne sound and vibration from rail traffic, Journal of Sound and Vibration 193 (1996) 175–184.

[19] A. Tadeu, J. António, L. Godinho, Green's function for two-and-a-half dimensional elastodynamic problems in a half-space, Computational Mechanics 27 (2001) 484–491.

[20] A. Tadeu, E. Kausel, Green's functions for two-and-a-half-dimensional elastodynamic problems, Journal of Engineering Mechanics - ASCE 126 (2000) 1093–1097.

[21] P. Amado-Mendes, P. Costa, L. Godinho, P. Lopes, 2.5D MFS–FEM model for the prediction of vibrations due to underground railway traffic, Engineering Structures 104 (2015) 141–154.

[22] M. Hussein, S. François, M. Schevenels, H. Hunt, J. Talbot, G. Degrande, The fictitious force method for efficient calculation of vibration from a tunnel embedded in a multi-layered half-space, Journal of Sound and Vibration 333 (2014) 6996–7018.

[23] A. Tadeu, J. António, L. Godinho, Defining an accurate MFS solution for 2.5D acoustic and elastic wave propagation, Engineering analysis with boundary elements 33 (2009) 1383–1395.

[24] A. Tadeu, J. António, D. Mateus, Sound insulation provided by single and double panel wallsa comparison of analytical solutions versus experimental results, Applied Acoustics 65 (2004) 15–29.

[25] L. Godinho, P. Amado-Mendes, A. Tadeu, Meshless analysis of soil–structure interaction using an MFS–MLPG coupled approach, Engineering Analysis with Boundary Elements 55 (2015) 80–92.

[26] A. Nayfeh, Wave propagation in layered anisotropic media: With application to composites, Elsevier, 1995.

[27] G. Waas, H. Riggs, H. Werkle, Displacement solutions for dynamic loads in transversely-isotropic stratified media, Earthquake engineering & structural dynamics 13 (1985) 173–193.

[28] E. Kausel, Wave propagation in anisotropic layered media, International Journal for Numerical Methods in Engineering 23 (1986) 1567–1578.

[29] B. Oliveira, M. João, E. Kausel, The thin-layer method in a cross-anisotropic 3D space, International journal for numerical methods in engineering 89 (2012) 537–560.

[30] J. Van Der Hijden, Propagation of transient elastic waves in stratified anisotropic media, volume 32, Elsevier, 2014.

[31] L. Chen, Three-dimensional greens function for an anisotropic multi-layered half-space, Computational Mechanics 56 (2015) 795–814.

[32] L. Chen, Greens function for a transversely isotropic multi-layered half-space: an application of the precise integration method, Acta Mechanica 226 (2015) 3881–3904.

[33] W. Thomson, Transmission of elastic waves through a stratified solid medium, Journal of Applied Physics 21 (1950) 89–93.

[34] N. Haskell, The dispersion of surface waves on multilayered media, Bulletin of the seismological Society of America 43 (1953) 17–34.

[35] E. Pan, M. Bevis, F. Han, H. Zhou, R. Zhu, Surface deformation due to loading of a layered elastic half-space: a rapid numerical kernel based on a circular loading element, Geophysical Journal International 171 (2007) 11–24.

[36] E. Pan, F. Han, Green's functions for transversely isotropic piezoelectric multilayered half-spaces, Journal of engineering mathematics 49 (2004) 271–288.

[37] B. Kennett, Reflections, rays, and reverberations, Bulletin of the Seismological Society of America 64 (1974) 1685–1696.

[38] M. Lowe, Matrix techniques for modeling ultrasonic-waves in multilayered media, Ieee Transactions on Ultrasonics Ferroelectrics and Frequency Control 42 (1995) 525–542.

[39] E. Kausel, J. Roësset, Stiffness matrices for layered soils, Bulletin of the Seismological Society of America 71 (1981) 1743–1761.

[40] S. Rokhlin, L. Wang, Stable recursive algorithm for elastic wave propagation in layered anisotropic media: Stiffness matrix method, The Journal of the Acoustical Society of America 112 (2002) 822.

[41] L. Wang, S. Rokhlin, Recursive stiffness matrix method for wave propagation in stratified media, Bulletin of the Seismological Society of Amercia 92 (2002) 1129–1135.

[42] E. Tan, Hybrid compliance-stiffness matrix method for stable analysis of elastic wave propagation in multilayered anisotropic media, The Journal of the Acoustical Society of America 119 (2006) 45–53.

[43] S. François, M. Schevenels, P. Galvín, G. Lombaert, G. Degrande, A 2.5D coupled FE–BE methodology for the dynamic interaction between longitudinally invariant structures and a layered halfspace, Computer Methods in Applied Mechanics and Engineering 199 (2010) 1536–1548.

[44] L. Andersen, C. J. C. Jones, Coupled boundary and finite element analysis of vibration from railway tunnels–a comparison of two- and three-dimensional models, Journal of Sound and Vibration 293 (2006) 611–625.

[45] G. Degrande, D. Clouteau, R. Othman, M. Arnst, H. Chebli, R. Klein, P. Chatterjee, B. Janssens, A numerical model for ground-borne vibrations from underground railway traffic based on a periodic finite element-boundary element formulation, Journal of Sound and Vibration 293 (2006) 645–666.

[46] X. Sheng, C. J. C. Jones, D. J. Thompson, Prediction of ground vibration from trains using the wavenumber finite and boundary element methods, Journal of Sound and Vibration 293 (2006) 575–586.

[47] S. François, M. Schevenels, P. Galvín, G. Lombaert, G. Degrande, A 2.5D coupled FE-BE methodology for the dynamic interaction between longitudinally invariant structures and a layered halfspace, Computer Methods in Applied Mechanics and Engineering 199 (2010) 1536–1548.

[48] P. Alves Costa, R. Calçada, A. Silva Cardoso, Track-ground vibrations induced by railway traffic: In-situ measurements and validation of a 2.5D FEM-BEM model, Soil Dynamics and Earthquake Engineering 32 (2012) 111–128.

[49] P. Amado-Mendes, P. Alves Costa, L. M. C. Godinho, P. Lopes, 2.5D MFS-FEM model for the prediction of vibrations due to underground railway traffic, Engineering Structures 104 (2015) 141–154.

[50] A. Yaseri, M. H. Bazyar, S. Javady, 2.5D coupled FEM-SBFEM analysis of ground vibrations induced by train movement, Soil Dynamics and Earthquake Engineering 104 (2018) 307–318.

[51] J. C. O. Nielsen, G. Lombaert, S. François, A hybrid model for prediction of ground-borne vibration due to discrete wheel/rail irregularities, Journal of Sound and Vibration 345 (2015) 103–120.

[52] K. A. Kuo, H. Verbraken, G. Degrande, G. Lombaert, Hybrid predictions of railway induced ground vibration using a combination of experimental measurements and numerical modelling, Journal of Sound and Vibration 373 (2016) 263–284.

[53] G. Kouroussis, K. E. Vogiatzis, D. P. Connolly, A combined numerical/experimental prediction method for urban railway vibration, Soil Dynamics and Earthquake Engineering 97 (2017) 377–386.

[54] D. López-Mendoza, A. Romero, D. Connolly, P. Galvín, Scoping assessment of building vibration induced by railway traffic, Soil Dynamics and Earthquake Engineering 93 (2017) 147–161.

[55] K. Kuo, H. Verbraken, G. Degrande, G. Lombaert, Hybrid predictions of railway induced ground vibration using a combination of experimental measurements and numerical modelling, Journal of Sound and Vibration 373 (2016) 263–284.

[56] X. Sheng, C. J. C. Jones, D. J. Thompson, A theoretical model for ground vibration from trains generated by vertical track irregularities, Journal of Sound and Vibration 272 (2004) 937–965.

[57] J. A. Forrest, H. E. M. Hunt, A three-dimensional tunnel model for calculation of train-induced ground vibration, Journal of Sound and Vibration 294 (2006) 678–705.

[58] J. A. Forrest, H. E. M. Hunt, Ground vibration generated by trains in underground tunnels, Journal of Sound and Vibration 294 (2006) 706–736.

[59] J. Han, X. Xiao, Y. Wu, Z. Wen, G. Zhao, Effect of rail corrugation on metro interior noise and its control, Applied Acoustics 130 (2018) 63–70.

[60] M. F. M. Hussein, H. E. M. Hunt, Modelling of floating-slab tracks with continuous slabs under oscillating moving loads, Journal of Sound and Vibration 297 (2006) 37–54.

[61] M. F. M. Hussein, H. E. M. Hunt, Modelling of floating-slab track with discontinuous slab Part 2: response to moving trains, Journal of Low Frequency Noise, Vibration and Active Control 25 (2006) 111–118.

[62] S. Gupta, G. Degrande, Modelling of continuous and discontinuous floating slab tracks in a tunnel using a periodic approach, Journal of Sound and Vibration 329 (2010) 1101–1125.

[63] G. Lombaert, G. Degrande, B. Vanhauwere, B. Vandeborght, S. François, The control of ground-borne vibrations from railway traffic by means of continuous floating slabs, Journal of Sound and Vibration 297 (2006) 946–961.

[64] F. Cui, C. H. Chew, The effectiveness of floating slab track system - Part I. Receptance methods, Applied Acoustics 61 (2000) 441–453.

[65] G. Wilson, H. Saurenman, J. Nelson, Control of ground-borne noise and vibration, Journal of Sound and Vibration 87 (1983) 339–350.

[66] P. Alves Costa, R. Calçada, A. Silva Cardoso, Ballast mats for the reduction of railway traffic vibrations. Numerical study, Soil Dynamics and Earthquake Engineering 42 (2012) 137–150.

[67] H. Loy, Mitigating vibration using under-sleeper pads, Railway Gazette International 168 (2012).

[68] R. Hildebrand, Effect of soil stabilization on audible band railway ground vibration, Soil dynamics and earthquake engineering 24 (2004) 411–424.

[69] J. Barbosa, P. Alves Costa, R. Calçada, Abatement of railway induced vibrations: Numerical comparison of trench solutions, Engineering Analysis with Boundary Elements 55 (2015) 122–139.

[70] J. Talbot, H. Hunt, On the performance of base-isolated buildings, Building Acoustics 7 (2000) 163–178.

[71] J. Talbot, W. Hamad, H. Hunt, Base-isolated buildings and the added-mass effect, in: Proceedings of ISMA 2014: International Conference on Noise and Vibration Engineering, 2014.

[72] F. Kawakami, T. Kobayashi, R. Cooper, M. Holden, C. Jaffe, Noise and vibration control in tokyo international forum, Journal of the Acoustical Society of America 103 (1998) 2994.

[73] P. Fiala, S. Gupta, G. Degrande, F. Augusztinovicz, A parametric study on countermeasures to mitigate sub–way traffic induced vibration and noise in buildings, in: Proceedings of ISMA2008 International Conference on Noise and Vibration Engineering, 2008, pp. 2751–2764.

[74] E. Celebi, F. Göktepe, Non–linear 2D FE analysis for the assessment of isolation performance of wave impeding barrier in reduction of railway-induced surface waves, Construction and Building Materials 36 (2012) 1–13.

[75] P. Coulier, S. François, G. Degrande, G. Lombaert, Subgrade stiffening next to the track as a wave impeding barrier for railway induced vibrations, Soil Dynamics and Earthquake Engineering 48 (2013) 119–131.

[76] T. M. Al-Hussaini, S. Ahmad, Design of wave barriers for reduction of horizontal ground vibration, Journal of geotechnical engineering 117 (1991) 616–636.

[77] S. François, M. Schevenels, A 2.5D finite element - boundary element model for vibration isolating screens, in: Proceedings of the ISMA2008, 2008, pp. 2765–2776.

[78] R. Shrivastava, N. K. Rao, Response of soil media due to impulse loads and isolation using trenches, Soil Dynamics and Earthquake Engineering 22 (2002) 695–702.

[79] S. Kattis, D. Polyzos, D. Beskos, Structural vibration isolation by rows of piles, in: Seventh International Conference on Soil Dynamics and Earthquake Engineering (SDEE 95) Hellenic Society of Soil Mechanics and Foundation Engineering, Greece., 1995.

[80] A. Clot, J. Romeu, R. Arcos, An energy flow study of a double-deck tunnel under quasi-static and harmonic excitations, Soil Dynamics and Earthquake Engineering 89 (2016) 1–4.

[81] J. Q. Sun, M. R. Jolly, M. A. Norris, Passive, Adaptive and Active Tuned Vibration AbsorbersA Survey, Journal of Mechanical Design 117 (1995) 234.

[82] L. Kela, P. Vähäoja, Recent studies of adaptive tuned vibration absorbers/neutralizers, Applied Mechanics Reviews 62 (2009) 060801.

[83] I. Kourakis, Structural systems and tuned mass dampers of super-tall buildings : case study of Taipei 101, Ph.D. thesis, Massachusetts Institute of Technology, 2007.

[84] D. E. Newland, Vibration of the London Millennium Bridge: cause and cure, International Journal of Acoustics and Vibration 8 (2003) 9–14.

[85] P. Nawrotzki, Tuned-mass systems for the dynamic upgrade of buildings and other structures, in: Eleventh East Asia-Pacific Conference on Structural Engineering & Construction (EASEC-11) Building a Sustainable Environment, Taipei Taiwan, Citeseer, 2008.

[86] P. Watts, On a method of reducing the rolling of ships at sea, Transactions of the Institution of Naval Architects 24 (1883) 165–190.

[87] H. Frahm, Device for damping vibration of bodies, U.S. Patent No. 989958 (1911).

[88] J. Ormondroyd, The theory of the dynamic vibration absorber, trans. asme, Journal of Applied Mechanics 50 (1928).

[89] M. Zilletti, S. J. Elliott, E. Rustighi, Optimisation of dynamic vibration absorbers to minimise kinetic energy and maximise internal power dissipation, Journal of sound and vibration 331 (2012) 4093–4100.

[90] R. W. Luft, Optimal tuned mass dampers for buildings, Journal of the Structural Division 105 (1979) 2766–2772.

[91] T. Asami, O. Nishihara, A. M. Baz, Analytical solutions to h and h2 optimization of dynamic vibration absorbers attached to damped linear systems, Journal of vibration and acoustics 124 (2002) 284–295.

[92] Y. Fujino, M. Abe, Design formulas for tuned mass dampers based on a perturbation technique, Earthquake engineering & structural dynamics 22 (1993) 833–854.

[93] M. N. Hadi, Y. Arfiadi, Optimum design of absorber for mdof structures, Journal of Structural Engineering 124 (1998) 1272–1280.

[94] B. Noori, A. Farshidianfar, Optimum design of dynamic vibration absorbers for a beam, based on H_∞ and H_2 optimization, Archive of Applied Mechanics 83 (2013) 1773–1787.

[95] S. Zhu, J. Yang, H. Yan, L. Zhang, C. Cai, Low-frequency vibration control of floating slab tracks using dynamic vibration absorbers, Vehicle System Dynamics 53 (2015) 1296–1314.

[96] J. P. Den Hartog, Mechanical vibrations, Courier Corporation, 1985.

[97] W. Ho, B. Wong, D. England, Tuned mass damper for rail noise control, in: Noise and Vibration Mitigation for Rail Transportation Systems, Springer, 2012, pp. 89–96.

[98] W. Ho, B. Wong, D. Tsui, C. Kong, Reducing rail corrugation growth by tuned mass damper, in: Proceedings of the 11th International Workshop of Railway Noise, 2013.

[99] M. P. Singh, S. Singh, L. M. Moreschi, Tuned mass dampers for response control of torsional buildings, Earthquake engineering & structural dynamics 31 (2002) 749–769.

[100] N. B. Desu, S. Deb, A. Dutta, Coupled tuned mass dampers for control of coupled vibrations in asymmetric buildings, Structural control and health monitoring 13 (2006) 897–916.

[101] Y. Arfiadi, M. Hadi, Optimum placement and properties of tuned mass dampers using hybrid genetic algorithms, Iran University of Science & Technology 1 (2011) 167–187.

[102] M. Mohebbi, K. Shakeri, Y. Ghanbarpour, H. Majzoub, Designing optimal multiple tuned mass dampers using genetic algorithms (gas) for mitigating the seismic response of structures, Journal of Vibration and Control 19 (2013) 605–625.

[103] E. Ntotsios, D. Thompson, M. Hussein, The effect of track load correlation on ground-borne vibration from railways, Journal of Sound and Vibration 402 (2017) 142–163.

[104] G. Lombaert, G. Degrande, Ground-borne vibration due to static and dynamic axle loads of InterCity and high-speed trains, Journal of Sound and Vibration 319 (2009) 1036–1066.

[105] X. Lei, N. A. Noda, Analyses of dynamic response of vehicle and track coupling system with random irregularity of track vertical profile, Journal of Sound and Vibration 258 (2002) 147–165.

[106] M. F. M. Hussein, H. E. M. Hunt, A power flow method for evaluating vibration from underground railways, Journal of Sound and Vibration 293 (2006) 667–679.

[107] S. Gupta, W. F. Liu, G. Degrande, G. Lombaert, W. N. Liu, Prediction of vibrations induced by underground railway traffic in Beijing, Journal of Sound and Vibration 310 (2008) 608–630.

[108] G. C. Marano, R. Greco, B. Chiaia, A comparison between different optimization criteria for tuned mass dampers design, Journal of Sound and Vibration 329 (2010) 4880–4890.

[109] MATLAB, version 9.2.0 (R2017a), The MathWorks Inc., Natick, Massachusetts, 2017.

[110] A. Boström, A. D. Burden, Propagation of elastic surface waves along a cylindrical cavity and their excitation by a point force, Journal of the Acoustical Society of America 72 (1982) 998–1004.

[111] D. Ghangale, A. Colaço, P. A. Costa, R. Arcos, A methodology based on structural finite element method-boundary element method and acoustic boundary element method models in 2.5 d for the prediction of reradiated noise in railway-induced ground-borne vibration problems, Journal of Vibration and Acoustics 141 (2019) 031011.

[112] R. Arcos, A. Clot, D. Ghangale, B. Noori, J. Romeu, Hybrid model for rail fasteners stiffness optimization in railway-induced ground-borne vibration problems, in: INTER-NOISE and NOISE-CON Congress and Conference Proceedings, volume 257, Institute of Noise Control Engineering, 2018, pp. 239–249.

[113] M. Bahrekazemi, Train-induced ground vibration and its prediction, Ph.D. thesis, Royal Institute of Technology, 2004.

[114] C. With, A. Bodare, Prediction of train-induced vibrations inside buildings using transfer functions, Soil Dynamics and Earthquake Engineering 27 (2007) 93–98.

[115] C. E. Hanson, J. C. Ross, D. A. Towers, M. Harris, et al., High-speed ground transportation noise and vibration impact assessment., Technical Report, United States. Federal Railroad Administration. Office of Railroad Policy , 2012.

[116] B. Noori, R. Arcos, J. Romeu, C. A., A method based on 3D stiffness matrices in Cartesian coordinates for computation of 2.5D elastodynamic Green's functions of layered half-spaces, Soil Dynamics and Earthquake Engineering 114 (2018) 154–158.

[117] E. Kausel, Fundamental solutions in elastodynamics: a compendium, Cambridge University Press, 2006.

[118] F. Graff, Wave motion in elastic solids, Dover Publications Inc., 1975.